DOE/ER/05490--107

DE90 002525

RESEARCH IN ELEMENTARY PARTICLE PHYSICS

Progress Report

Lai-Him Chan and Richard Haymaker

and

Richard Imlay, Roger McNeil and William Metcalf

Louisiana State University
Baton Rouge, Louisiana

March 1, 1989 to February 28, 1990

Prepared for the U. S. Department of Energy under
Contract # DE-AS05-77-ER05490

DISCLAIMER

This report was prepared as an account of work sponsored by an agency of the United States Government. Neither the United States Government nor any agency thereof, nor any of their employees, makes any warranty, express or implied, or assumes any legal liability or responsibility for the accuracy, completeness, or usefulness of any information, apparatus, product, or process disclosed, or represents that its use would not infringe privately owned rights. Reference herein to any specific commercial product, process, or service by trade name, trademark, manufacturer, or otherwise does not necessarily constitute or imply its endorsement, recommendation, or favoring by the United States Government or any agency thereof. The views and opinions of authors expressed herein do not necessarily state or reflect those of the United States Government or any agency thereof.

MASTER

DISTRIBUTION OF THIS DOCUMENT IS UNLIMITED

DISCLAIMER

This report was prepared as an account of work sponsored by an agency of the United States Government. Neither the United States Government nor any agency thereof, nor any of their employees, makes any warranty, express or implied, or assumes any legal liability or responsibility for the accuracy, completeness, or usefulness of any information, apparatus, product, or process disclosed, or represents that its use would not infringe privately owned rights. Reference herein to any specific commercial product, process, or service by trade name, trademark, manufacturer, or otherwise does not necessarily constitute or imply its endorsement, recommendation, or favoring by the United States Government or any agency thereof. The views and opinions of authors expressed herein do not necessarily state or reflect those of the United States Government or any agency thereof.

DISCLAIMER

Portions of this document may be illegible in electronic image products. Images are produced from the best available original document.

Abstract

We describe theoretical work on effective action expansion of an effective low energy theory of hadrons, dynamical symmetry breaking, and lattice gauge theories.

The high energy experimental group at Louisiana State University has finished taking data on a neutrino oscillation experiment at LAMPF. Results for the 1987 data have been published. Analysis of 1988 and 1989 data is in progress. LSU is also participating on an electron-positron experiment, AMY, that is running at TRISTAN in Japan. LSU is responsible for the muon detector for AMY. Many results have been published. We have recently joined an electron-proton experiment, ZEUS.

TABLE OF CONTENTS

Page

THEORETICAL - TASK A

Introduction 1

A. Low energy particle dyanmics and effective field theories, L-H. Chan. 2

B. Problems in Lattace QCD, R. Haymaker. 19

C. Statistics and Quantum Field Theory in Three Space-Time Dimensions, Chen-Han Lee. 48

EXPERIMENTAL - TASK B

A. Introduction. 50

B. The Neutrino Oscillation Experiment 51

C. The AMY Experiment at TRISTAN. 69

D. The ZEUS Experiment at HERA 100

E. The SSC Facilities 113

F. References 117

Reports 122

THEORETICAL - Task A

Introduction

This report describes work on various problems in particle physics. The work includes an effective low energy theory of hadrons, the effective-action expansion, and lattice gauge theories.

Co-principal investigators R. Haymaker and L.-H Chan have devoted 100% of their time in the summer and 50% of their time during the academic year to this project. Our research associate, W. F. Kao has returned to the Republic of China to take on a faculty position at Fu-Jen University.

J. Wosiek from Hagellonian University in Krakow will be back at LSU for three months next March to continue the joint project on lattice gauge theories with R. Haymaker.

II. THEORETICAL – TASK A

A Low-energy particle dynamics and effective field theories (Lai-Him Chan)

The emphasis of theoretical particle physics has been centered on higher energy and shorter distance where the dynamics of particles and fields is presumably more fundamental and perhaps simpler. However particle phenomenology as observed in laboratories occurs at low energy. In many cases there is no first principle method of calculation to relate theories directly and experimental observations. Therefore it is vitally important to develop theoretical tools and conjectures which serve as intermediate stepping stones for the construction of an effective theory that would eventually lead the ultimate understanding of particle physics at the fundamental level.

In the past years I have pursued this endeavor successfully in a number of ways as will be described in more detail in the following sections. My general approaches are:

1. to use a set of acceptable principles or scenarios together with model-independent assumptions, which are either derivable or believed to be derivable from a more fundamental theory, to extrapolate from existing data predictions which may be useful either as relevant information for further data analysis or as a theoretical check on the validity of the general assumptions. The example for this approach is my work on the isospin mass splittings [1,2,3].

2. to extract from experimental observations some general properties or structures of the dynamics which may not be anticipated directly from the fundamental interactions. The recognition of such principles or structures may give insight to the ultimate solution to the dynamical problem. The example of my work in this direction is my conjecture on the scalar quark confinement which have been finally confirmed theoretically and experimentally only very recently after many years [4].

3. to develop mathematical tools which may be used to extract from a fundamental theory at shorter distance an effective field theory for low-energy dynamics. A series of my recent papers on effective action expansions contributes toward this end [5,6,7,8,9,10].

4. to develop an effective field theory for the low-energy hadron dynamics using effective action expansion and assumptions from QCD [6,8].

In the following pages, I shall first describe some major innovation in mathematical tool in doing theoretical physics at LSU, the coming of *Mathematica*. Then I shall report the progress and the future direction on a few research programs.

A.1 A New Analytical Tool — Mathematica

In contrast to heavily computational oriented approaches such as the lattice gauge theories, analytical approaches may shed more light on the real physical dynamics which may otherwise be difficult to be recognized. However analytical tools necessary for interesting physical processes are very complex and cumbersome, in particular when dealing with nonabelian algebra. Symbolic manipulation programing languages such as MACSYMA, REDUCE and SMP have been available in mainframe computers but they are cumbersome to use and far less than a truly interactive style a normal theoretician would like to work with. Therefore they have been applied to handle some straightforward but tedious chores in particular problem rather than being used as a problem solving tool.

Recently a powerful new mathematics program *Mathematica* from Wolfram research, when integrated with the Macintosh II front end, has succeeded in fulfilling many requirements of being the ideal analytical tools. It does symbolic mathematics, manipulating algebraic formulae with ease. It produces two- and three-dimensional graphic and can even animate them. a substantial part of known mathematics is already built in, and additional functions can be added through Mathematica's expressive new programming language. The software of Mathematica are divided into two parts: (1) the front end which takes advantage of the particular feature of the host computer and the kernel which is machine independent and is available in most

advantage, it is necessary to upgrade the computer to more powerful new models, Mac IIx or Mac IIci which will also solve the speed problem. I am looking forward to upgrade our system next year.

A.2 Isospin mass splittings

The isospin mass splitting arises from two different sources: (1) the one-photon exchange and (2) the strong isospin violation due to intrinsic up and down quark mass difference.

The one-photon exchange representing the electromagnetic interaction energy between the constituent quarks is well understood. In most cases it contributes less than 2 MeV or less than 40% of the mass difference. Its contributions are not sensitive to the theoretical models.

A nonelectromagnetic isospin-breaking mechanism, necessary to explain $m_N > m_P$ and $m_{K^0} > m_{K^+}$, has been attributed to the difference in the up and down quark masses. In a series of papers a few years ago I have proposed that associated with this mass difference there must be an induced dynamical isospin-breaking effect due to the quark mass dependence of the interaction mainly from the hyperfine interaction and that its contribution to the hadron isospin mass splittings (for the presently existing hadrons as well as those heavy hadrons yet to be discovered) can be estimated very reliably from some general assumptions consistent with the QCD hypotheses in a model independent way [1,2,3]. Because the induced dynamical effect is very sensitive to the quark mass, my predictions of the isospin splittings for hadrons with heavy quark are uniquely different from the conventional models. It was emphasized that the prediction $M_{B^0} - M_{B^+} = 2.3 \pm 0.3 MeV$ can be checked by precise measurement. If the measured value is found outside the acceptable region, some of the general assumptions used must be reexamined very carefully. The $M_{B^0} - M_{B^+}$ mass difference is very important since it must be used to estimate the relative proportions of the $B^0\bar{B}^0$ and B^+B^- final state in the $\Upsilon(4S)$ decays.

Table I summarizes the present status of isospin splittings, a comparison of my calculation and the experimental values. Two latest results are highlighted by bold-

face types. The $\Xi_c^0 - \Xi_c^+$ value represents the first reliable measurement on this splitting [12]. Although it has a large error, it agrees fairly well with my predicted value. This measurement will surely be refined in the near future and gives further support to this calculation.

TABLE I. Baryon isomultiplet splittings in MeV.

	Strong	Electric	Magnetic	Total	Expt.
$n-p$	1.9	–1.0	0.4	1.3	1.2933
$\Sigma^- - \Sigma^+$	5.6	1.0	1.4	8.0	7.97 ± 0.07
$\Sigma^- - \Sigma^0$	2.8	2.0	0.1	4.9	4.88 ± 0.06
$\Sigma^+ + \Sigma^- - 2\Sigma^0$	0.0	3.0	–1.2	1.8	1.79 ± 0.14
$\Sigma^{*-} - \Sigma^{*+}$	4.0	1.0	–0.1	4.9	4.4 ± 0.6
$\Sigma^{*-} - \Sigma^{*0}$	2.0	2.0	–0.7	3.3	3.5 ± 1.0
$\Xi^- - \Xi^0$	3.7	2.0	1.0	6.7	6.4 ± 0.6
$\Xi^{*-} - \Xi^{*0}$	2.1	2.0	–0.5	3.6	3.2 ± 0.6
$\Sigma_c^0 - \Sigma_c^{++}$	4.9	–4.9	–0.3	–0.3	$-.5 \pm 0.6 \pm 0.2$ [a]
$\Sigma_c^0 - \Sigma_c^+$	2.4	–1.0	–0.7	0.7	
$\Sigma_c^{*0} - \Sigma_c^{*++}$	4.4	–4.9	0.7	–0.2	
$\Sigma_c^{*0} - \Sigma_c^{*+}$	2.2	–1.0	–0.2	1.0	
$\Xi_c^0 - \Xi_c^+$	3.4	-1.0	0.8	3.2	$5 \pm 4 \pm 1$ [b]
$\Sigma_b^- - \Sigma_b^+$	4.7	1.0	0.4	6.0	
$\Sigma_b^- - \Sigma_b^0$	2.3	2.0	–0.3	4.0	
$\Sigma_b^{*-} - \Sigma_b^{*+}$	4.5	1.0	0.3	5.8	
$\Sigma_b^{*-} - \Sigma_b^{*0}$	2.5	2.0	–0.4	3.8	
$D^+ - D^0$	2.66	1.00	.32	4.7	4.74 ± 0.28
$D^{*+} - D^{*0}$	2.42	1.00	–.11	3.3	2.90 ± 1.30
$B^0 - B^+$	2.90	–0.50	–.06	2.3	2.00 ± 1.10
$B^{*0} - B^{*+}$	2.58	–.050	.02	2.1	

(a) Average value of Ref. 14 and Ref.15
(b) Ref. 12.

The other recent measurement is of particular interest. Lichtenberg [13] had suggested that the best way for distinguishing among various theoretical models would come from measurement of the mass difference $\Sigma_c^{++} - \Sigma_c^0$. The final result of

the mass splitting comes from a cancellation of two large contributions, strong and electrostatic, with opposite signs; the magnetic contribution is small as in all cases (see Table I). A relatively small uncertainty in determining the exact contribution in each of the large contribution can therefore give a large variation in the final result after the cancellation. It is among the very few instance that theoretical predictions are extremely sensitive to the theoretical models as illustrated in Table II. They range from 3 to -18 MeV. Table II also shows values of experimental measurements. The 1986 and 1987 values are as scattered as the theoretical predictions. A better measurement by ARGUS group[24] gives $\Sigma_c^{++} - \Sigma_c^0 = 1.2 \pm 0.7 \pm 0.3 MeV$. The latest measurement by CLEO group[15] $\Sigma_c^{++} - \Sigma_c^0 = -0.1 \pm 0.6 \pm 0.1 MeV$ rules out all other models and therefore gives strong confirmation of my calculation.

Table II. A comparison of some calculated and experimental values of the mass difference $\Sigma_c^{++} - \Sigma_c^0$.

	Reference	$\Sigma_c^{++} - \Sigma_c^0$ (MeV)
Theory	Lichtenberg[13]	3.5
	Itoh[16]	6.5
	Ono[17]	6.1
	Lane & Weinberg[18]	–6
	MIT bag model[19]	–3 to –18
	Chan[1]	0.4
	Kalman[20]	–2.7
	Richard[21]	–3 or +2
	Chan[2]	0.3
	Lichtenberg & Hwang[22]	3.0
	Capstick[23]	1.4
Experiment	ARGUS (1986)[24]	2.5 ± 1.0
	Fermi Lab (1987)[25]	-10.8 ± 2.9
	ARGOS (1988)[14]	1.2 ± 0.7 ± 0.3
	CLEO (1989) [15]	–.1 ± 0.6 ± 0.2

Recently Shuryak and Rosner[26] show that an instanton picture provides as satisfactory a description of mass splittings in octet and decimet baryons as the more conventional picture based on hyperfine interactions due to single-gluon exchange. Their calculation is based on a single instanton property that the instanton interaction between quarks is appreciable (and attractive) only for diquarks in a spin-zero state. Although the dynamical origin of the instanton may be quite different from that of the color magnetic moment interaction. I can show that their particular way of implementation can easily be integrated into my model by recognizing that the spin 0 projection operator of the diquark,

$$P_0 = \frac{1}{4} - \vec{s}_1 \cdot \vec{s}_2,$$

is trivially related to the spin-spin term. Therefore the S–wave hadron mass matrix element

$$M = \mu_p + \sum_i m_i + \alpha_s^{(p)} k_p D_p m_u^2 4 \sum_{i>j} \frac{\vec{S}_i}{m_i} \cdot \frac{\vec{S}_j}{m_j}$$

can easily rewritten into the following expression

$$M = \mu_p + \sum_i m_i + \frac{1}{4}\alpha_s^{(p)} k_p D_p m_u^2 4 \sum_{i>j} \frac{1}{(m_i m_j)} + \alpha_s^{(p)} k_p D_p m_u^2 4 \sum_{i>j} \frac{1}{(m_i m_j)} \left(\vec{S}_i \cdot \vec{S}_j - \frac{1}{4} \right),$$

The last term is the instanton contribution. The above expression differs from that of Shuryak and Rosner by the extra spin-independent term $\sum_{i>j} \frac{1}{(m_i m_j)}$. If at least one of the quark is heavy, the the contribution is very small. If both quarks are light as in the case considered in that paper, one can then rewrite

$$\frac{2}{m_i m_j} = \frac{1}{m_i^2} + \frac{1}{m_j^2} - \left(\frac{1}{m_i} - \frac{1}{m_j} \right)^2$$

The second term is small, of the second order of $SU(3)$ breaking. The first two terms depend on a single quark mass only and can be absorbed into the redefinition of the quark mass. This explains completely the discrepancy in quark masses between the two models. The crossing between the hyperfine interaction interpretation and the instanton interpretation make it possible to have the best of both features. In this formulation, I use my model to predict all parameters for the instanton

model. On the other hand, the instanton interpretation allow me to calculate the η and η' masses which would otherwise not be possible.

A.3 Derivative expansion and effective action expansion

Much progress and speculations in fundamental particles interactions in the recent years have based on hierarchy of levels of effective dynamics. While the fundamental field theories may appear to be simple and perhaps elegant at very short distance, the connection to the observable dynamics at low energy level are extremely complex and remote. With the emerging problems such as the Skyrmion physics, strongly interacting Higgs sector of the standard model, supersymmetric nonlinear σ model, supergravity, anomalies etc., there has been increasing interest toward effective field theories with higher derivative couplings. Important progresses have been achieved for the efficient derivation of the derivative (effective action) expansions by integrating out the non-observable quantum degrees of freedom associated with the short distant dynamics [5,6,7,8,9,27,28,29,30,38]. In particular my method has been followed by works from major groups such as Berkeley [29,30,31,32,33,34,35,36,37] and Seattle Washington [39,40,41], in diversified areas from nuclear and soliton physics to supersymmetry and supergravity. This new tool opens up many applications as well as many questions which has not been raised before. In addition there may be also improvements on the technique and generalizations to more complex and realistic problem such as the non-abelian-gauge-meson-loop.

An important aspect of my formulation is that the derivative expansion can be developed systematically in a straightforward manner without having to solve any equation. I have used this method to calculate the four derivative terms in a number of models. In a number of problems it is clear that it may be useful to go beyond the four-derivative terms. However the algebra for the computation becomes unmanageable. With the help of Mathematica, hopefully this task can be accomplished.

I am going to describe only a few examples in this proposal my research in this direction.

A.3.1 On the improvement of the derivative expansion

In spite of its many possible applications, the criteria of the usefulness determined by the properties of convergence of these derivative expansions has not been established, since most of the realistic models are unsolvable. One would expect that the radius of convergence of the derivative expansion should be determined by the next mass scale of the original Lagrangian. Such connection may not necessarily be obvious if there are dynamically generated particles (including solitons) of lower mass scale. In that case resummation and analytical continuation techniques must be employed in order to make use of the derivative expansion to describe the low energy phenomenology.

In a recent paper I propose an algebraic resummation method to improve the convergence of the derivative expansion [10]. This method, originally designed to improve the convergence of the derivative expansion of the two- dimension ϕ^4 field theory, can be easily adopted for field theory in any dimension. While this method may appear to be naive as well as far from being mathematically rigorous and unique, and the example seems to be unrealistic, it opens up the possibility that a clever resummation technique with proper analytic continuation can turn the derivative expansion into a useful tool in studying the effective low energy phenomenology.

It may be perhaps more useful if we can apply the resummation method locally on the effective Lagrangian density expansion rather than globally on the effective action expansion. Indeed the arguments leading to the final result would be even stronger when they are applied locally. However the Lagrangian density can only be defined up to a total derivative term. This freedom of adding an arbitrary total derivative term can alter the convergence properties substantially while it would have no effect on the effective action expansion. Since adding a total derivative term does not commute with the construction of the resummation, the end result depends crucially on the initial choice of the form of the Lagrangian density. It is possible that eventually one may be able to utilize this degree of freedom properly to obtain the best improved series with the required convergence properties. This aspect is under current investigation.

In some theories with spontaneous symmetry breaking, the effective actions be-

come complex when the effective mass becomes negative and therefore unphysical beyond this critical point. The classical potential is nonconvex and the conventional loop expansion breaks down. The singularity is the artifact of the perturbation expansion rather than that of the derivative expansion. A possible way to resolve this problem is to use nonstandard perturbation expansion techniques such as the mean-field expansion [42] and others [43,44,45,46,47] that includes an infinite partial summation of higher order loop contributions such that the effective potential remain real and physical for all values of $\Phi(x)$. The derivative expansion of the corresponding action should be improved accordingly.

A.3.2 Effective action expansion for the nonlinear σ model — the normal coordinate method

I have proposed to investigate whether the $SO(N)$ nonlinear σ model is equivalent to the $m_\sigma \to \infty$ limit of the linear σ model by comparing the corresponding one-loop effective action expansions up to the 4-derivative terms and including the symmetry breaking term [9].

For this purpose I use a new background field method to calculate the effective action expansion directly. In the case of the linear σ model the renormalization procedure is implemented carefully before the $m_\sigma \to \infty$ limit is taken. For the nonlinear σ model I introduce a new and intuitive covariant treatment for the perturbation calculation of the field theory with nonlinear constraint. I do not find any noninvariant terms in either case [50,51,52,53]. I show that the divergent parts of the effective Lagrangians due to $m_\pi \to 0$, $m_\sigma \to \infty$, or $N \to \infty$ are equivalent in the two models. However the nonleading finite parts of the effective Lagrangians are different. Therefore the two operations, taking the $m_\sigma \to \infty$ limit and calculating the quantum corrections, do not commute. The origin of this difference may be a violation of decoupling.

To make sure that my new method for calculating the effective Lagrangian for the nonlinear σ model is reliable, I have also carried out the corresponding calculation using the normal coordinate method of Ref. [54] and obtained the same result[55].

It is interesting that one can actually identify the corresponding expressions and contributions such as those in Eq. (6.28) between the two methods.

However there may be some subtle difficulties not anticipated in the construction of the effective action for the nonlinear σ model due to the constraint, such that Eq.(6.30) may not be valid even to the one-loop order Lagrangian.[56] The investigation of this aspect is presently in progress.

For the time being, the linear σ model and the nonlinear σ model are the only viable models to provide the spontaneous symmetry breaking urgently needed to understand any unified picture in particle physics. Even with the limited scope of applicability, our new method and analysis have taken a new small step toward the understanding of this fundamental problem.

A.3.3 Nonlinear σ model from linear σ model

The minimal nonlinear σ model is conventionally regarded as the formal limit of the linear σ model at $m_\sigma \to \infty$. While this idea may be correct in the tree level, there is no compelling reason that the nonlinear σ model is completely equivalent to the linear σ model at $m_\sigma \to \infty$ when quantum corrections are included. More precisely one should integrate out the heavy σ field to obtain a chiral invariant effective action. Such task turns out to be nontrivial and has not been successfully carried out. Since the decoupling theorem is not applicable in this model, there will be observable consequences in the light meson sector at low energy from the one-loop correction due to the heavy σ meson loop. The resulting nonlinear σ model is non-renormalizable.[7]

A new functional integration method is developed for integrating out the heavy chiral scalar field in the linear σ model to render a finite chiral invariant effective Lagrangian in the one-loop approximation after proper renormalization at $m_\sigma \to \infty$. In addition to the minimal nonlinear σ model term, the effective Lagrangian also contains a finite chiral invariant quantum correction term with four derivatives. This term has the correct sign for the stability of the skyrmion solution.

A.3.4 Effective Lagrangians from chiral quark dynamics

The Skyrme model has been very successful in unifying the low-energy hadron physics [48]. However it can only be considered as a phenomenological field theory. Ultimately the Skyrmion Lagrangian must be an effective Lagrangian derivable from a more fundamental Lagrangian valid at a shorter distant scale. Ideally it should possess the following properties: (1) baryons as topological solitons, (2) a satisfactory description of low energy phenomenology in the meson sector and the baryon sector and (3) the correct nuclear force. A majority of recent works have concentrated on the search for possible effective Lagrangians phenomenologically, especially by nuclear physicists [59,60,61,62,63,64,65].

The great theoretical fascination with the skyrme model is that it represents a dynamical system wherein one might hope to comprehend all low-energy hadronic phenomenology directly in terms of a nonlinear σ model effective Lagrangian. Our goal is to be able to derive such an effective Lagrangian with few if any adjustable parameters.

Theoretical derivation of the effective Lagrangian has been hindered by the major problem of solving QCD at low energy and the lack of a systematic method for the effective action expansion. While solving QCD remains an outstanding problem there has been tremendous progress in finding a simple and systematic method for the effective action expansion. The availability of such a method would offer an opportunity to obtain effective Lagrangians by exploring various scenarios from QCD.

The spontaneously broken chiral symmetry scenario of quantum chromodynamics (QCD) together with the Veltman theorem implies that the low energy effective Lagrangian of QCD must be of the nonlinear σ model type[58]. The effective Lagrangians resulting from integrating the quark fields from the gauged or nongauged chiral quark model Lagrangian in a Skyrme-type scenario may be completely equivalent to QCD in the large N_c limit at low energy and therefore may serve as realistic models for low energy hadron dynamics.

For this purpose, I have presented in detail the recent development of the effective

action expansion, in particular the evaluation of the fermion determinant of these models [6,8,57]. The implications on the low energy phenomenology associated with these effective Lagrangians have been discussed.

I plan to use Mathematica to generate the six-derivative terms for the effective Lagrangian to investigate the effect on both the meson and the baryon dynamics, especially on whether these term can help to stabilize the skyrmion solution.

In a recent paper in Physics Letters, Novozhilov[66] calculated the effective QCD chiral Lagrangian for pions and vector mesons with the chiral symmetry group G and the hidden local symmetry group $G_h = SU(2)_{hL} \times SU(2)_{hR}$ where the ρ meson is the composite guage field of the hidden local symmetry group[67]. The amazing result of his calculation is that he can determine the ρ meson parameter completely,

$$g^2 = \frac{12\pi^2}{N_c} = 4\pi^2,\ m_\rho = g^2 F_\pi^2 \text{ and } g_{\rho\gamma} = 2F_\pi^2 g_{\rho\pi\pi},$$

which are identical to what I have found from the effective Lagrangian of the chiral quark model albeit the ρ meson is dynamically generated from the pion form factor rather than built in as the gauge meson of the hidden symmetry. It will be very interesting to find out how this two model are related and it may shed some light on the origin of the hidden symmetry.

A.3.5 A new background field method for effective action and its derivative expansion in field theories with nonlinear constraint

In the recent years, there has been more and more attention on the field theories with higher derivative couplings and systems with nonlinear constraints. Some examples are the ordinary and supersymmetric σ model, the strongly interacting heavy Higgs sector of the standard model, Skyrmion physics, and various types of gauge theories. The background field method in the effective action formalism has been very useful method for such investigation.

Quantum field theories with constraint have long been recognized to be problematic. The best example is the nonlinear σ model. The most convenient treatment is to use the normal coordinate path integration method of Honerkamp [54]. In this method the parametrization of the fields is manifestly noncovariant. A

reparametrization invariance of the field transformation is necessary to guarantee that the S-matrix is covariant. Such procedure is very cumbersome. Moreover there appears no simple way to define a unique effective action [56].

I have formulated a new background field method to evaluate the effective action and its derivative expansion for field theories with an arbitrary number of nonlinear constraints. In this method the constraints are not actually used to eliminate any component of the background field. Therefore the question of reparameterization invariance never arises. I have applied this method for the special case of the nonlinear σ model and obtained the effective action expansion in agreement with the my previous result[9]. The detail of this work will be reported in a paper under preparation. The application of this method to gauge field theories is nontrivial since the constraints in gauge theories are not explicit. This aspect will be further investigated.

A.3.6 Berry's phases and the Wess and Zumino terms

A very important progress in particle physics and quantum field theory in the recent years is the understanding of why some symmetries in classical physics may disappear when symmetry violating quantum processes are taken into account. The anomalous symmetry breaking term in the effective Lagrangian is known as the Wess-Zumino term[68]. The existence of the the Wess-Zumino term or the anomaly depends on the highly nontrivial topology of the mapping between the internal symmetry space and the configuration space. Not only the derivation of this term is mathematically involved, even the form cannot be written in a conventional expression[49]. It is of no surprise that such a term would have been missed in the naive calculation of the derivative expansion of the effective action which emphasizes the local aspect of the geometry rather than the global aspect of mapping. It is highly desirable to understand how one can integrate the global topological aspect into the derivative expansion to provide a simple derivation and understanding of the Wess-Zumino term.

Berry's elegant work[69] on the modification of the quantum adiabatic theorem

provides a general framework to understand the non-integrable phase in dynamical system in which the Wess-Zumino term is a special case in quantum field theories[70]. Berry discovered that when a system traverse a closed path in an external parameters space, the wave function acquires an additional nonintegrable geometrical phase factor not included in the more familiar dynamical phase factor. This phase factor is amazingly universal [71]. Since quantum mechanics can be considered as a zero dimension field theory, adiabatic expansion is the derivative expansion , as the Berry's phase corresponds to the Wess-Zumino term, a quantum mechanics model in which Berry's phase is realized would provide a simple laboratory to explore our ideas of derivative expansion. Conversely our techniques in derivative expansion and topological consideration can be applied to give a simple understanding and derivation of the Berry's phase.

I have found that the derivative expansion method which I developed in Ref. [6] is the only method suitable for this purpose, although not anticipated at that time. In order to by-pass some technical problems, this systematical method contains a little twist, namely to functionally differentiate the fermion determinant before the derivative expansion and to functionally integrate back. However it can now be seen that the final functional integration can be used as an important way to tie the derivative expansion to to topological structure of the mapping between the internal space and the configuration space. This can be illustrated by a very simple model of a spin-$\frac{1}{2}$ particle (fast degrees of freedom) coupled to a time-dependent external magnetic field (slow degrees of freedom). The effective action can be defined by integrating out the fast degrees of freedom (the spin-$\frac{1}{2}$ field). The effective action term corresponding to the Berry's phase can then be obtained by the derivative expansion method thus described. The similarity between the Berry's phase and the Wess-Zumino term becomes obvious. Therefore the techniques can equally be applied to the calculation of the Wess-Zumino terms. A paper to report this work is in preparation.

References

[1] L.-H. Chan, *Phys. Rev.* **D15** , 2478 (1977).

[2] L.-H. Chan, *Phys. Rev. Lett.* **51** , 253 (1983).

[3] L.-H. Chan, *Phys. Rev.* **D31** , 204 (1985).

[4] L.-H. Chan, *Phys. Lett.* **71B** , 422 (1977).

[5] L.-H. Chan, *Phys. Rev. Lett.* **55** , 21 (1985).

[6] L.-H. Chan, *Phys. Rev. Lett.* **54** , 1222 (1985); **56** , 404 (1985).

[7] L.-H. Chan, *Phys. Rev. Lett.* **57** , 1199 (1986).

[8] L.-H. Chan, *Chiral Soliton* Chapter 2, edited by K. F. Liu world Scientific, Singapore, 1987.

[9] L.-H. Chan, *Phys. Rev.* **D36**, 3755 (1986).

[10] L.-H. Chan, to be published in *Phys. Rev.* (1988).

[11] Stephen Wolfram,*Mathematica - A System of Doing Mathematics by Computer*, Addison Wesley (1988)

[12] M. S. Alam et al., *Phys. Lett.* **B226**, 401 (1989).

[13] Lichtenberg *Phys. Rev.* **D16** , 231 (1977).

[14] ARGUS Collaboration *Phys. Lett.* **B211** , 489 (1988).

[15] T. Bowcock et al., *Phys. Rev. Lett.* **62**, 1240 (1989).

[16] C. Itoh, T. Minamikawa, K. Miura, and T. Watanabe, *Prog. Theor. Phys.* **54** , 908 (1975).

[17] S. Ono, *Phys. Rev.* **D15** , 3492 (1977).

[18] K. Lane and S. Weinberg, *Phys. Rev. Lett.* **37** , 717 (1976).

[19] N. Deshpande, D. Dicus, K. Johnson, and V. Teplitz, *Phys. Rev.* **D15**, 1885 (1977).

[20] C. S. Kalman and G. Jakimov, *Lett. Nuovo Cimento* **19**, 403 (1977).

[21] J. M. Richard and P. Taxil, *Z. Phys.* **C26**, 421 (1984).

[22] W-Y. P. Hwang and D. B. Lichtenberg, *Phys. Rev.* **D35** , 3526 (1987).

[23] Simon Capstick, *Phys. Rev.* **D36** , 2800 (1987).

[24] D. B. MacFarlane, in *Proceedings of the twenty-Third international Conference on High Energy Phyics, Berkeley, California,1986,* Edited by S. Loken (World Scientific, Singapore, 1987)' P.664.

[25] M. Diesburg *et al.,Phys. Rev. Lett.* **59** , 2711 (1987).

[26] E. V. Shuryak and Rosner,*Phys. Lett.* **B218**, 72 (1989).

[27] C. M. Fraser, *Z. Phys.* **C28** , 101 (1985).

[28] I. J. R. Aitchison and C. M. Fraser, *Phys. Lett.* **146B** , 63 (1984); *Phys. Rev. D* **31**, 2605 (1985).

[29] O. Cheyette, *Phys. Rev. Lett.* **55** , 2394 (1985).

[30] M. K. Gaillard, *Nucl. Phys.* **B268** , 669 (1986); (1986).

[31] O. Cheyette, M. K. Gaillard, *Phys. Lett.* **B197** , 205 (1987).

[32] M. K. Gaillard, *Carese Summer School 1987:189.*

[33] P. Binetruy, S. Dawson, M. K. Gaillard and I. Hinchliffe, *Phys. Rev.* **D37**, 2633 (1988).

[34] P. Binetruy and M. K. Gaillard, *Nucl. Phys.* **B312**, 341 (1989).

[35] P. Binetruy and M. K. Gaillard, *Phys. Lett.* **B220**, 68 (1989).

[36] M. K. Gaillard and V. Jain, *Phys. Rev.* **D39**, 3755 (1989).

[37] V. Jain, *Phy. Rev.* **D40**, 1213 (1989).

[38] R. Ball and H. Osborn, *Nucl. Phys.* **B263** , 245 (1986).

[39] M. Li. R. Perry and L. Wilets, *Phys. Rev.* **D36**, 596 (1987) .

[40] R. Perry and M. Li, *Mod. Phys. Lett.* **A2**, 353(1987).

[41] R. J. Perry, *Phys. Lett.* **B182**,269 (1986); University of Washington Preprint 40048-38-N6 (1986).

[42] F. Cooper, G. S. Guralnik and S. H. Kadan, *Phys. Rev.* **D14**, 1607 (1976).

[43] C. M. Bender, F. Cooper and G. S. Guralnik, *Ann. Phys.* (N. Y.) **109**, 165 (1977).

[44] Y. Fujimoto, L. O'Raifeartaigh and G. Parrvicini, *Nucl. Phys.* **B212**, 268 (1983).

[45] J. M. Cornwall, R. Jackiw, and E. Tomboulis, *Phys. Rev.* **D10**, 2428 (1974).

[46] T. Barnes and G. I. Ghandour, *Phys. Rev.* **D22**, 924 (1980) .

[47] A. Okopińska, *Phys. Rev.* **D35** 1835, (1987).

[48] T. H. R. Skyrme, *Proc. Roy. Soc.* **A260**, 127 (1961) and **A262**, 237 (1961); G. Adkins, C. R. Nappi and E. Witten, *Nucl. Phys.* **228**, 552 (1983); J. Goldstone and F. Wilczek. *Phys. Rev. Lett.* **47**, 986 (1981); A. P. Balachandran, V. P. Nair and S. G. Rajeev, *Phys. Rev. Lett.* **49**, 1124 (1982).

[49] E. Witten, *Nucl. Phys.* **B223**, 422 (1983); **ibid** 433 (1983);

[50] T. Appelquist and C. Bernard, *Phys. Rev.* **D22**, 200 (1980) and *Phys. Rev.* **D23**,425 (1981);

[51] J.M. Cornwall, *Nucl. Phys.* **B157**,392 (1979).

[52] R. Akhoury and Y. P. Yao, *Phys. Rev.* **D25**, 3361 (1982)

[53] I. J. R. Aitchison and C. M. Fraser, *Phys. Rev.* **D32**, 2190 (1985)

[54] J. Honerkamp, *Nucl. Phys.* **B36**, 130 (1972); L. Tataru, *Phys. Rev.* **D12**,335 (1975); D. I. Kazookov, V. N. Pervushin and S. V. Pushkin, *Teor. Mat. Fiz.*, **31**, 169 (1977) [*Theor. Math. Phys.* (USSR) **31**, 389 (1977)].

[55] "*Effective Action Expansion for the Nonlinear σ Model — the Normal Coordinate Method*", L.-H. Chan W. F. Kao and T. Matsuki, LSU preprint, Oct. 1988.

[56] C. P. Burgess and G. Kunstatter,Princeton Institute of Advanced Study preprint IASSNS-HEP 87/34 (1987); G.A. Vilkovisky, in *Quantum Theory Gravity*, edited by S. Christensen, (Adam Hilger, Bristol, 1984); G. A. Vikovisky, Nucl. Phys. **B234** (1984) 125; B. S. DeWitt, to appear in *E. S. Fradkin's 60^{th} Birthday Volume*, (Adam Hilger Lt., Bristol, 1986).

[57] E. D'Hoker and E. Farhi, *Nucl. Phys.* **B248** , 59 (1984); **B248**, 77 (1984).

[58] M. Veltman, *Nucl. Phys.* **B123**, 89 (1977).

[59] A. Jackson, A. D. Jackson and V. Pasquier, *Nucl. Phys.* **A432**, 567 (1985).

[60] U. B. Kaulfuss and U.-G. Meissner, *Phys. Rev.* **C30**, 2058 (1985); *Phys. Rev.* **D31**, 3024 (1985).

[61] V. Vento, *Phys. Lett.* **153B**, 198 (1985).

[62] R. Vinh Mau, M. Lacombe, B. Loiseau, W. N. Cottingham and P. Lisboa, *Phys. Lett.* **B150**, 259 (1985).

[63] H. M. Sommermann, H. W. Wyld and C. J. Pethick, *Phys. Rev. Lett.* **55**, 476 (1985).

[64] U.-G. Meissner and I. Zahed, *Phys. Rev. Lett.* **56**, 1035 (1986).

[65] M. Lacombe, B. Loiseau, R. Vinh Mau and W. N. Cottingham , *Phys. Rev. Lett.* **57**, 170 (1986).

[66] V. Y. Novozhilov, *Phys. Lett.* **B228**, 240 (1989).

[67] M. Bando, T. Kugo, S. Uehara, K. Yamawaki and T. Yanagida, *Phys. Rev. Lett.* **54**, 1215 (1985).

[68] J. Wess and B. Zumino, *Phys. Lett.* **37B**, 95 (1971).

[69] M. V. Berry, *Proc. R. Soc.*, **A392**, 45 (1984).

[70] P. Nelson and L. Alvarez-Gaumé, *Comm. Math. Phys.* **99**, 103 (1985); H.somoda, *phys. Lett.* **156B**, 220 (1985), *Nucl. Phys.* **B266**, 410 (1986); A. Niemi and G. Semenoff, *Phys Rev. Lett.* **55**, 927 (1985);**56**,1019 (1986), *Phys. Lett.* **B175**, 439 (1986); A. Niemi, G. Semenoff and Y.-S. Wu, *Nucl. Phys.* **B276**, 173 (1986).

[71] C. A. Mead and D. G. Truhlar, *J. Chem. Phys.* **70**, 2284 (1984); F. Wilczek and A. Zee, *Phys. Rev. Lett* **52**, 211 (1984); J. Moody, A. Shapere, and F. Wilczek, *Phys. Rev. Lett* **56**, 893 (1986); H. Kuratsuji and S. Iida, *Phys. Rev. Lett* **56**, 1003 (1986); D. Arovas, J. R. Schrieffer, and F. Wilczek, *Phys. Rev. Lett* **53**, 722 (1984)

B. 2 Problems in Lattice QCD (R. Haymaker)

My major efforts at present are going into building up a lattice gauge theory group at LSU. Jacek Wosiek from the Jagellonian University in Cracow and I have collaborated in this area for three years. I have two students, Vandana Singh and Yingcai Peng. This past Spring Professor Andrzej Kotanski also from the Jagellonian University visited LSU for three months. Chris Heller at Trieste is currently porting the program I wrote to their Convex computer. I have obtained funding through the Louisiana Board of Regents for another visitor from Cracow for three months. LSU has continued to upgrade its computer facilities. We have three FPS AP264 array processors. Last fall, the IBM mainframe was upgraded to a 3090 with vector processors. In addition we are making use of an image processor in the Astronomy group. Our present efforts are on various aspects of color flux in the presence of static charges. Much of the effort is in Monte Carlo simulations. We also are studying semi-analytic variational methods. We now have a running $SU(3)$ monte carlo code, although all the results reported here will be on $SU(2)$. Finally we have continued investigating the complex Langevin method for doing averages over complex distribution functions.

2.1 Monte Carlo Flux Simulation

I would like describe the flux problem for $q\bar{q}$ in $SU(2)$ for quark separations of up to 9 lattice units. I presented this work at XXIX Crakow School of Theoretical Physics, June 1989, Zakopane, Poland [1]. This will also be presented at the 1989 Lattice Symposium in Capri.

Papers in preparation are the following

1. Expanded version of my Zakopane paper to be published in Acta Physica Polonica (with Jacek Wosiek)

2. Non-perturbative scaling analysis and transfer matrix study of large T dependence (with Jacek Wosiek)
3. Results as of September will be published in the proceedings of the Capri Lattice 89 Symposium. (with Jacek Wosiek, Vandana Singh, and Yingcai Peng)
4. Systematic study of flux, studying the shape and R and T dependence of the flux tube. (with Jacek, Wosiek, Vandana Singh and Yingcai Peng)

Although the basic picture of a flux tube between a heavy quark - antiquark pair is well established, the detailed distribution of the flux is just now being elucidated. Early work on this problem was done by M. Fukugita and I. Niuya [2] and J. Flower and S. Otto [3]. Our Wilson loop values have statistical errors comparable to the earlier calculation of Gutbrot [4]. Jorysz and Michael [5] have studied the static adjoint source in $SU(2)$. Michael [6] has also derived sum rules relating a sum over energy density to the total energy of the system and a similar relation for the gluon condensate. J. Wosiek and I [7] reported on measurements of the parallel component of the chromoelectric flux for $SU(2)$ for static quarks represented by Wilson loops. R. Sommer [8] investigated thoroughly all flux components for $SU(2)$ using Polyakov lines as sources for quark separations up to four lattice units.

One of the interesting results in these studies is that there are large cancellations between electric and magnetic components of the energy distribution giving a much smaller flux tube than one would estimate based on a single component. Sommer [8] saw this effect in his data in the mid-point slice at quark separations of four lattice spacings. We elucidate this cancellation over a large fiducial volume, and large separations.

There are many complications beyond the lattice granularity in trying to develop a picture of color fields comparable to the highly intuitive classical

electric and magnetic field lines. The self interactions of these fields play a central role in determining the distribution which destroys the linearity in the picture. In addition the non-abelian and quantum aspects of the problem further limit the appliction of simple intuition to speculate about the field lines. In our investigations, we employ Wilson loops to represent source world lines. It is then necessary to extrapolate to loops with large time extent to supress the effects of creation and annihilation of charges. Interest lies the shape of the flux tube for large space separations. However large space and/or large time separations are very hard to achieve because of the exponential suppression of the signal with the area of the Wilson loop. The concept of field lines in this problem is not applicable since one can measure only the square of the components. Of course one is primarily interested in the continuum limit and hence in the scaling and renormalization of the lattice results. The Michael sum rules [6] show that the energy density scales, whereas the gluon condensate does not. Hence the behaviors of the electric and magnetic components separately are lattice properties only. Finally we find that the magnetic component of the energy is negative.

2.1.1 Results and Work in Progress

The correlation that is needed to measure flux is the following

$$\begin{aligned} \frac{1}{2}\epsilon^{\mu\nu}(x) &= \frac{\beta}{a^4}\left(\frac{\langle W P_x^{\mu\nu}\rangle}{\langle W\rangle} - \langle P\rangle\right) \approx \frac{\beta}{a^4}\left(\frac{\langle W P_x^{\mu\nu} - W P_\infty^{\mu\nu}\rangle}{\langle W\rangle}\right) \\ &: \quad \frac{1}{2}(-B_1^2, -B_2^2, -B_3^2; E_1^2, E_2^2, E_3^2) \end{aligned} \tag{1}$$

where W is the Wilson loop, $P_x^{\mu\nu}$ the plaquette and a the lattice spacing. We incorporate a minus sign into the definition of the chromomagnetic components since that gives the conventional sign in Minkowski space. The energy density is

$$\frac{1}{2}\epsilon = \frac{1}{2}(E^2 + B^2) \tag{2}$$

β	a lat. spacing	N_{therm}	Sweeps between meas.	no. of meas.
2.5	0.13 f	2200 ovrrl., 2200 metr.	5 ovrrl. 5 metr.	200
2.4	0.16 f	1700 ovrrl., 1700 metr.	5 ovrrl. 5 metr.	230
2.3	0.21 f	2862 ovrrl., 2862 metr.	5 ovrrl. 5 metr.	240

Table 1: Parameters used in simulation

The computations were done on the FPS AP264 array processor at LSU. Our lattice size was a $17^3 \times 20$ hypercube with helical boundary conditions based on a configuration program made available by Mike Creutz Updating was done checkerboard fashion which requires space dimensions odd and the time dimensions even. We also use Creutz's overrelaxation algorithm [9] alternated with a one or two hit Metropolis. For $SU(2)$ overrelaxation is microcanonical and hence Metropolis is needed to sample different energies. We measured all rectangular loop sizes from 1×1 to 6×9. Because of the large amount of data generated and because of the difficulty of getting good statistics, the data was folded on rectangular symmetry planes. We also limited the measured flux to a fiducial volume consisting of a closed volume four lattice spacings in every direction surrounding the Wilson loop. We measured all six components of the flux.

Table 1 gives the parameters for our measurements. We used perturbative scaling to arrive at the lattice spacing a in physical units[7]. Non-perturbative scaling analysis [8] give somewhat smaller values. We have yet to complete the corresponding analysis on our data.

The straightforward measurement of these quantities would lead to prohibitive computer time or intolerable errors. Enhancements of the measurements are essential to beat down the errors. One enhancement is almost trivial but contributed significantly in reducing errors. That is indicated in Eqn.(1) in which the flux is measured relative to a point at infinity. This does not change the average but some of the fluctuations of the Wilson loops themselves cancels

when the difference is taken between two positions. By taking a point where the correlation vanishes the two forms in Eqn.(1) are equal. In practice we take a corner of the hypercubic fiducial volume as the point at infinity.

The second important enhancement was to do as many integrals analytically as is practical[10]. For example the one link integral can be done using

$$\int [dU] U e^{\frac{\beta}{2} tr[UK^\dagger]} = \frac{I_2(\beta b)}{I_1(\beta b)} V \int [dU] e^{\frac{\beta}{2} tr[UK^\dagger]}. \tag{3}$$

where K is the sum of six 'staples' coupling to U in the action. The sum of $SU(2)$ matrices in the $j = \frac{1}{2}$ representation is a multiple of an $SU(2)$ matrix which we denote by V

$$K = bV; \;\; b \equiv (detK)^{\frac{1}{2}}, \tag{4}$$

The effect of Eqn.(3) when applied to a simulation is to replace a link U occurring in the Wilson loop by a corresponding sum of 'staples' K. This is indicated in Fig. 1. Since K involves 18 links, one can expect the fluctuations of the ensemble of K's to be suppressed compared to a single link U in each measurement.

This result is useful as long as subsequent analytic integration does not involve one of the links in K. For example this will work for those links that make up the sides of a Wilson loop of size 2×2 or larger as long as one link on each corner is left in its original form. This result must be generalized to handle the four links in a plaquette and the the two links that form corners. This has been done by B. Bunk [12] in an unpublished report which he kindly made available to us.

To do the plaquette integral consider the following four-link integral

$$Z(\gamma, \beta) \equiv \int [dU_1 dU_2 dU_3 dU_4] \, e^{-S}, \tag{5}$$

where

$$-S \equiv (\frac{\gamma}{2} tr[U_4^\dagger U_3^\dagger U_2 U_1] + \frac{\beta}{2} \sum_{k=1}^{4} tr[U_k K_k^\dagger]). \tag{6}$$

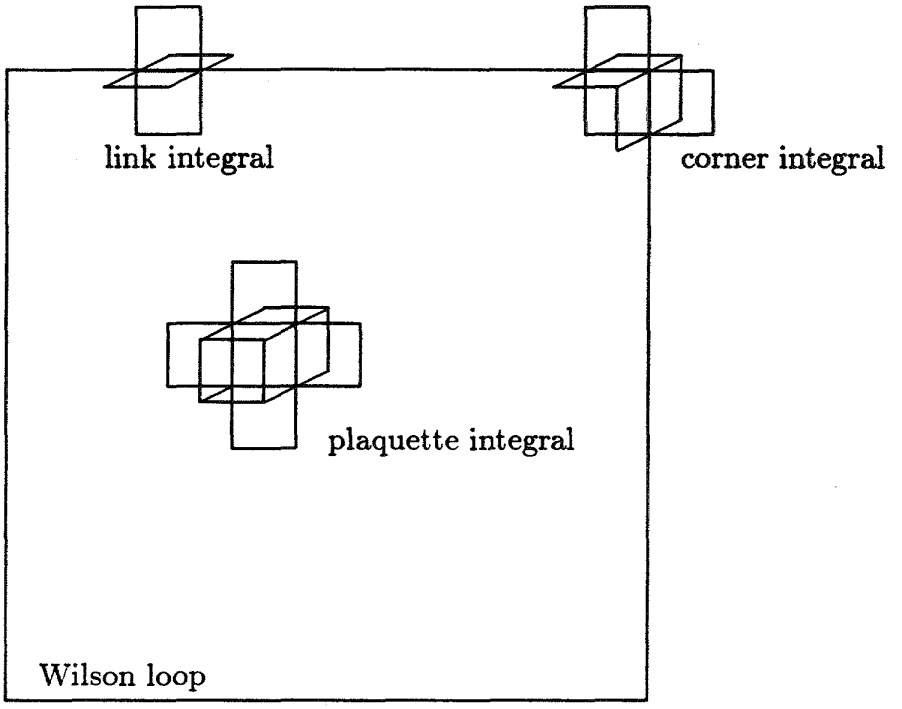

Figure 1: Links involved in link, corner and plaquette integrals

We can reduce this four link integral to a single sum using $SU(2)$ character expansions. The result is

$$\int [\prod_l dU_l] \frac{1}{2} tr(U_4^\dagger U_3^\dagger U_2 U_1)\, e^{-S} = \frac{\frac{\partial Z(\gamma,\beta)}{\partial \gamma}|_{\gamma=\beta}}{Z(\beta,\beta)} \int [\prod_l dU_l]\, e^{-S} \qquad (7)$$

where

$$Z(\gamma,\beta) = \sum_j c_j(\gamma) \frac{1}{(2j+1)^4} \prod_{k=1}^{4} c_j(\beta b_j) \chi^{(j)}(V_4^\dagger V_3^\dagger V_2 V_1) \qquad (8)$$

The $c's$ are coefficients of the expansions of the exponential in characters of $SU(2)$, $\chi^{(j)}(V)$. Full details will be given a subsequent paper. By doing the link integrals in a plaquette, the result is expressed in terms of the links pictured in Fig. 1. Again the value of the plaquette is spread over many more links and the subsequent simulation will see a smaller sweep to sweep spread in the values of this 'fat' operator. Similarly the corner integral can be done, but the result which is more complicated will be presented in a subsequent paper.

In the vectorized code, we save the long vectors of Wilson loops (or fat Wilson loops) corresponding to all locations of the loop and similarly for all locations and orientations of the plaquette. We then calculate the cross correlation between these two long vectors. To do a naive correlation measurement an estimate of computer time, T,gives

$$T \propto V_{lattice} \times V_{fiducial} \tag{9}$$

whereas if one employes fast fourier transforms we obtain

$$T \propto V_{lattice} \times ln_2(V_{lattice}) \tag{10}$$

Given the size of our fiducial volume, the fast fourier transform was essential to beat down computer time.

The fast fourier transforms give all the correlations, not just those in the fiducial volume. However when the fat operators indicated in Fig. 1 get too close together, the analytic integrals break down. Therefore one must recalculate those correlations, dropping the analytic integrations for one or the other or both operators. As a consequence self energies i.e. when plaquette is touching the Wilson loop, are harder to measure than more distant correlations. When a link of a plaquette overlaps a link of the Wilson loop analytic integrals must be dropped on both operators. Correlations measured with completely unenhanced operators have unacceptable errors. Measurements of self energies with an improved treatment will be reported later.

2.1.2 Results

We first look at the heavy quark potential

$$\langle W(R,T)\rangle = \exp\left(-VT + C(T)\right) \tag{11}$$

One can argue that $C(T)$ becomes independent of T for large T. Hence we can obtain $V(R)$ by plotting $\frac{-1}{T} ln\langle W(R,T)\rangle$ vs. $\frac{1}{T}$, and looking for the intercept of

a linear fit. One can also make a time dependent estimate of $V(R)$ using

$$V(R) \approx ln\left(\frac{\langle W(R,T)\rangle}{\langle W(R,T+1)\rangle}\right) \tag{12}$$

These two methods agree very well and give the potential consistent with the now standard results. This is shown by the 'dots' in Fig. 2.

Let us start the discussion of flux by looking at the value of the correlation at the center of the Wilson loop as a function of spatial extent, R and time extent T. These are shown in Fig. 3. The central value gives the flux at the midpoint between the quarks and for the middle time slice. Fig. 3 show how well the flux data extrapolates to large T. This is the first indication that one does not need to go to very large T to get reliable data, at least for these components. We are presently exploiting the transfer matrix formalism, fitting all components to exponential forms in T to extrapolate to large times, which will be reported later.

One of our primary goals in this work is to explore the shape of the flux tube. In particular we look at the transverse shape of the tube at the middle time slice, and at the z slice mid-way between the quarks. Fig. 4 show the typical behavior of individual components plotted against the transverse distance. Except for a small rounding at the point on the axis, they are all consistent with exponential behavior, presumably determined by the lowest glueball mass.

Fig. 5 shows the value of the flux at the mid-point of the flux tube as a function of quark separations up to $R = 9$ in physical units. These were all done for $T = 5$. For all but the 3 largest $R's$, we have data for larger T. Increasing T up to 9 changes only the $E_{\|}$ component and the change resulting from increasing T to 9 is indicated with the arrows.

From Fig. 5 we can get a very crude estimate of the energy density at the center point of the flux tube [11]. Extrapolating the last three R values to large T, and recalling that the magnetic components subtract from the electric

components we estimate the energy density at the center to be approximately

$$Energy\ density\ at\ center\ of\ flux\ tube \sim 1.0 \pm 0.5 \frac{gev}{f^3} \tag{13}$$

For the purposes of comparison we would like to point out that this is far from the MIT bag [13] constant value

$$B_{MIT}(bag\ constant) = 0.14 gev^4 = 0.05 \frac{gev}{f^3} \tag{14}$$

Therefore it is unlikely that a volume energy alone can account for the cavity states and at the same time give enough pressure to confine the flux to such a small flux tube. Since our errors are large, we are not able to confront the discrepency properly, however it seems unlikely that our estimates are off by a factor of 20. We are presently doing fits to this data which will allow a more careful estimate of this number. Also the sum rules of the next section will provide an independent estimate.

Fig. 6 shows the high quality of the $B_{\|}$ data. Shown is the profile of the $B_{\|}$ component along the axis connecting the charges for T from 2 to 9. Clearly it is not necessary to take T larger than 4 or 5 here.

There is a very interesting check on our flux data provided by sum rules derived by C. Michael [6]. The energy it takes to pull quarks apart as measured by the potential must be accounted for by an energy density integrated over all space. The lattice version is the Michael energy sum rule.

$$\frac{1}{2} \sum_{\vec{x}} a^3 [E^2(\vec{x}) + B^2(\vec{x})] = V(R) + \frac{f(\beta)}{a} \tag{15}$$

Recall that the measured magnetic component of the energy is negative. Therefore there is a cancellation in Eqn.(15) in calculating energy. To test this relation, we need to sum over all space. Unfortunately we have very poor data for plaquettes that touch the Wilson loop. We will assume that these contributions are approximately independent of the the separation R and discard them. Hence we can check the R dependence of Eqn.(15) up to a constant. The results are shown in Fig. 7. Errors preclude a definitive check but the behavior is correct.

A rather important test of the volume sum of flux is to see if our fiducial volume is large enough. Fig. 8 gives the sum rule as a function of fiducial volume. The value 4 is the maximum volume we measured, being a closed region of 4 lattice units in all directions surrounding the Wilson loop. Fig. 8) Shows the effect of dropping back to 3,2,and 1 lattice units. Hence 4 units is clearly adequate.

There is a second sum rule for the gluon condensate:

$$\frac{1}{2}\sum_{\vec{x}} a^3[E^2(\vec{x}) - B^2(\vec{x})] = -\beta\frac{\partial \ln a}{\partial\beta}V(R) - \frac{\beta}{a}\frac{\partial f}{\partial\beta} \tag{16}$$

We attempted to measure this quantity. However, because there is no cancellation between electric and magnetic components this extends over a much larger volume and we do not have a large enough fiducial volume to test the sum rule.

The general picture of the flux tube leads to another sum rule that is much simpler to measure. Rather than looking at the potential itself, lets look at the work reqired to pull a $q\bar{q}$ apart by one lattice spacing. The potential rises by this quantity of work. If the effect is merely to stretch the flux tube, leaving the end configurations unchanged, then we should be able to account for this work by a volume integral of the flux over a transverse slice of the string one lattice spacing thick at for example the mid-point of the tube. Fig. 2 gives the result. The upper numbers at each step are the differences between the potential as R increases by 1 unit. The lower number is the result from the transverse sum rule. For small R the flux tube is just forming, and the agreement is poor. For a well formed flux tube, $R = 4, 5$, the agreement is good.

Again we need to do a test of the fiducial volume. This is shown in Fig. 9. The important result is that the sum rule is being saturated within the fiducial volume of one lattice unit surrounding the $q\bar{q}$ axis. For large separations, $R = 5, 6$ the sum rule is saturated between 1 and 2 lattice units. In none of these cases do we need 3 or 4 units. The cancellation is rather dramatic. The gluon condensate sum rule is quite a different matter. For this case there is

no cancellation and the fiducial volume dependence is totally different. And for $R \geq 4$ the measured fiducial volume is clearly inadequate. As indicated in Fig. 9 the shaded area in each case indicates schematically the region required to saturate the sum rule.

Our results on the smallness of the flux tube are consistent with Sommer's result [8]. If we take Sommer's value for $-\beta\frac{\partial \ln a}{\partial \beta} \approx 10$ we are consistent with the gluon condensate sum rule being about a factor of 10 larger than the energy.

Let us use this transverse energy sum rule to estimate independently the energy density at the mid-point of the flux tube. First in lattice units, the total energy in a transverse slice, taken from Fig. 2 is $\approx 0.07a^{-1}$ As a conservative estimate, take the radius of the flux tube to be 2 lattice units. Then the energy is spread over a volume of $\pi(2a)^2 a$. Therefore in physical units

$$Energydensity \approx 0.0056a^{-4} \approx 1.7\frac{gev}{f^3}. \tag{17}$$

We used $a = .16f$. Non-perturbative analysis [8] [4] leads to a smaller number hence it would tend to raise the estimate. The error in this estimate could easily be a factor of 2. Improved estimates of this number will be given in a subsequent paper.

One of the consequences of this cancellation is that we know very little about the shape of the flux tube since it is contained in a size comparable to the lattice spacing. Although the individual components have a very clear exponential behavior as shown in Fig. 4 the underlying energy distribution need not be exponential. We are not yet in a position to see if the profile is gaussian [15], [14].

Figure 10 gives our major conclusions. The presence of heavy quark sources distorts the gluon condensate from its vacuum value in a large region around the quarks. However there is a conspiracy among the electric and magnetic contributions to the energy to cancel everywhere except in the neighborhood of th charges where the electric part dominates, and within a rather slim flux

tube connecting the quarks. The energy flux extends farther out in the region surrounding the charges. Our data shows this in that the fiducial volume dependence of the volume sum rule is saturated more slowly than the transverse slice sum rule.

A second point is that it is reasonable to do this calculation with Wilson loops. Since one is always fighting the area law this has the advantage over Polyakov lines which must of course be as long as the time extent of the lattice. The dominant component, $E_{\|}$ turns out to be the most difficult component to measure.

To complete this study in a systematic way we need to fit this data. This is in large part completed. We have concentrated on fitting the profile of the flux tube. We have used these fits to generate color pictures of the flux tube. Figure 11 gives a sample of the pictures we are able to generate. Figure 12 gives a 3-d plot of the same data.

2.1.3 Proposed Work

There is much work to do to complete the projects already described in this report. Beyond that there are many directions this work could go.

- Different representations of the source, e.g. adjoint representation.
- Baryons in SU(3), after developing fluctuation suppression for SU(3).
- Sources connected by a diagonal to see if the small flux tube is artefact of world lines lying on symmetry planes of the lattice
- Larger values of β to explore the flux tube in more detail.
- Smaller lattice volumes to compare the flux tube configuration with the semi-analytic studies of small volumes.

2.2 Convergence of Langevin Simulation for Complex Gaussian Integrals

Simulations in lattice gauge theories over non-positive or complex Boltzman factors remains problematic. A fully reliable method to perform such averages could be a significant advance in lattice theories. The majority of the work in lattice gauge theories builds up observables from vacuum configurations in the functional integral. Absorbing an operator into the distribution function raises the possiblity of generating configurations relevant to the operator being measured. The complex Langevin method [16] [17] proposed a possible solution to this problem. Although there are some successes, its correctness in general is not known. Ambjorn and Yang [18] analyzed some of the numerical problems raised by this method in simulating integrals. Ambjorn, Flensberg and Peterson [19] [20] and Flower, Otto and Callahan [21] applied this method to pure gauge simulations in various space-time dimensions. In these applications, definitive successes are limited to simulations of soluble problems. These authors showed that the method may fail even for soluble models and were able to trace the failure to a pathology of the method applied to a single integral. Haymaker and Wosiek [22] were able to overcome these difficulties in prototype integrals and had limited success in the soluble SU(2) 2-dimensional gauge theory.

We have made progress in a more elementary problem of a complex gaussian integral and are able to prove convergence of the complex Langevin method[23]. The theory of convergence of the real Langevin method relies on the proof that the corresponding Fokker-Planck equation for the distribution function e^{-S} has a time independent solution giving the desired distribution. Further the real part of the eigenvalues of the Fokker-Planck operator must be positive to insure that all other solutions are transient. One can introduce complex parameters smoothly and repeat the analysis. The analytic continuation of the Fokker-Planck equation will have solutions smoothly connected to the real problem.

But now its solution being a complex function bears no relationship to the real probability distribution generated by the corresponding complex Langevin equation. The latter generates a distribution $P(x, y)$ in the complex plane. It is this true probability distribution which governs the convergence properties of the Langevin method. Unlike the real Langevin method, this distribution is unknown until the problem has been solved.

Here we give only the results[23] . We have been able to solve the eigenvalue problem for the 2 variable Fokker-Planck equation. The eigenvalues are shown in Fig. 13. Since the real part of all these eigenvalues is positive, all states except the lowest state will decay away. This proves convergence of the Langevin method. A further result is that there is a close relationship between this pattern and the eigenvalues of the analytic continuation of the Fokker-Planck equation, Fig 14 i.e. the top diagonal row is the same. Further there is a simple relationship between the corresponding eigenvectors. Whether an interesting relationship exists in more complicated examples remains to be seen. This solution is applicable to any complex Langevin simulation which is dominated by an attractive fixed point. It is hoped that this work provides possibly a set of expansion functions to explore integrals that could arise in lattice simulations.

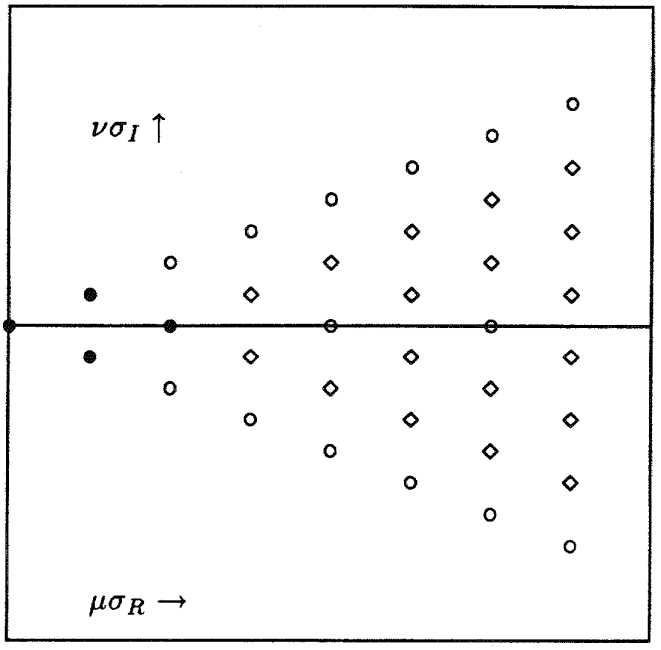

Figure 13: Eigenvalues of L

References

[1] R. Haymaker 'Color Flux Distribution on the Lattice', LSU preprint. Talk given at the XXIX Cracow School of Theoretical Physics, June 1989, Zakopane, Poland.

[2] M. Fukugita and I. Niuya, Phys. Lett.,**132B**, 374(1983).

[3] J. Flower and S. Otto, Phys. Lett., **160B**, 128 (1985).

[4] F. Gutbrod, Z. Phys., **C30**, 585 (1986).

[5] I.H.Jorzsz and C.Michael, Nucl. Phys **B302** 448, (1987)

[6] C.Michael,Nucl. Phys. **B280 [FS18]** 13, (1987).

[7] J. Wosiek and R. Haymaker Phys.Rev. Rapid Commun. **D36**, 3297, (1987).

[8] R.Sommer Nucl. Phys. **B306** 180, (1988),see also thesis, Wuppertal preprint, WUB 86-13, May 1986.

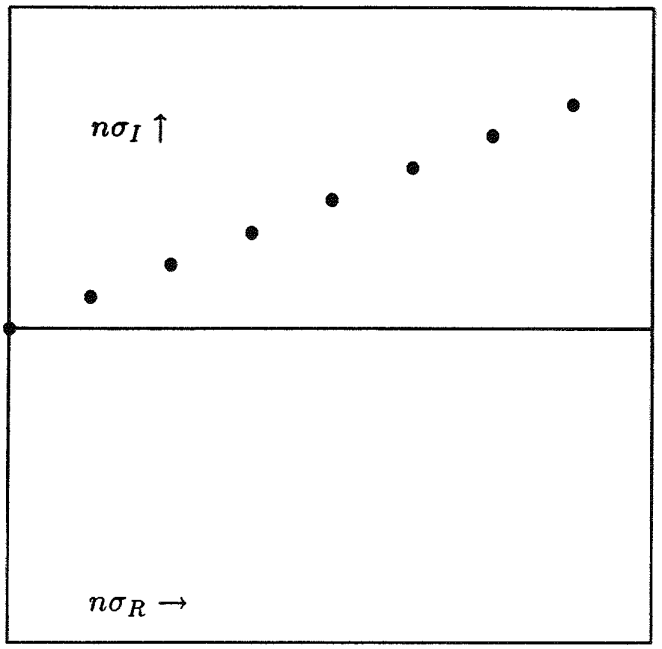

Figure 14: Eigenvalues of complex oscillator

[9] M. Creutz, Phys.Rev. **D36**, 515, (1987).

[10] G. Parisi, R. Petronzio and F. Rapuano, Phys. Lett., **128B**, 418 (1983).

[11] J. D. Bjorken, Phys. Rev., **D27**, 140 (1983). 399 (1984).

[12] B. Bunk, unpublished notes

[13] MIT bag reference.

[14] C. Peterson and L. Sköld, Nucl. Phys., **B255** , 365 (1985).

[15] M. Lüscher, G. Münster and P. Weisz, Nucl. Phys., **B180[FS2]**, 1 (1981).

[16] J. Klauder, Acta Physica Austriaca Suppl. **XXV**, 251 (1983)

[17] G. Parisi, Phys. Lett. **131B**, 393 (1983).

[18] J. Ambjorn and S. Yang, Nucl. Phys. **B275[FS17]**, 18 (1986).

[19] J. Ambjorn, M. Flensburg, and C. Peterson, Phys. Lett. **159B**,335 (1985).

[20] J. Ambjorn, M. Flensburg and C. Peterson, Nucl. Phys. **B275[FS17]**, 375 (1986).

[21] J. Flower, S. Otto and S. Callahan, Phys. Rev. **D34**, 598 (1986).

[22] R. W. Haymaker and J. Wosiek, Phys. Rev. **D37**, 969,(1988)

[23] R. W. Haymaker and Y. Peng, LSU preprint 'Convergence of Langevin Simulation for Complex Gaussian Integrals'

[24] F. Langouche, D. Roekaerts and E. Tirapegui, Prog. Theor. Phys. **61**, 1617 (1979).

[25] J.B.Kogut **Strings, Lattice Gauge Theory and High Energy Phenomenology** editors V. Singh, and S.R. Wadia, Proceedings of the Tata Institute Winter School, Panchgani, p.261, 1987,World Scientific.

[26] L. Pesquera and M.A. Rodriquez, **Stochastic Processes Applied to Physics**, World Scientific, 1985

3 Figure Captions

Fig.1 (figure in the text)

Fig.2. Heavy quark potential in lattice units. The upper numbers are the differences between the potential at neighboring points. The lower numbers are obtained from the transverse energy sum rule.

Fig.3 Flux at the center of the Wilson loop in lattice units as a function of T, for R= 2 - 5. Ordinate is log_10 of components indicated. $\beta = 2.4$

Fig.4 Transverse profile of the flux tube for particular components at the mid-point as a function of distance in fermis. Ordinate is log_10(component of energy density in units gev/f^3) R=4, T=4 E_z component.

Fig.5 Flux at the center of the Wilson loop in physical units for fixed T= 5, and For R = 1 to 9 lattice units. Measurements were taken for larger T but only for $R \leq 6$. Arrows indicate the values of the flux for for T=9. Only the $E_{\|}$ points were affected.

Fig.6 Component in lattice units.

Fig. 7 Test of Michael volume energy sum rule up to a constant. Self energies were discarded and the value normalized at R = 2.

Fig. 8 Test of fiducial volume dependence of the Michael volume energy sum rule for a fiducial volumes of 1 to 4 lattice units surrounding the Wilson loop.

Fig. 9 Fiducial volume dependence of energy and action (gluon condensate) sum rules measured on the transverse slice of the flux tube at the midpoint. The shaded areas contrast the small size of the energy flux compared to the gluon condensate.

Fig.10 Schematic behavior of the flux distribution surrounding $q\bar{q}$.

Fig.11 Photographs taken of the LSU astronomy image processor of the flux tube. The left pictures are the energy distribution, and the right pictures are the gluon condensate.

Fig.12 Three dimensional plot of $-\frac{1}{2}B_{\|}^2$.

Fig.13,14 (figures in the text)

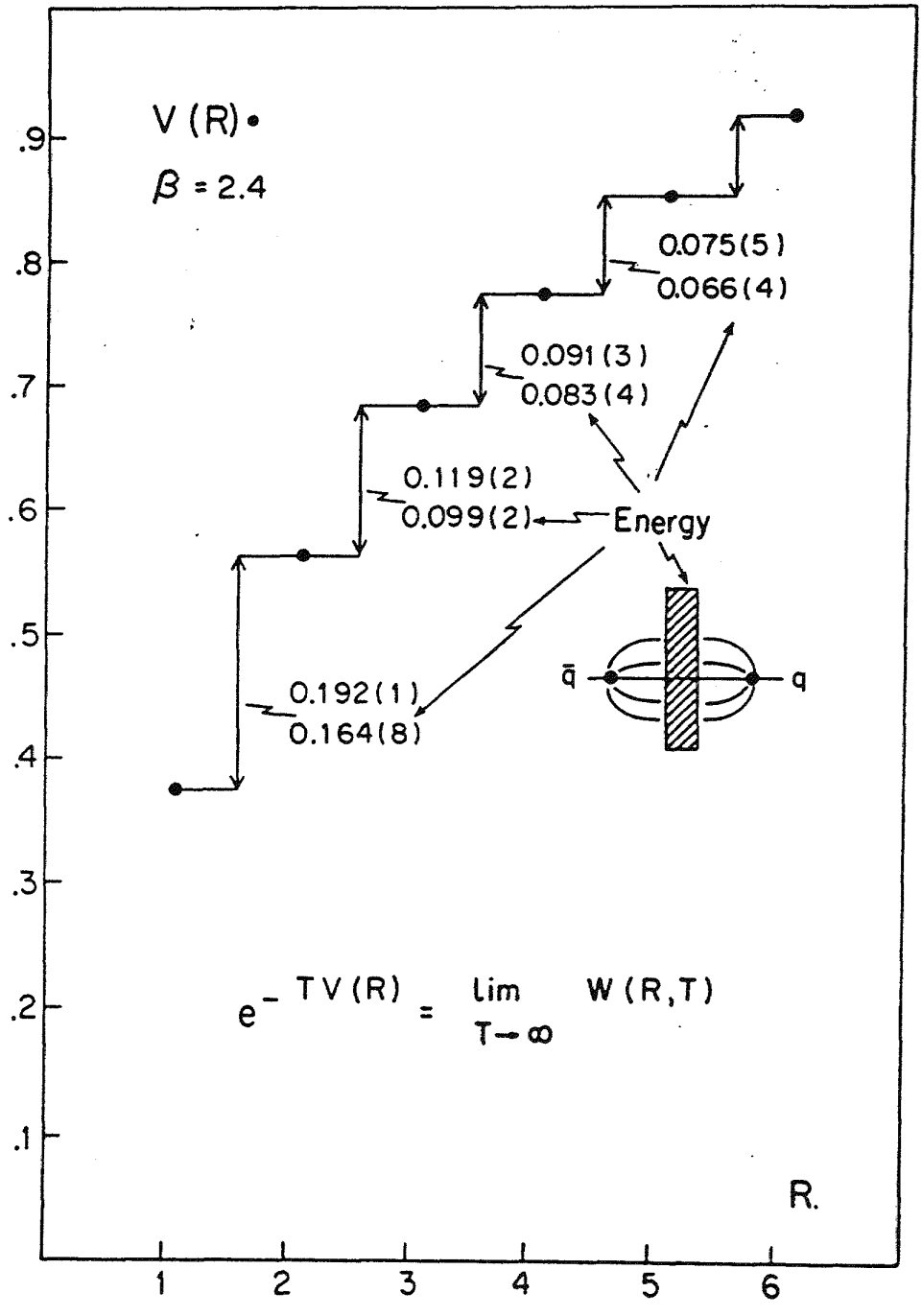
V (R)•
β = 2.4
0.075(5)
0.066(4)
0.091(3)
0.083(4)
0.119(2)
0.099(2)
Energy
0.192(1)
0.164(8)
q̄
q
e^- TV(R) = lim W(R,T)
T→∞
R.
.9
.8
.7
.6
.5
.4
.3
.2
.1
1
2
3
4
5
6

Fig.2

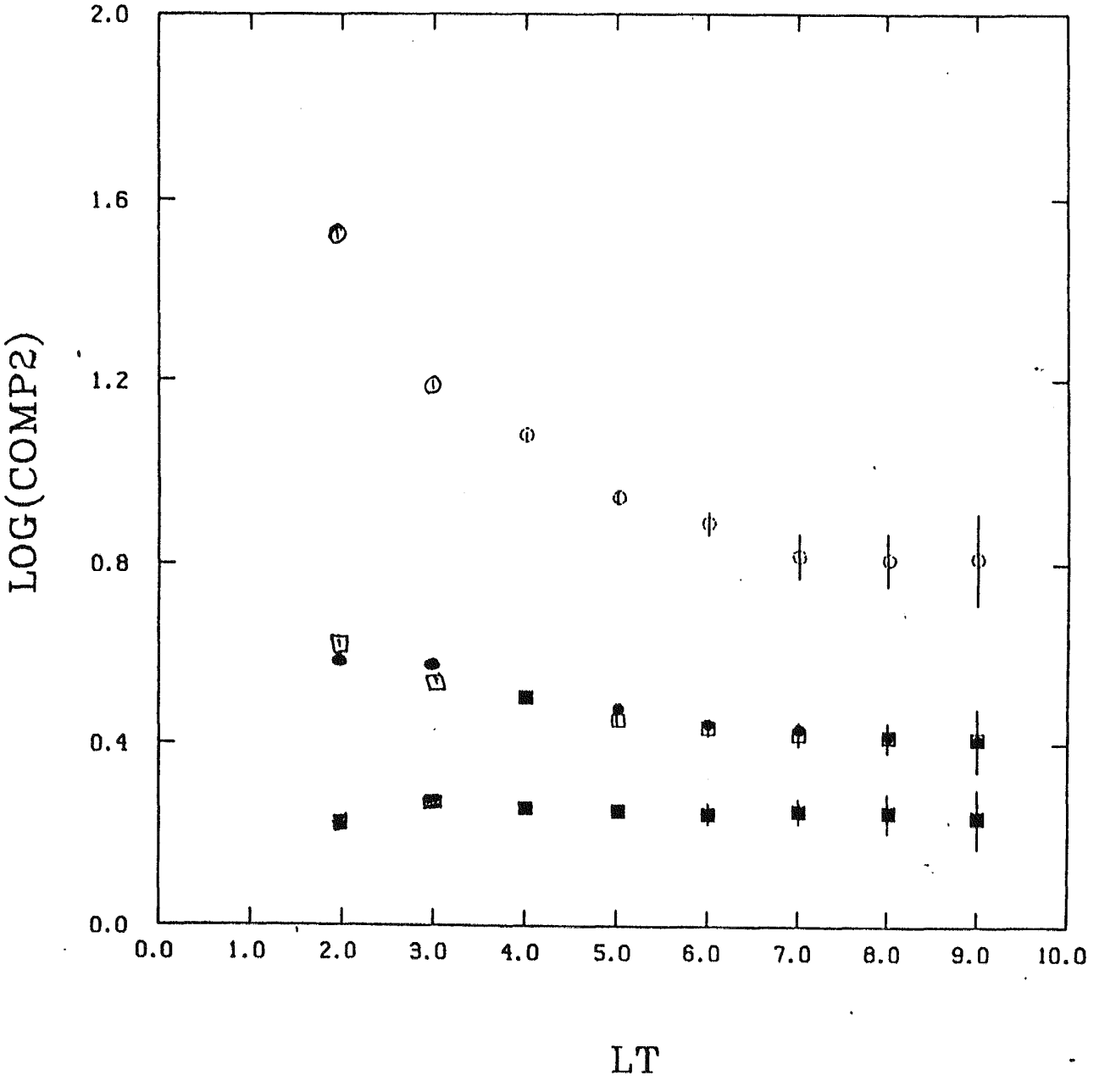
B=2.4 R= 4
LOG(COMP2)
LT
2.0
1.6
1.2
0.8
0.4
0.0
0.0
1.0
2.0
3.0
4.0
5.0
6.0
7.0
8.0
9.0
10.0
$\frac{1}{2}E_z^2$
$\frac{1}{2}E_x^2$
$-\frac{1}{2}B_y^2$
$-\frac{1}{2}B_z^2$

Fig.3

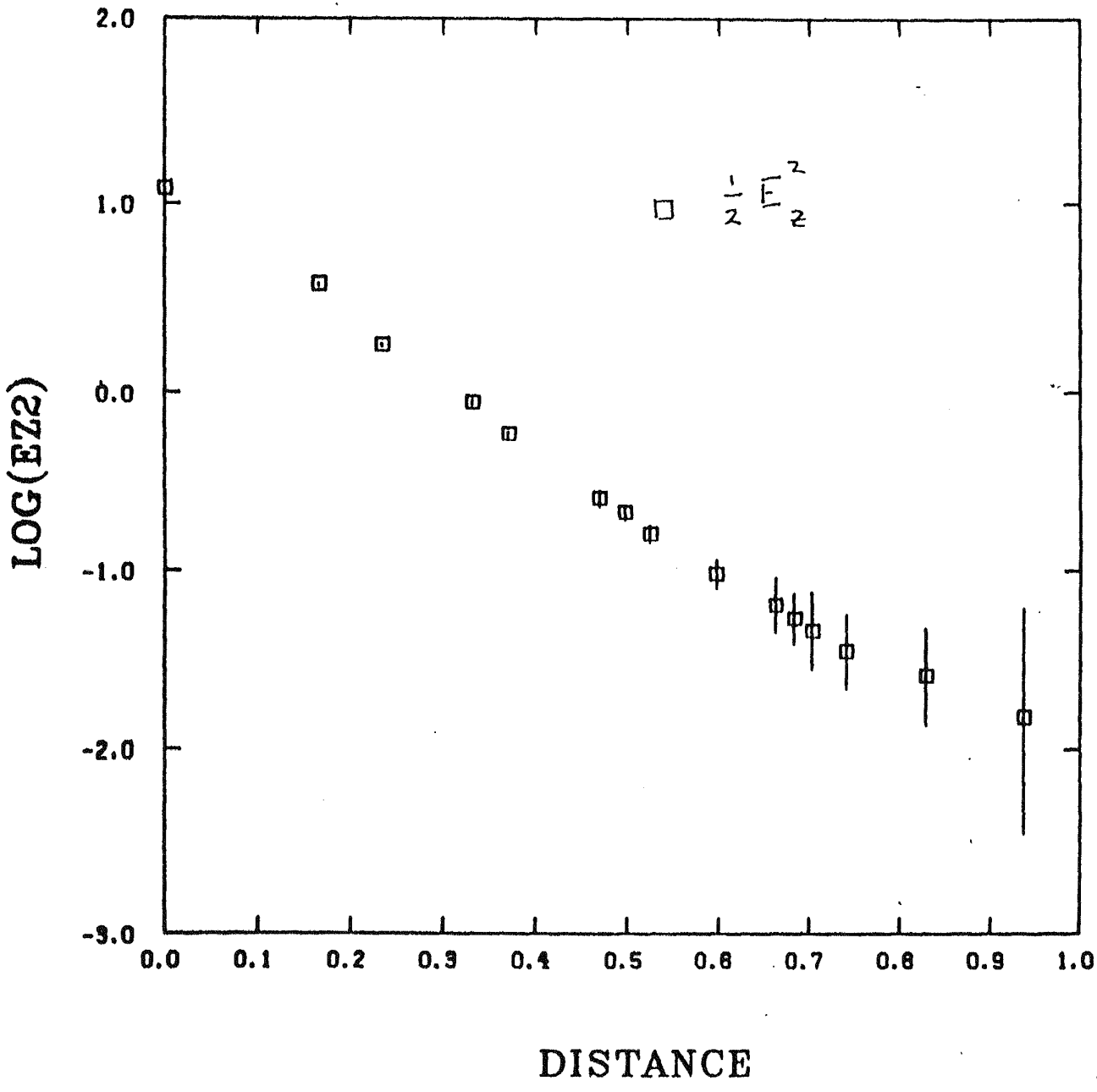
B=2.4 WL=44 ST=66
2.0
1.0
0.0
-1.0
-2.0
-3.0
LOG(EZ2)
0.0
0.1
0.2
0.3
0.4
0.5
0.6
0.7
0.8
0.9
1.0
DISTANCE

Fig.4

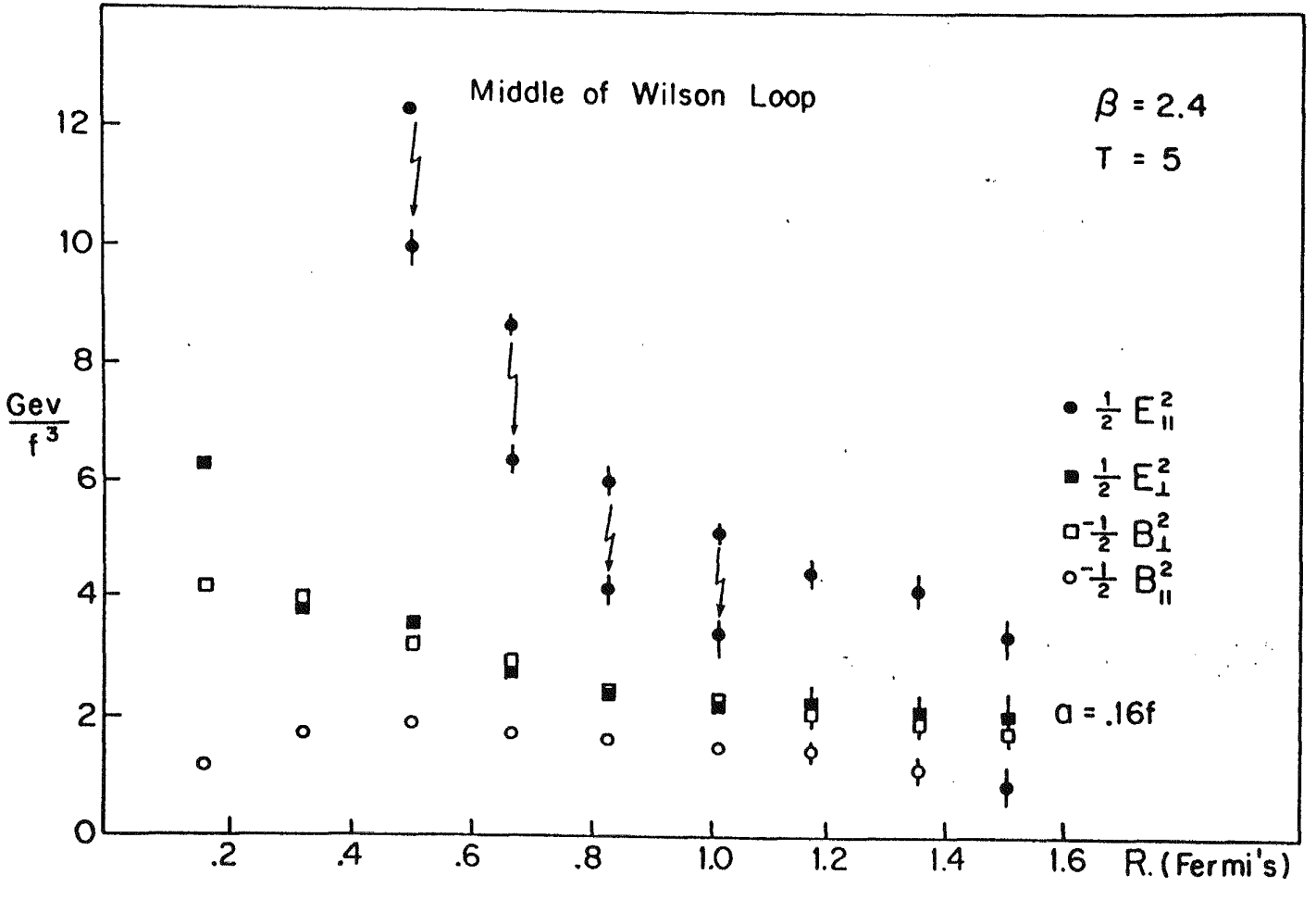
Middle of Wilson Loop
β = 2.4
T = 5
Gev/f³
12
10
8
6
4
2
0
.2
.4
.6
.8
1.0
1.2
1.4
1.6
R. (Fermi's)
½ E²∥
½ E²⊥
-½ B²⊥
-½ B²∥
a = .16f

Fig.5

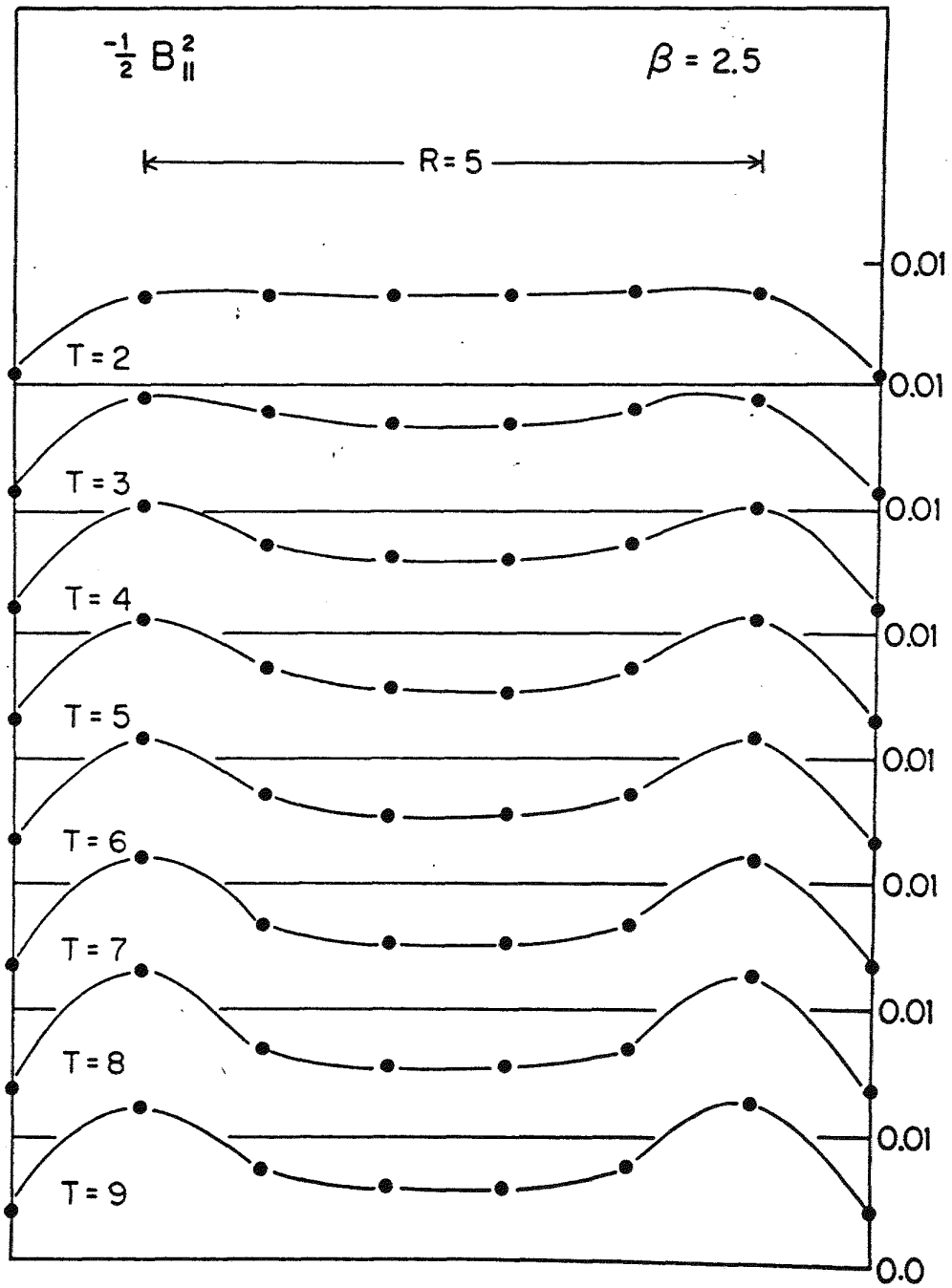
$-\frac{1}{2} B_{\parallel}^2$
$\beta = 2.5$
R = 5
0.01
T = 2
0.01
T = 3
0.01
T = 4
0.01
T = 5
0.01
T = 6
0.01
T = 7
0.01
T = 8
0.01
T = 9
0.0

Fig.6

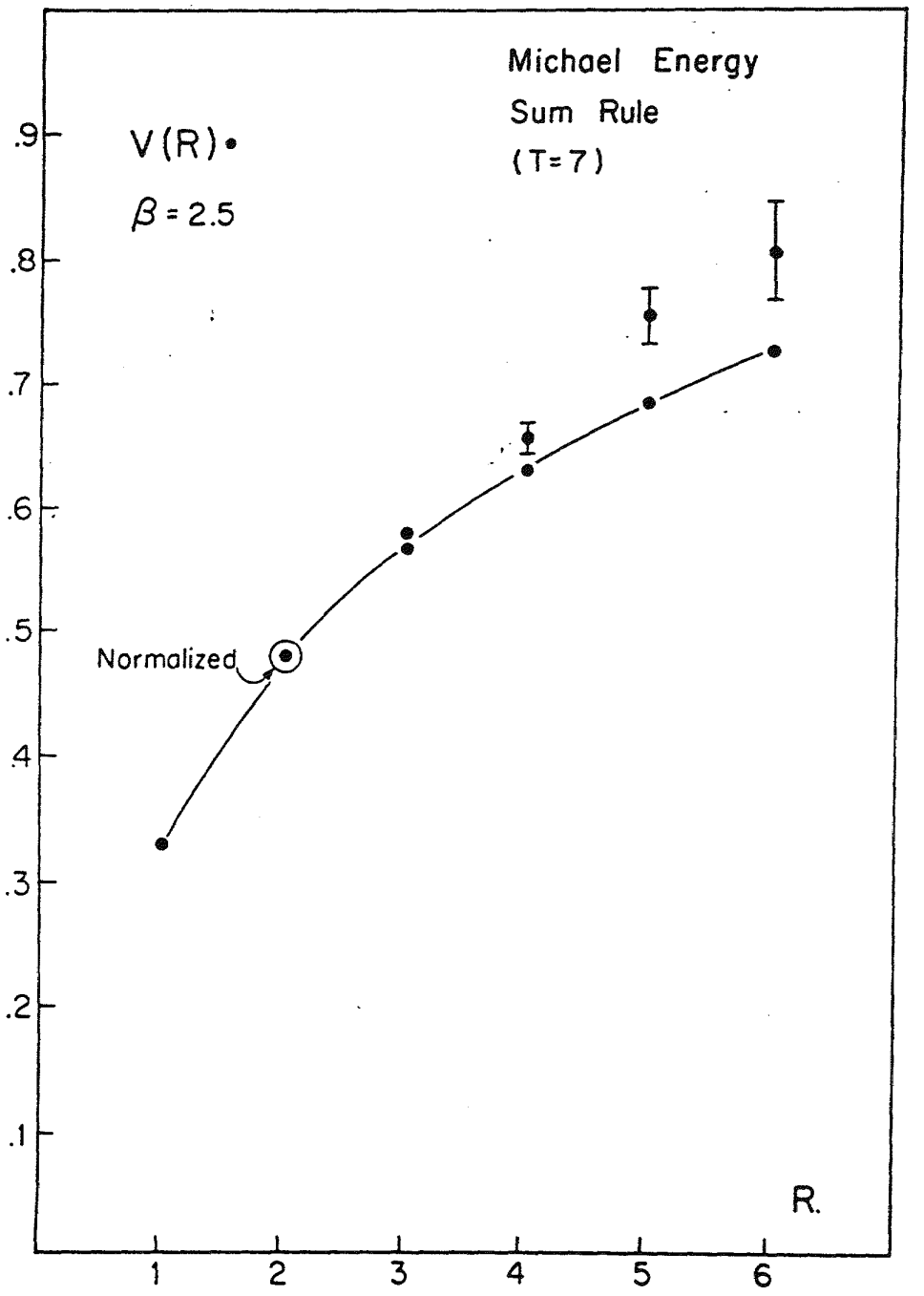
Michael Energy
Sum Rule
(T=7)
V(R)•
β = 2.5
Normalized
R.
.9
.8
.7
.6
.5
.4
.3
.2
.1
1
2
3
4
5
6

Fig.7

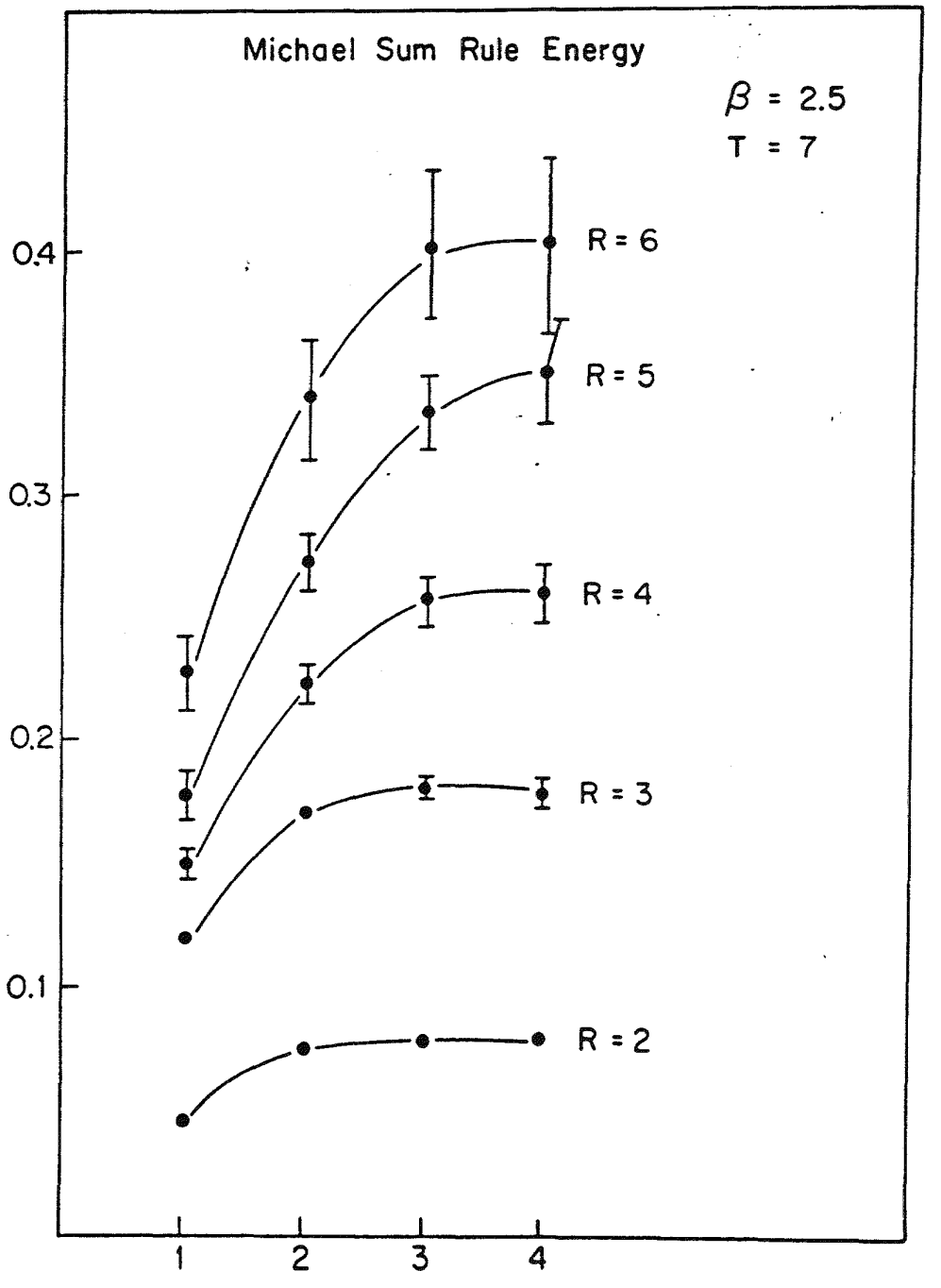

Fig.8

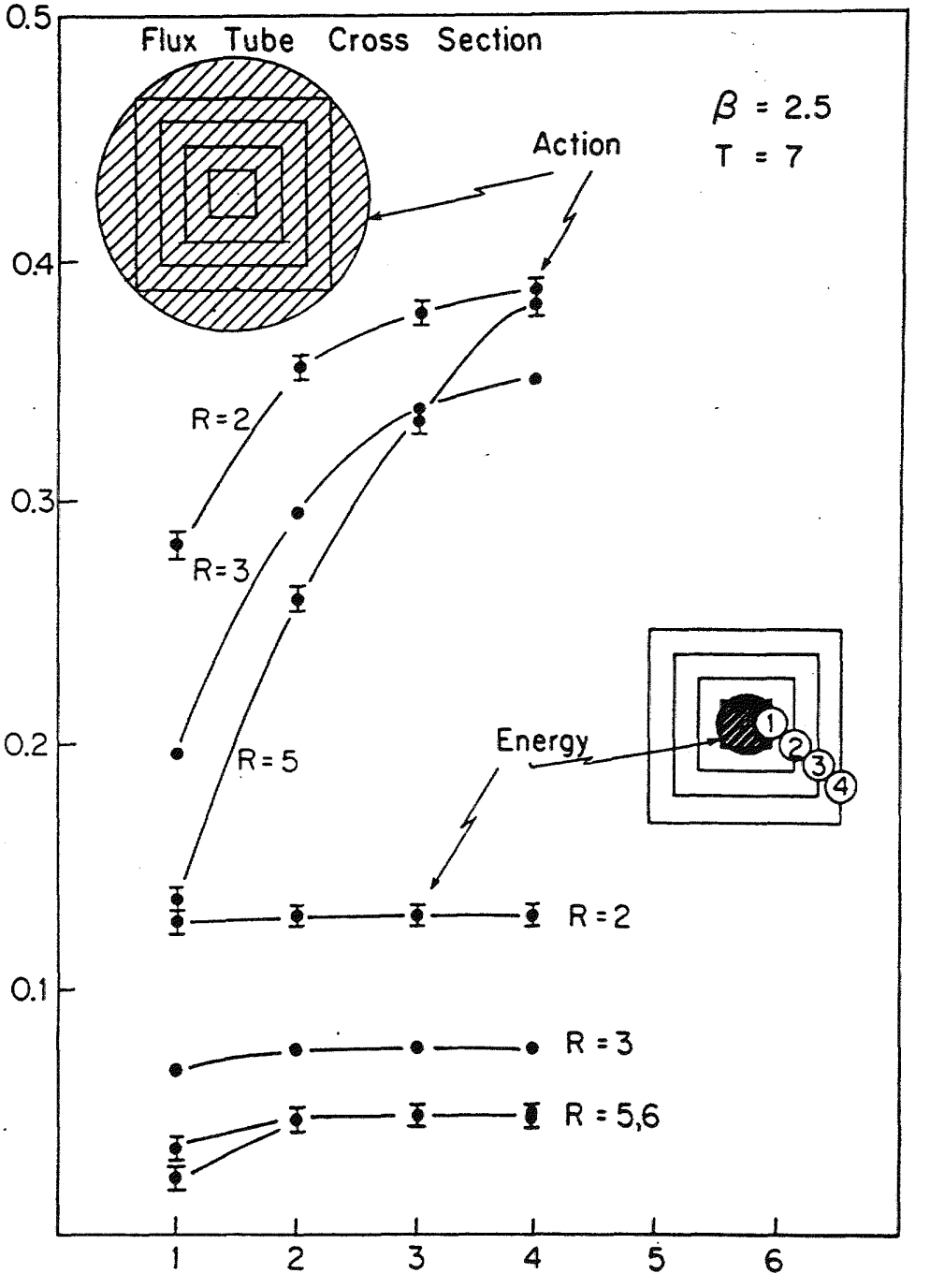
Flux Tube Cross Section
β = 2.5
T = 7
Action
Energy
R=2
R=3
R=5
R=2
R=3
R=5,6
0.5
0.4
0.3
0.2
0.1
1
2
3
4
5
6

Fig.9

Flux Distribution around $q\bar{q}$

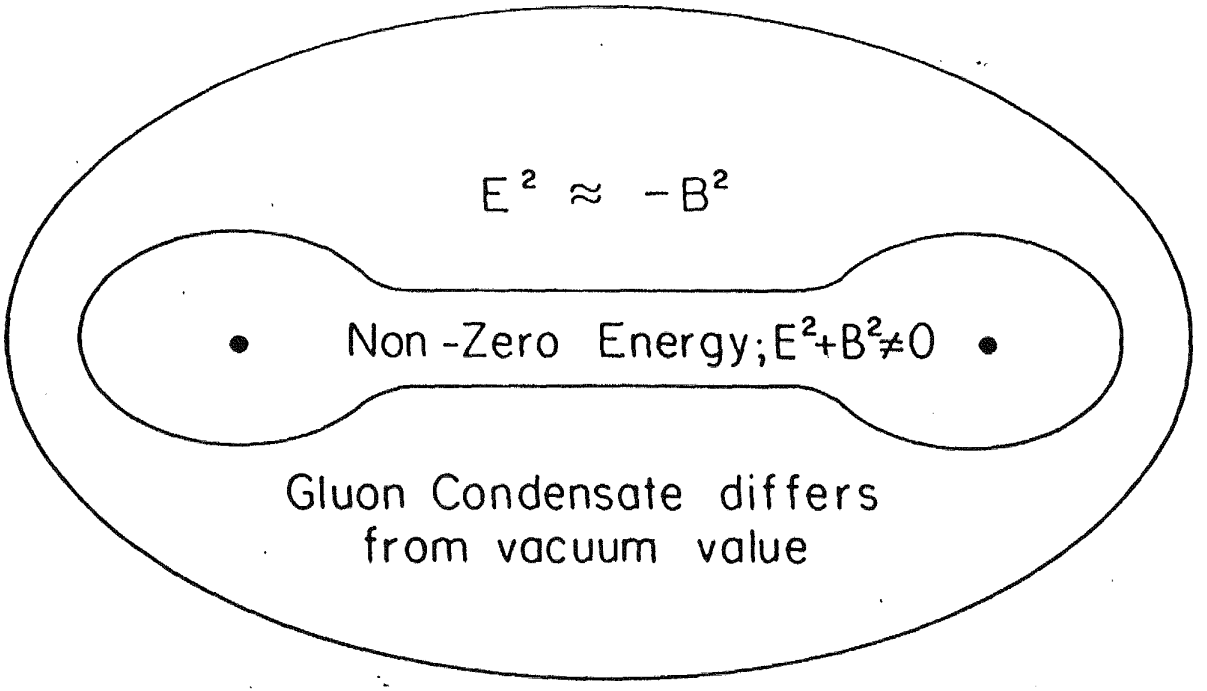

$E^2 \approx 0$

$B^2 \approx 0$

Fig.10

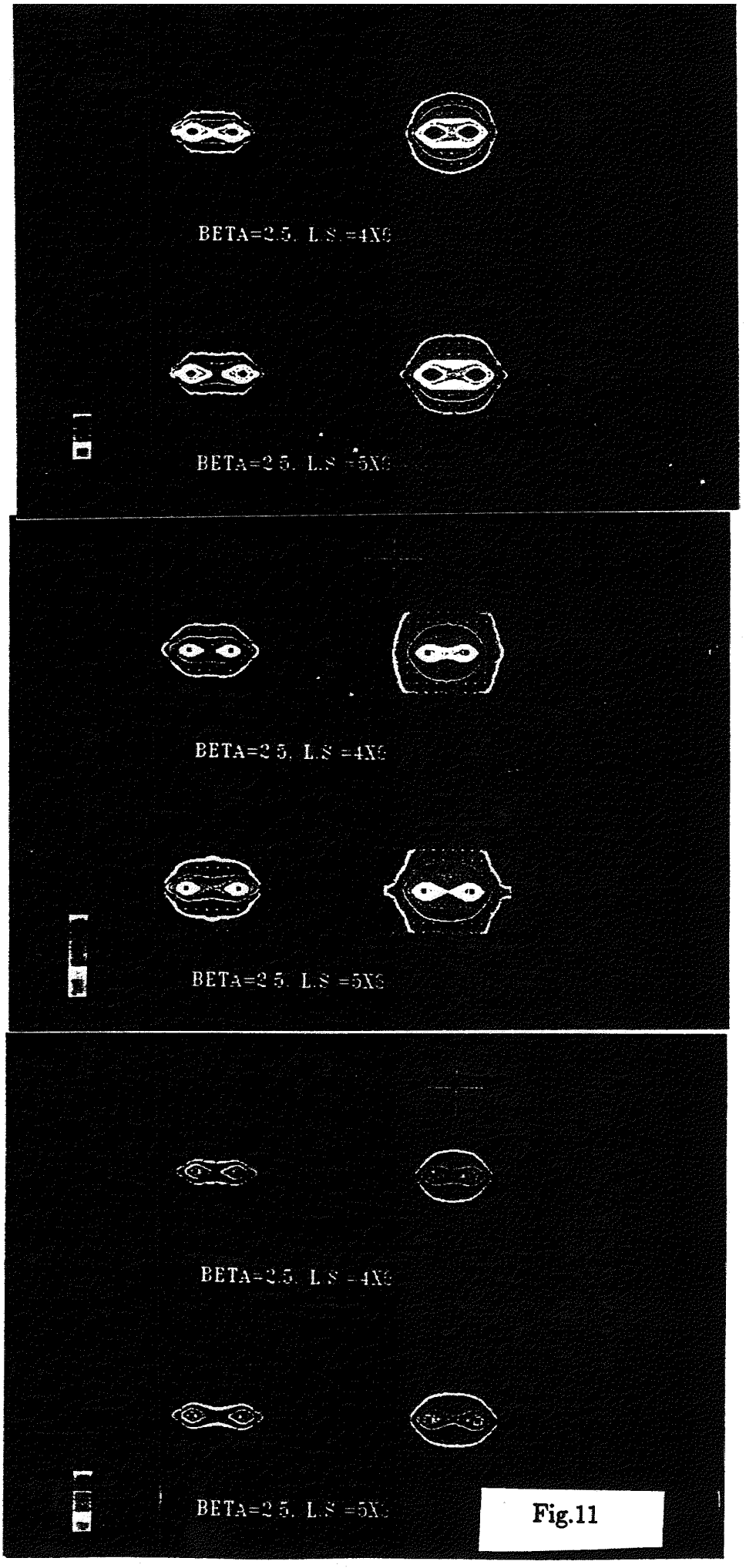
BETA=2.5. L.S.=4X6
BETA=2.5. L.S.=5X6
BETA=2.5. L.S.=4X6
BETA=2.5. L.S.=5X6
BETA=2.5. L.S.=4X6
BETA=2.5. L.S.=5X6

Fig.11

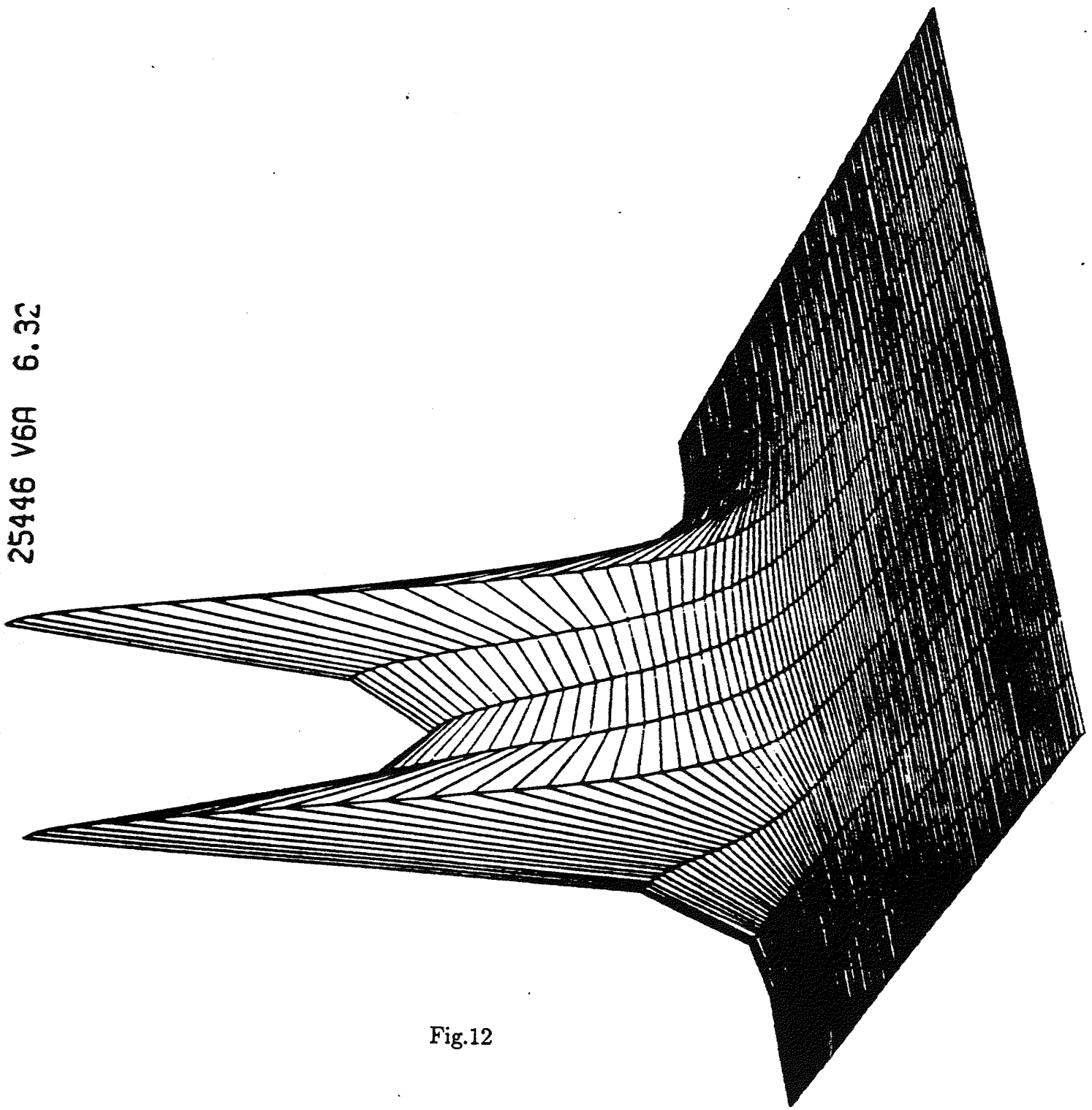

Fig.12

C Statistics and Quantum Field Theory in Three Space-Time Dimensions(Chen-Han Lee)

It has been shown that the quantum mechanical systems in three space-time dimensions carry fractional statistics and fractional spin.[1] In three dimensional field theory, the statistics transmutation of various models with the abelian Chern-Simons term[2] has also been observed.[3]

Although the applications of the statistics transmutation in fractional quantum Hall effect[4] and high T_c superconductivity[5] have activated investigation of Chern-Simons term related models in three space-time dimensions, we still lack a model-independent understanding of these peculiar behaviors of spin and statistics in the framework of three dimensional quantum field theory. We propose to study three dimensional quantum field theory in the $SL(2,R)$ spinor formulation. Among our goals are better understanding of fractional spin and statistics and the connection between them and to clearify the role of the Chern-Simons term, both abelian and non-abelian, in providing the statistics transmutation. The corresponding supersymmetric formulation will also be studied.

References

[1] J. Leinaas and J. Myrlheim, Nuovo Cimento, B37(1977), 1. F. Wilczek, Phys. Rev. Lett., 49(1982), 957. F. Wilczek and A. Zee, Phys. Rev. Lett., 48(1982), 1144.

[2] S. Deser, R. Jackiw and S. Templeton, Ann. Phys., 140(1982), 372.

[3] F. Wilczek and A. Zee, Phys. Rev. Lett., 51(1983), 2250. I. Dzyaloshinskii, A. Polyakov and P. Wiegmann, Phys. Lett., A127(1988), 112. A. Polyakov, Mod. Phys. Lett., A3(1988), 325.

[4] R.B. Laughlin, Phys. Rev. Lett., 50(1983), 1395. B.J. Halperin, Phys. Rev. Lett., 52(1984), 1583. D.A. Arovas, R. Schrieffer and A. Zee, Nucl. Phys., B251(1985), 117.

[5] Y.-H. Chen, F. Wilczek and E. Witten, "On Anyon Superconductivity", IASSNS-HEP-89/27, and the references listed there.

III. EXPERIMENTAL - TASK B

A. INTRODUCTION

Louisiana State University started a high energy experimental program July 1, 1979. The new group collaborated from 1979 to 1984 on a very successful electron-positron colliding beam experiment at CESR.

In 1980 LSU joined neutrino oscillation experiment E645 at LAMPF which is looking for possible oscillations of the type $\bar{\nu}_\mu \rightarrow \bar{\nu}_e$ or $\nu_e \rightarrow \bar{\nu}_e$. [1] Data taken in 1986 was used to check out the detector, identify shielding problems and make a preliminary search for oscillations. Data taking resumed in June 1987 with substantially improved shielding. Limits obtained from 1987 data have been published .[2] We have just completed the final run for the experiment.. Imlay and Metcalf of LSU were the spokesmen for this final run. We expect to complete the analysis of the experiment in the Spring of 1990.

In late 1984 we joined an electron-positron experiment, AMY, at the TRISTAN storage ring in Japan. The LSU high energy group had primary responsibility for building the muon identifier. Data taking began in 1987. The muon detector has worked well and results have been reported for both isolated single muon events[3] and for $ee \rightarrow \mu\mu$ events.[4] We have recently reported on the charge asymmetry for $e^+e^- \rightarrow b\bar{b}$ for events with a subsequent semileptonic decay $b \rightarrow \mu^-$ or $\bar{b} \rightarrow \mu^+$. [5] We plan to continue our participation on AMY this year. We also note that Professor Paul Kirk of LSU is participating on AMY in addition to his Intermediate Energy program.

We have recently joined the electron-proton experiment, ZEUS, at the HERA facility in Germany. LSU has taken responsibility for building the optical readout of the electromagnetic part of the barrel calorimeter. We have spent the last six months getting setup for this task and our facility is now in operation.

Finally we are interested in participating in SSC physics. We have attended various meetings on SSC physics and joined two subsystem proposals.

B. THE NEUTRINO OSCILLATION EXPERIMENT

1. Introduction

In 1980 LSU, OSU, ANL, and CIT proposed experiment E645 for LAMPF which is searching for neutrino oscillations in two channels $\bar{\nu}_\mu \rightarrow \bar{\nu}_e$ and $\nu_e \rightarrow \bar{\nu}_e$. [1] Our neutrino source consists of an equal admixture of ν_μ,$\bar{\nu}_\mu$, and ν_e arising from decays of stopping π^+ and μ^+ in a beam stop. The appearance of $\bar{\nu}_e$ in our detector would indicate the occurrence of neutrino oscillations. We see no evidence for neutrino oscillations. Figure 1 shows limits we obtained on the two oscillation parameters δm^2 and $\sin^2 2\theta$ from our 1987 data. Also shown are the estimated limits we may obtain from our 1988 and 1989 data.

In this appearance experiment we are looking for the reaction $\bar{\nu}_e + p \rightarrow e^+ + n$ in 20 tons of liquid scintillator arranged in 40 planes, each 3.6 m x 3.6 m x 3 cm. A plane has 12 lucite containers (3.6 m x 30 cm x 3 cm) filled with scintillator. Each container is viewed by a phototube at each end. Our trigger requires that 3 out of 4 consecutive planes fire. Each plane of scintillator is followed by x and y planes of proportional drift tubes to measure the electron trajectories. Pulse height information is recorded for all phototubes and drift tubes for a period of 160 μs on each event ,approximately 60 μs before and 100 μs of time after the trigger. This permits rejection of electrons from stopped cosmic ray muons and possibly detection of neutrons. (Layers of gadolinium allow us to identify the neutron on some fraction of the events through a capture reaction that gives off several photons within 100 μs of the trigger.) The entire detector is surrounded by a 200 ton passive iron/lead shield and an active liquid scintillator cosmic ray veto. A schematic drawing of the apparatus in its tunnel is shown in Figure 2.

Two faculty members, (Imlay and Metcalf), a Research Associate (Fazely) and a technician (Marterer) from LSU are now working on the experiment. Our graduate student, Cathy Choi, finished her thesis on the neutrino experiment last year.

Figure 1

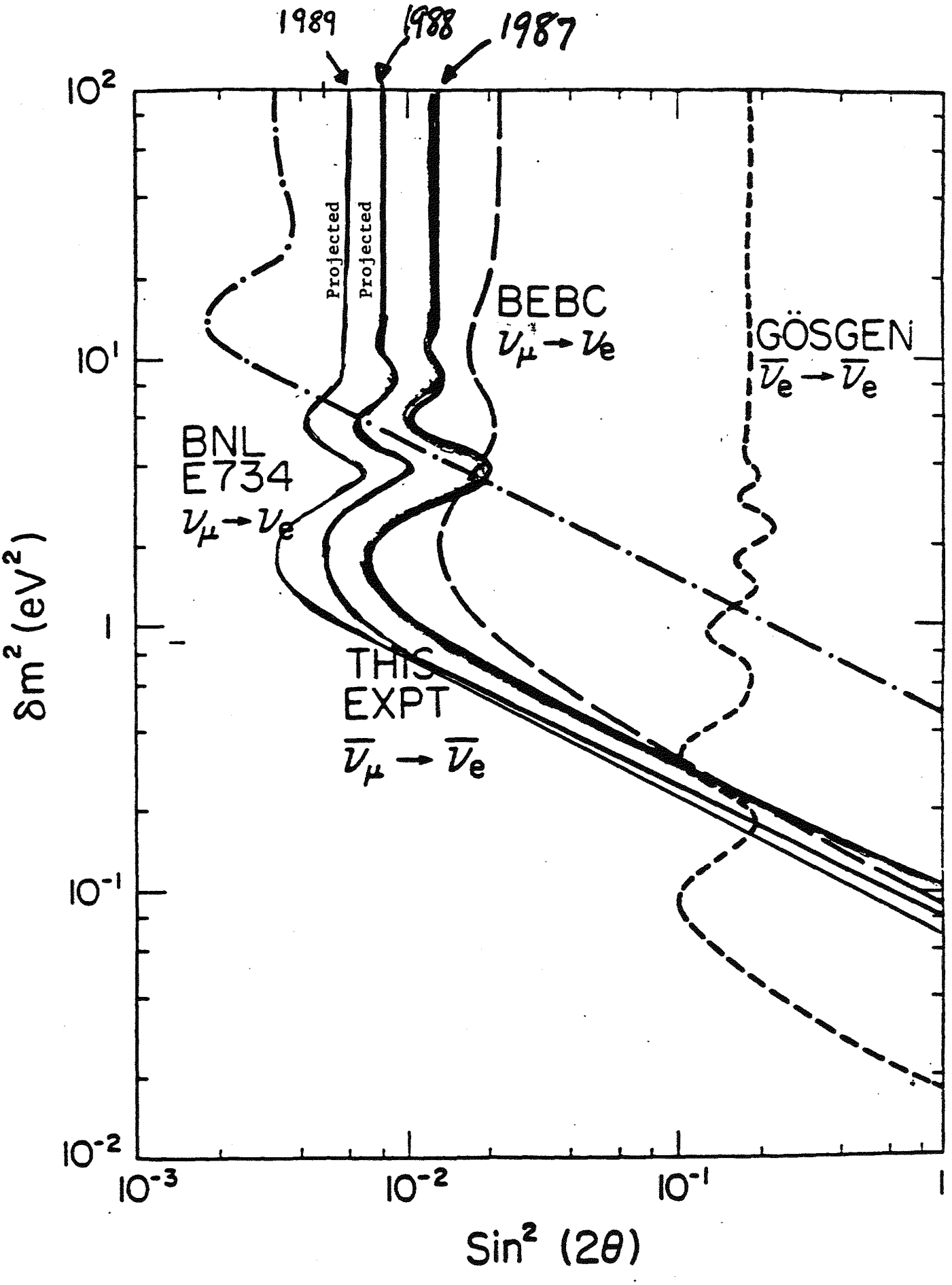
1989
1988
1987
Projected
Projected
BEBC
$\nu_\mu \rightarrow \nu_e$
GÖSGEN
$\overline{\nu}_e \rightarrow \overline{\nu}_e$
BNL
E734
$\nu_\mu \rightarrow \nu_e$
THIS
EXPT
$\overline{\nu}_\mu \rightarrow \overline{\nu}_e$
10^2
10^1
1
10^{-1}
10^{-2}
δm^2 (eV^2)
10^{-3}
10^{-2}
10^{-1}
1
Sin^2 (2θ)

E645 COSMIC RAY SHIELD

Side Elevation Section

1 August 1987

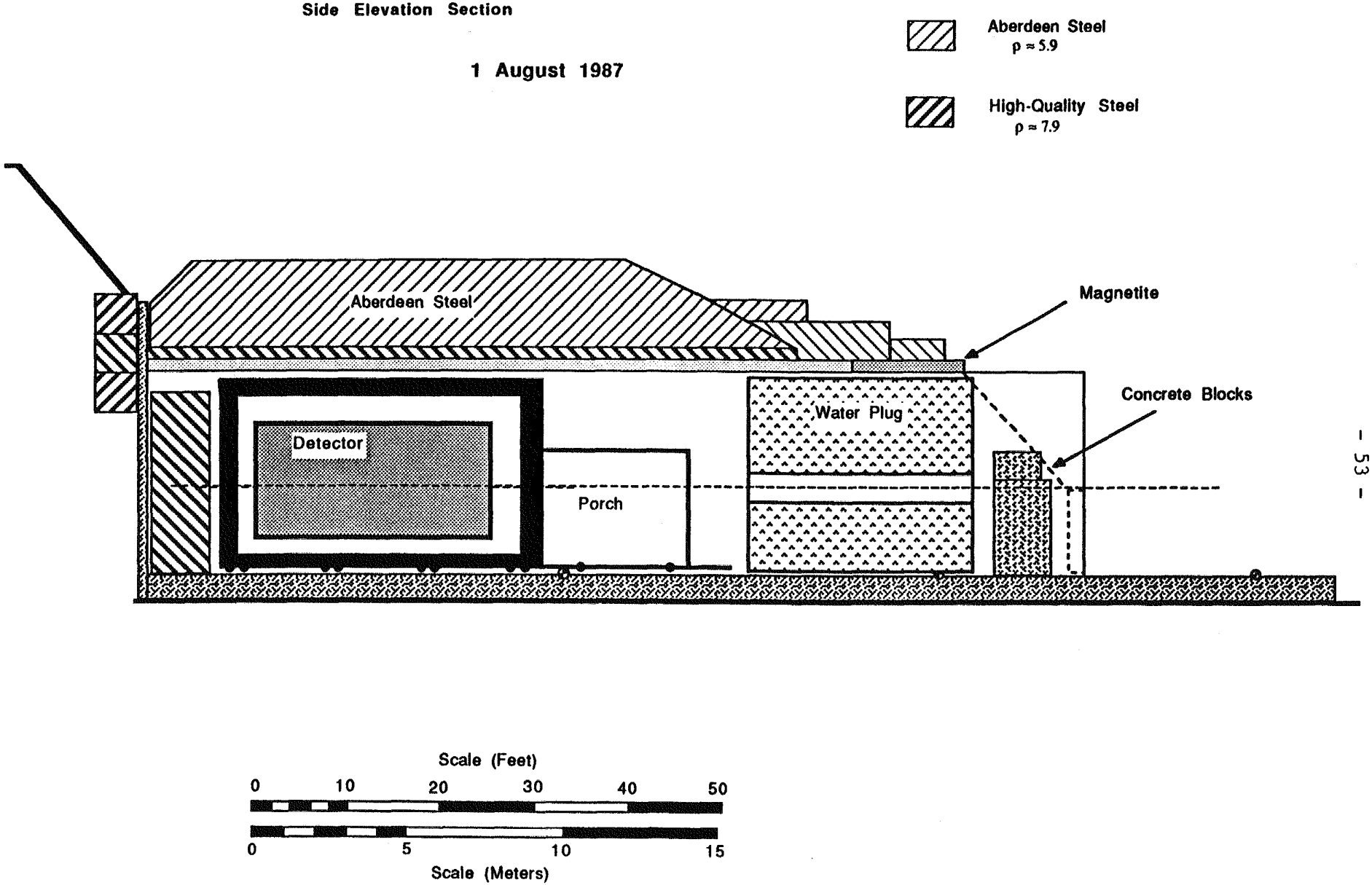

Figure 2

2. Components of the Experiment

a. Tunnel for the Experiment

J. Donahue of Los Alamos kept track of construction of the tunnel and service building for the collaboration. Construction started in August 1984 and was completed a year later.

b. Cosmic Ray Shield

The active and passive cosmic ray shield (a large tank of liquid scintillator and 7" of iron/lead respectively) was handled primarily by the ANL physicists. It was installed at the experimental site in the fall of 1985. ANL conducted extensive studies of cosmic rays in a tunnel with variable overburden at Los Alamos. On the basis of these studies we decided it was necessary to place at least 2000 gm/cm2 of iron and tuft shielding over the detector to reduce the hadronic component of the cosmic rays to an acceptable level. The installation of the overburden was directed by J. Donahue of LAMPF and completed in 1987.

c. The Detector

OSU and LSU were responsible for the construction and operation of the 20 ton neutrino detector. Details of its operation are presented in a recent NIM article.[6] OSU conducted the prototype work on the liquid scintillator counters which are used for the neutrino target. LSU shared on the preparation, testing and calibration of these counters.

LSU produced half of the necessary 4000 drift tubes along with the associated electronics. The drift tubes are of an unique cardboard design(with thin aluminum layers for ground planes) to limit the amount of aluminum, a necessity at these neutrino energies to avoid unwanted backgrounds.

In early 1984 we tested a small scale version of the detector in a charged particle beam at LAMPF. The response of the detector to electrons and protons above 30 MeV was measured. It was found that for events traversing 3 or more modules we could distinguish electrons from protons at the 5 x 10-4 level. These results have been confirmed by measurements of stopping muons and proton recoils from neutron interactions in the actual detector. The response of the detector to electrons agrees very well with the EGS Monte Carlo calculations done by the LSU group.

R. McKeown of CIT developed a scheme for the detection of the neutron produced in $\overline{\nu}_e + p \rightarrow e^+ + n$ for some fraction (about 30%) of the events. Photons are detected from a capture reaction of thermalized neutrons in gadolinium layers in the detector. The usefulness of this slow neutron detection depends both on the efficiency for detecting neutrons and on the background level without neutron detection.

d. Software and data analysis

LSU assumed major software responsibilities on the experiment. The graduate student, C. Choi, mentioned above worked with William Metcalf on a Monte Carlo simulation of the detector that has been used extensively in acceptance and background studies as well as providing fake data to debug many of the analysis routines. Metcalf wrote various routines for data analysis including the drift chamber tracking routine. Choi wrote most of the routines necessary for detector calibration. As an example of the results of the calibration work Figures 3 and 4 shows the corrected pulse height distribution for muons in a typical scintillation counter and in a PDT while Figure 5 shows the attenuation length calculation for the counters. Figure 6 shows a typical stopping muon event with the decay clearly visible.

3. The 1986 Run

The running period of LAMPF, (June-December, 1986) was used to shake down the detector and collect the first set of data. Minimal cosmic ray shielding was completed by November 15, 1986, but even this was not adequate. More seriously we had a substantial beam associated neutron background. (See next section). Nevertheless, analysis of 1986 data prepared us for the much cleaner 1987 data.[7]

4. Beam and Cosmic Ray Shielding

The 1986 data showed a large beam neutron background. Improved shielding, including the plugging of a 0° pipe in the berm, reduced this background by much more than a factor of 100 to an insignificant level. The cosmic ray hadronic background was also reduced by a factor of 10 to an acceptable level.

A concrete retaining wall was added at the open end of the tunnel and on the south side. Magnetite and tuff were added on the south side before beam started in June 1987. Pan Am continued stacking steel in the weakest areas as indicated by recoil proton distributions for cosmic ray data. Recoil protons which trigger the detector provide a clean sample of neutron induced events and thus are used as a monitor of neutron distributions

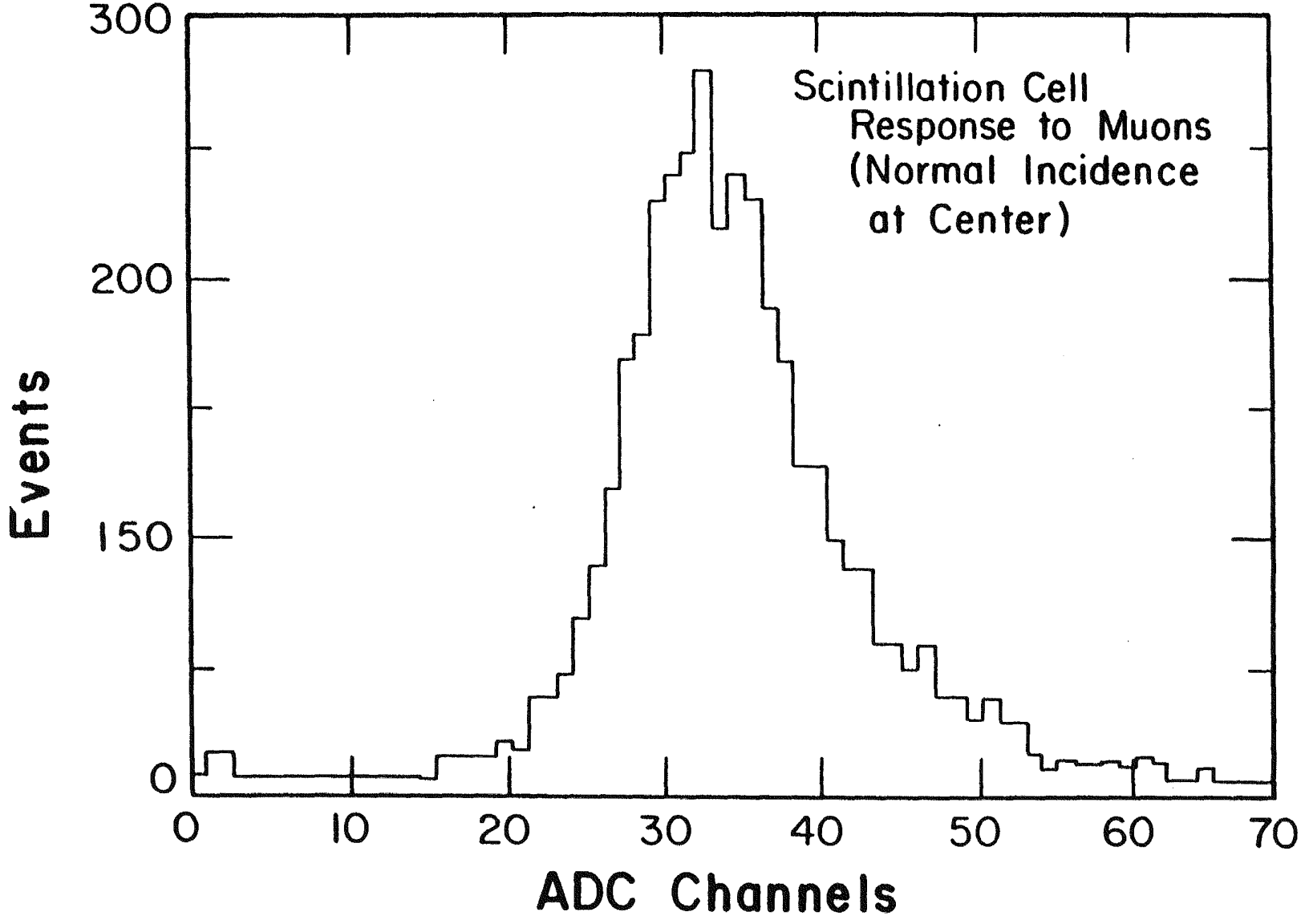
Scintillation Cell
Response to Muons
(Normal Incidence
at Center)
Events
300
200
150
0
0
10
20
30
40
50
60
70
ADC Channels

Figure 3

Figure 4

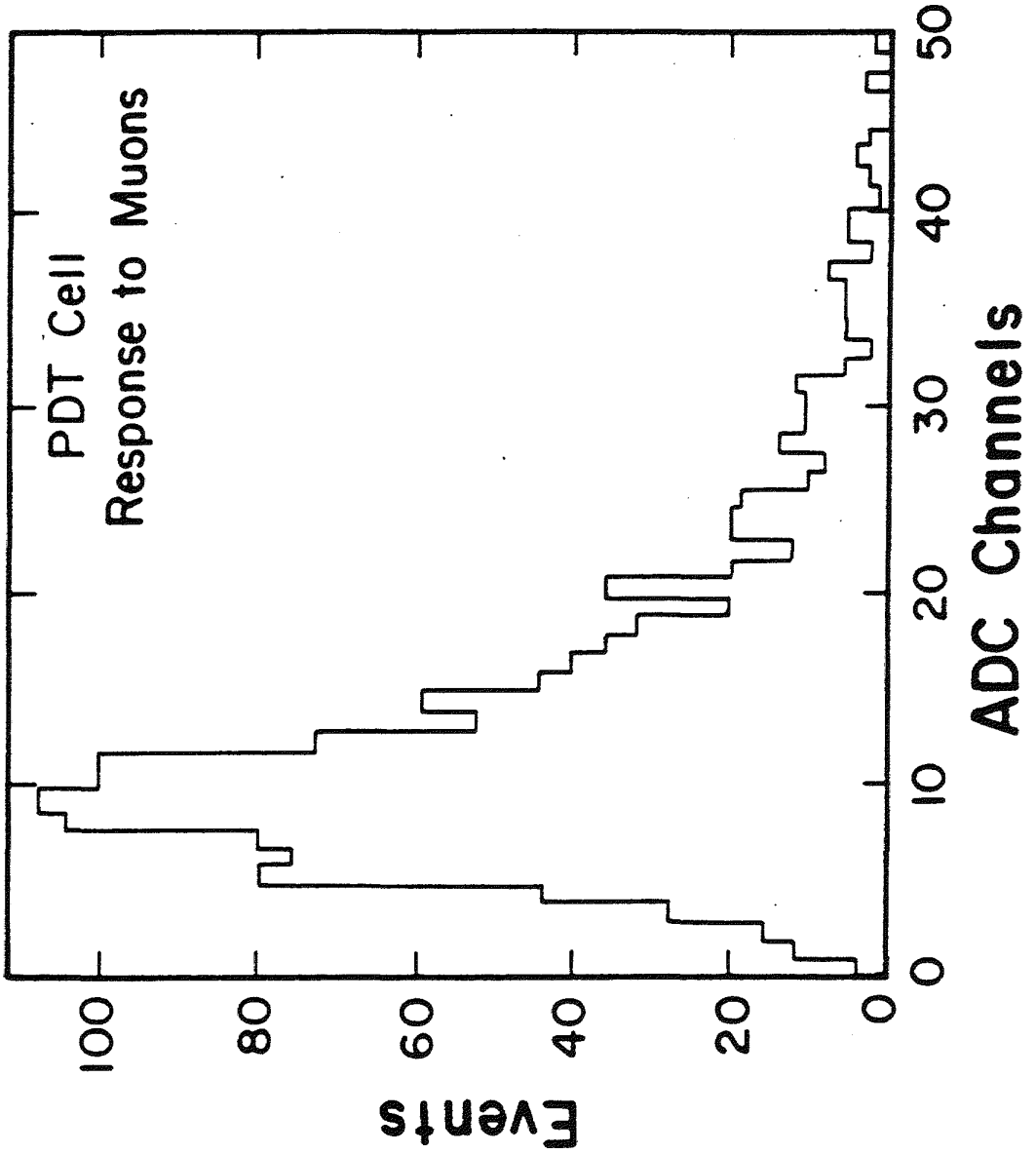
PDT Cell
Response to Muons
Events
ADC Channels
0
20
40
60
80
100
0
10
20
30
40
50

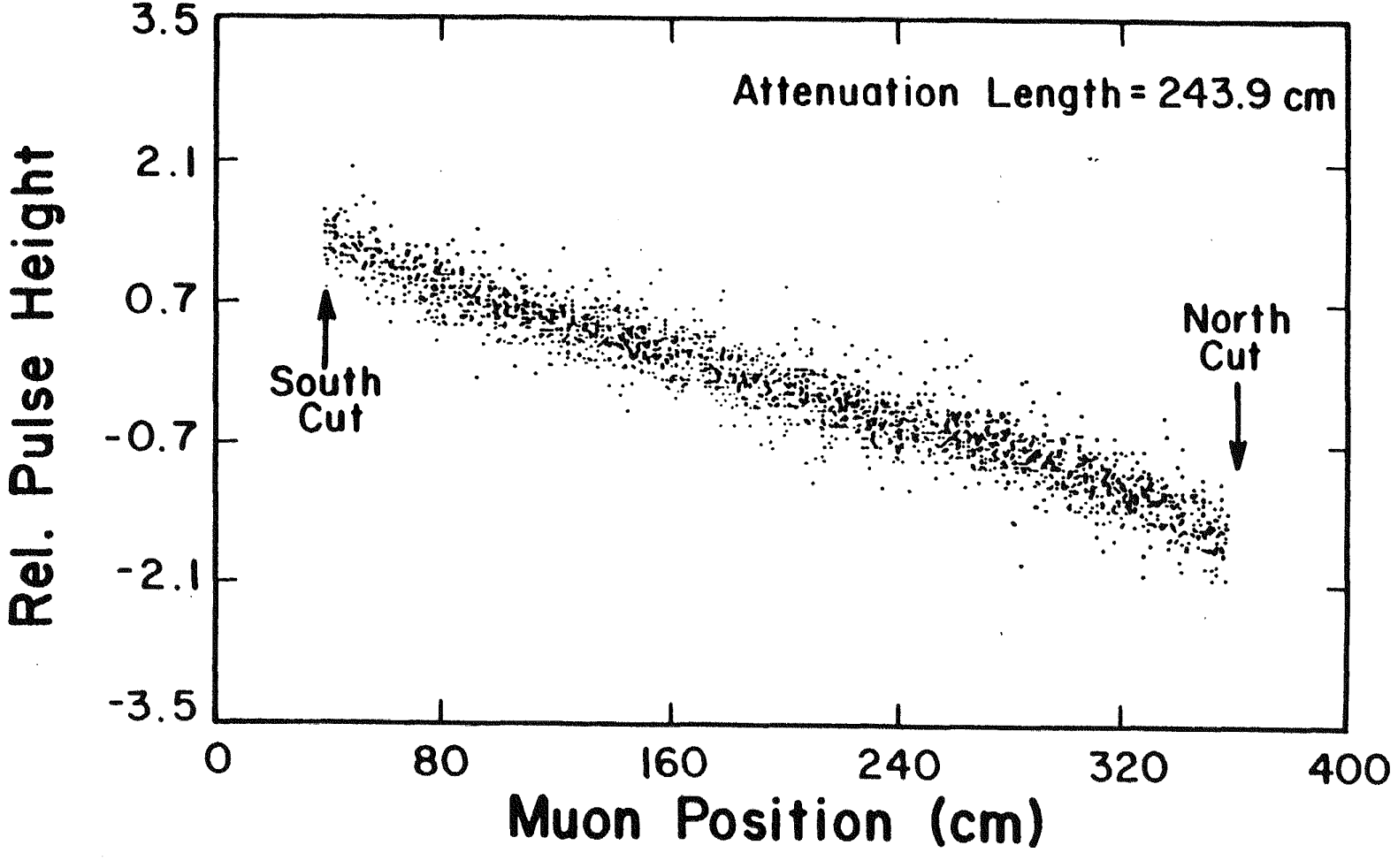
Attenuation Length = 243.9 cm
Rel. Pulse Height
3.5
2.1
0.7
-0.7
-2.1
-3.5
South Cut
North Cut
0
80
160
240
320
400
Muon Position (cm)

Figure 5a

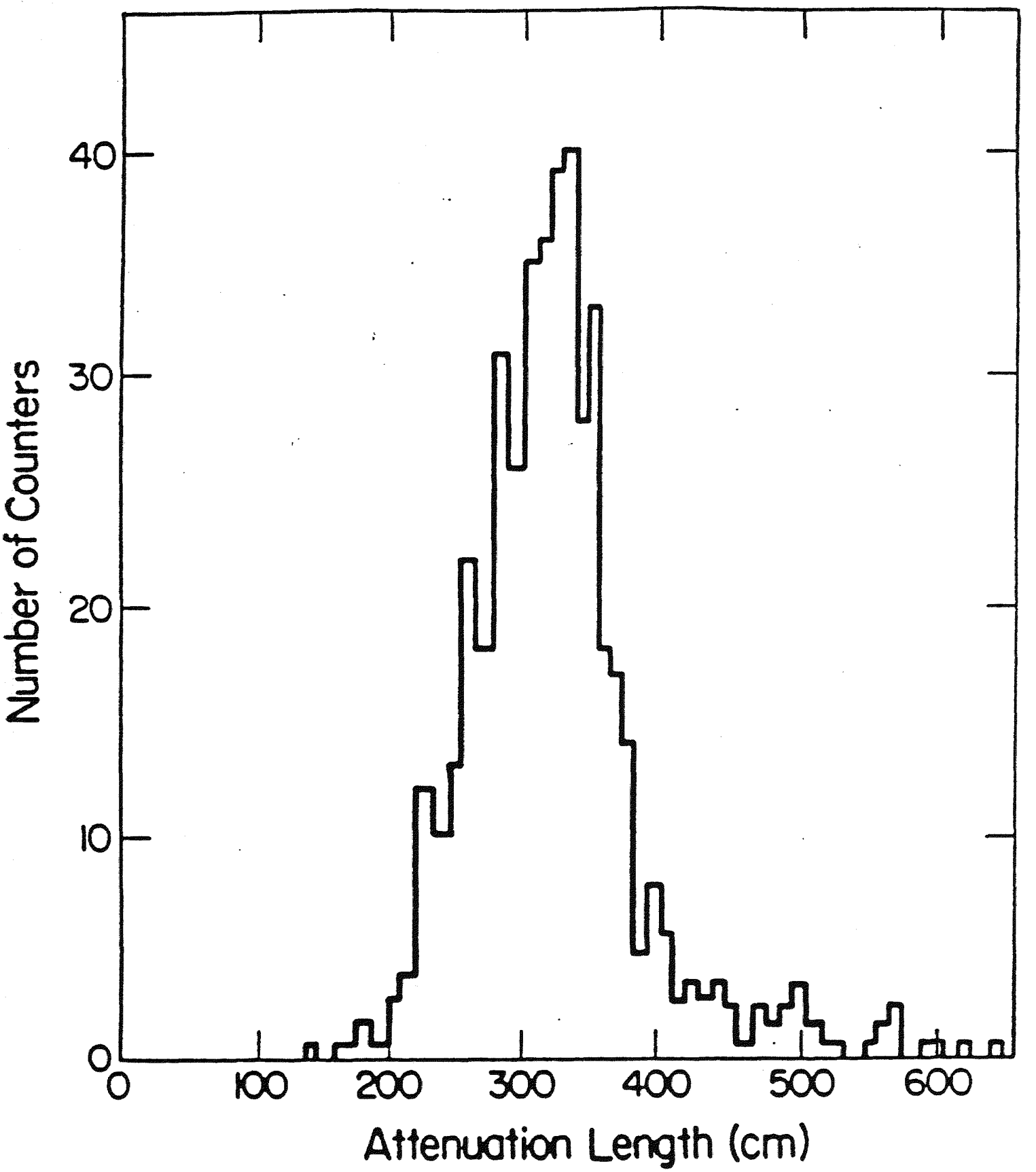
Number of Counters
0
10
20
30
40
0
100
200
300
400
500
600
Attenuation Length (cm)

Figure 5b

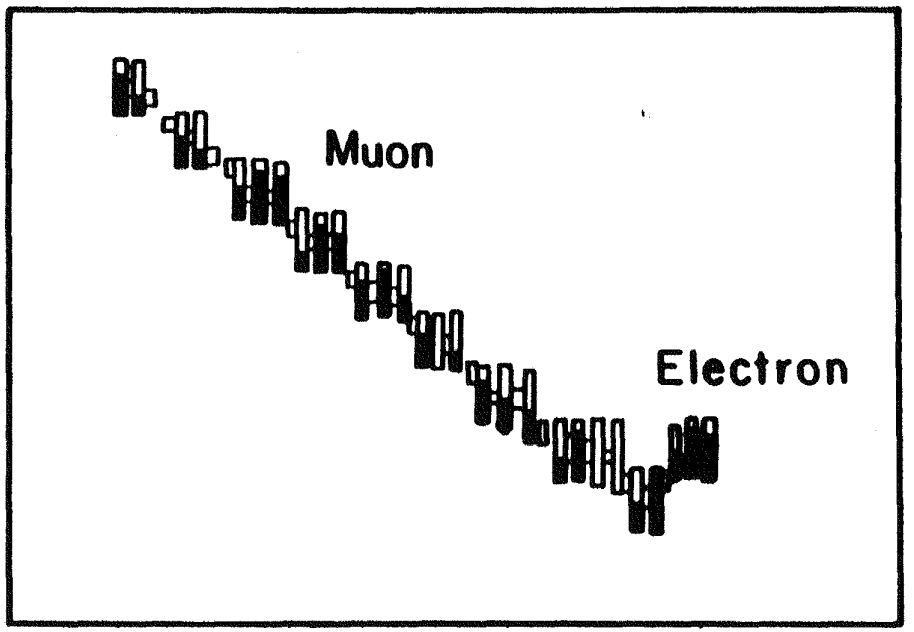

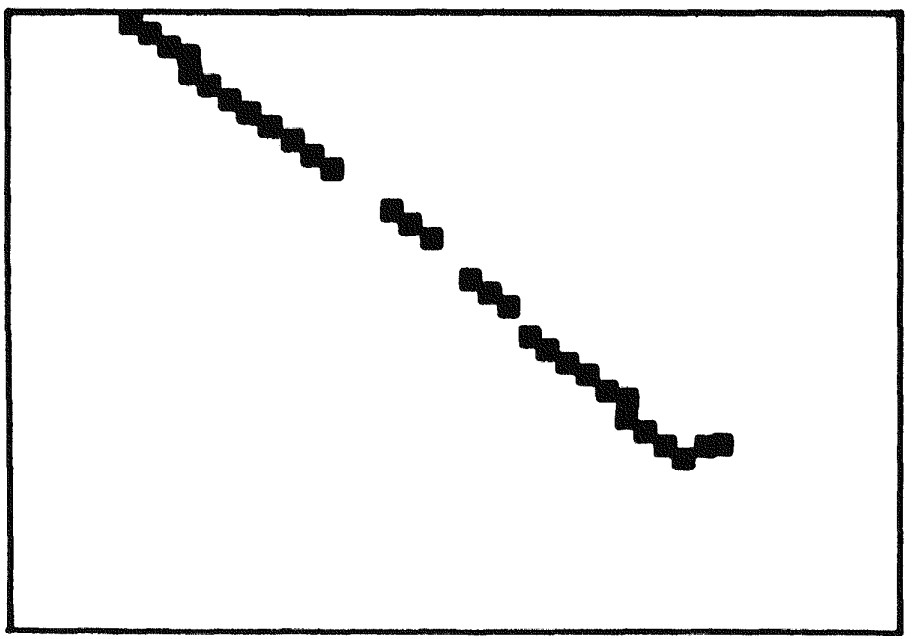

Stopping μ Decay

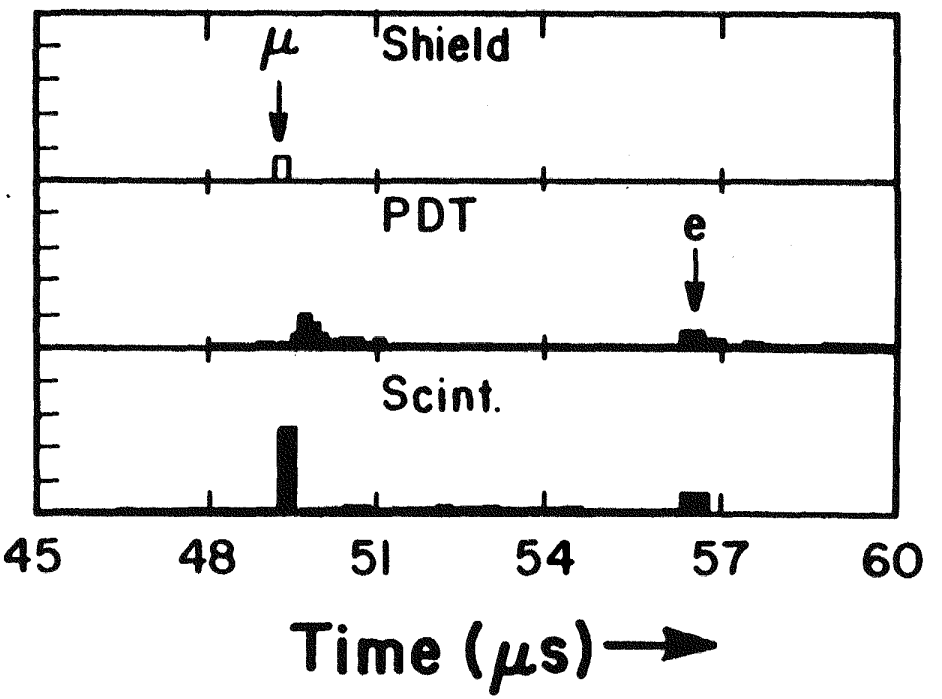

Figure 6

and rates. Recoil proton rates dropped each week and by October, 1987 were down a factor of 10 to 25 protons per LAMPF day which is an acceptable level. (See Figure 7). The recoil proton rates in the beam gate and cosmic ray gate are consistent with each other (± 2%). Thus, there is no evidence for beam associated recoil protons from neutrons.

5. Results from the 1987 Run

The 1987 data has been analyzed. The observed electron energy spectrum, shown in Figure 8b, is completely consistent with that expected from backgrounds, primarily ν_e C and ν_e electron elastic scattering. Thus we have no evidence for neutrino oscillation and can set the limits shown in Figure 1. Details of the analysis are provided in the paper[2] and Joe Mitchell's thesis.[8]

Electrons from muons which stop in the detector and decay provide an important control sample of electrons for the experiment. Figure 8a shows the energy distribution of electrons from stopped muon decay. Figure 9 shows the observed muon lifetime. We use the pulse height in the scintillators and proportional drift chambers to provide particle ID. Likelihood distributions obtained from muon decay electrons are shown in Figure 10a. The distribution should be flat. The dashed lines show where cuts are made to remove non electrons in our data sample shown in Figure 10b.

6. Status of the 1988 Run

The 1988 Run (June - October) almost doubled our data sample. A preliminary analysis of this run yielded a sample of events completely consistent with the 1987 sample.

The operation of the experiment for this run was handled by OSU and LSU personnel with help from two of our LAMPF collaborators. Data taking, calibration and analysis had become much more routine. Two technicians (Anderson of OSU and Marterer of LSU) ran half the shifts and learned how to process the data through the initial steps of the data analysis. They could also fix most of the hardware problems that occurred.

7. Status of the 1989 Run

After the 1988 run we decided to run the experiment one more year. The motivations were (1) to completely rule out hints of oscillations seen in other experiments

Figure 7

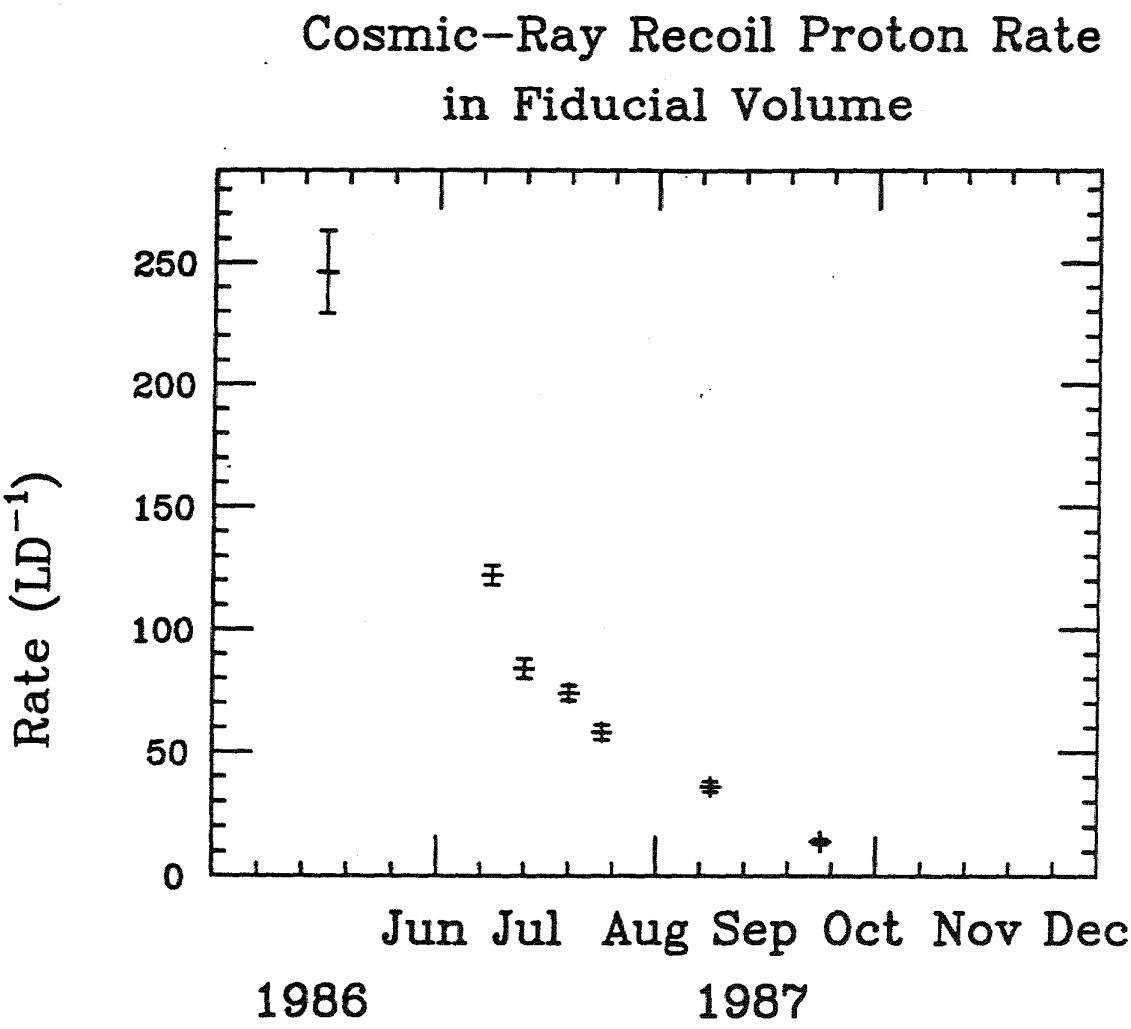
Cosmic-Ray Recoil Proton Rate
in Fiducial Volume
Rate (LD^{-1})
250
200
150
100
50
0
Jun Jul Aug Sep Oct Nov Dec
1986
1987

Figure 8

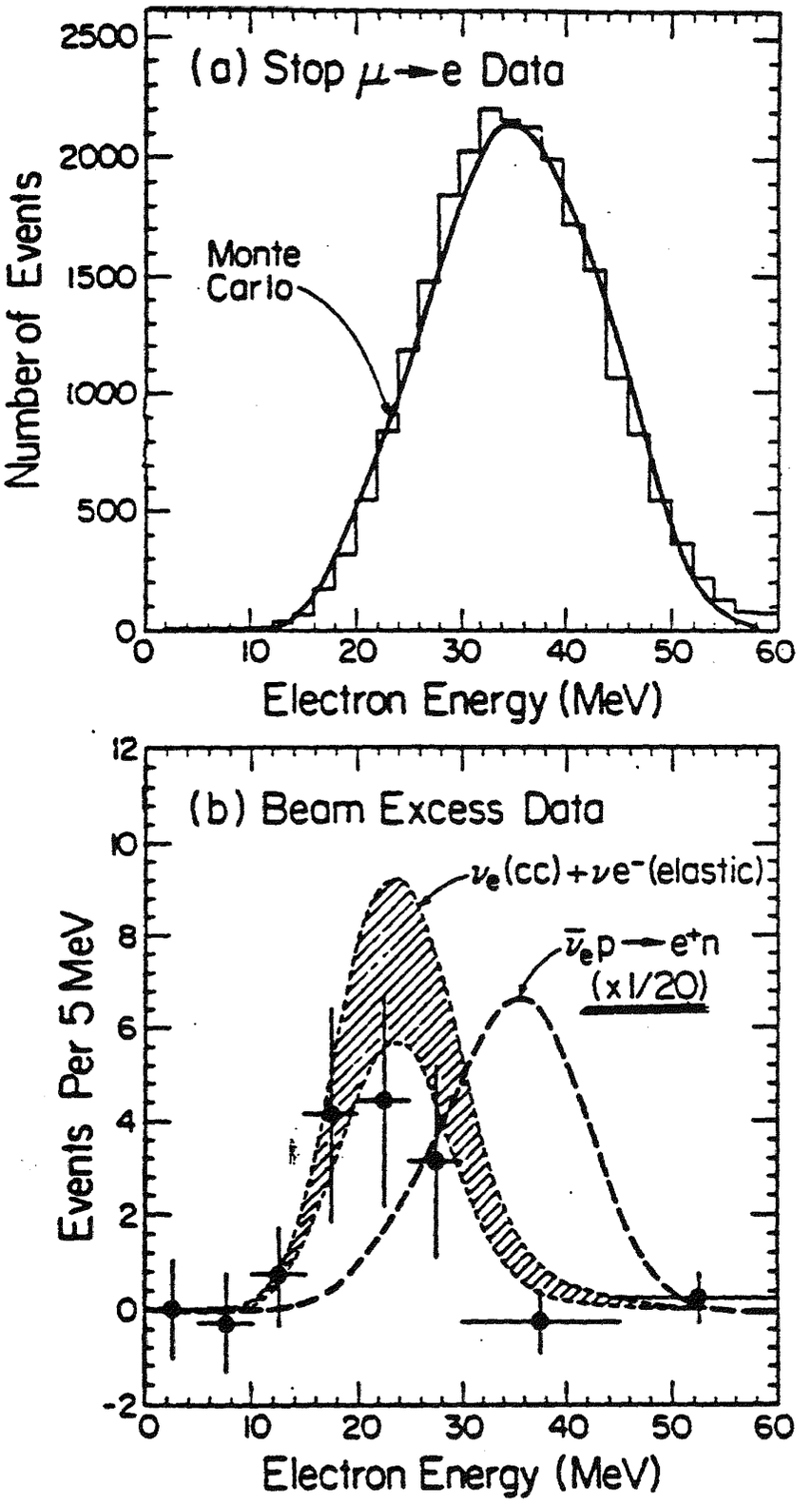
(a) Stop μ→e Data
Monte Carlo
Number of Events
Electron Energy (MeV)
(b) Beam Excess Data
νe(cc)+νe⁻(elastic)
ν̄ep→e⁺n
(x1/20)
Events Per 5 MeV
Electron Energy (MeV)

Figure 9

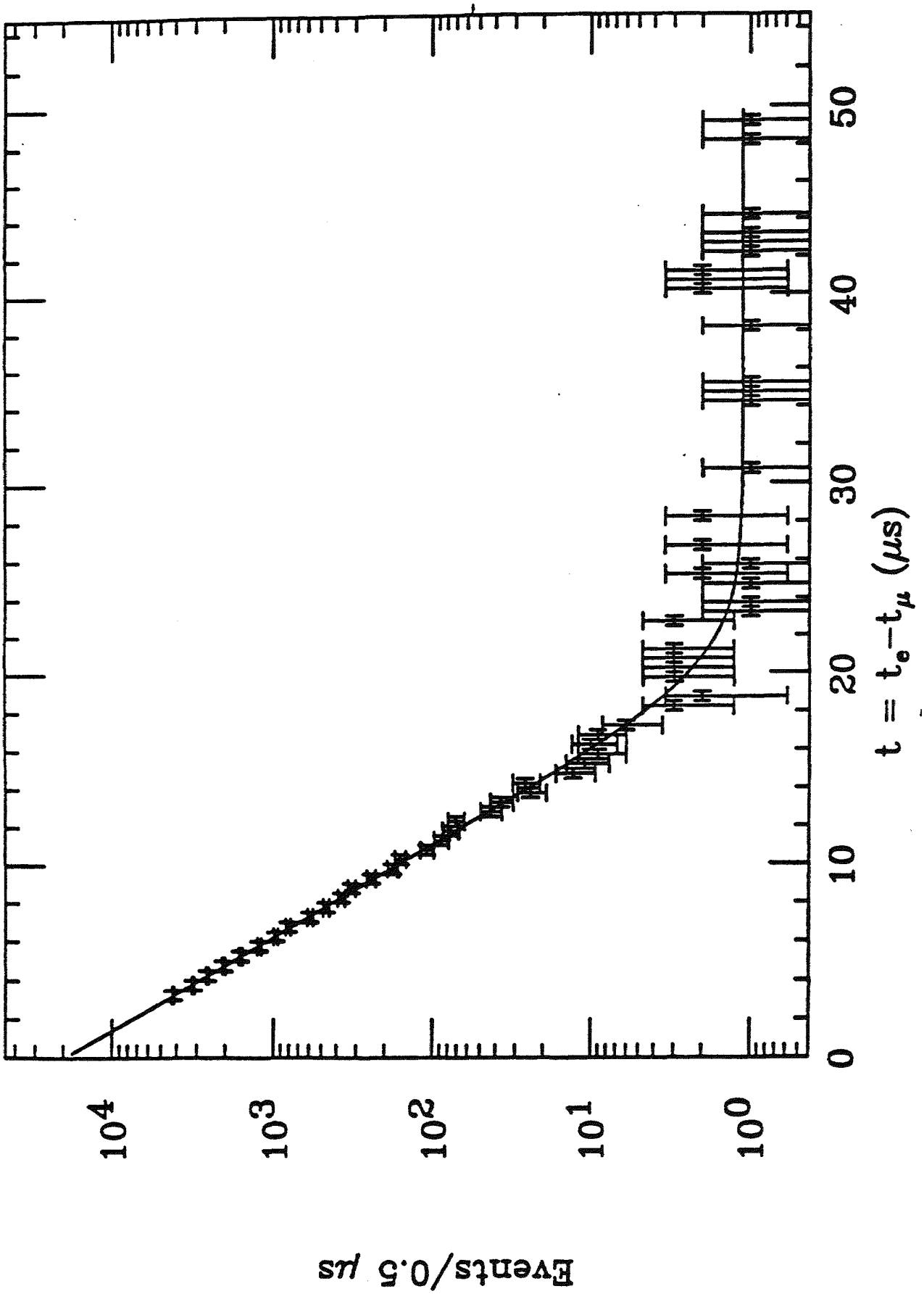

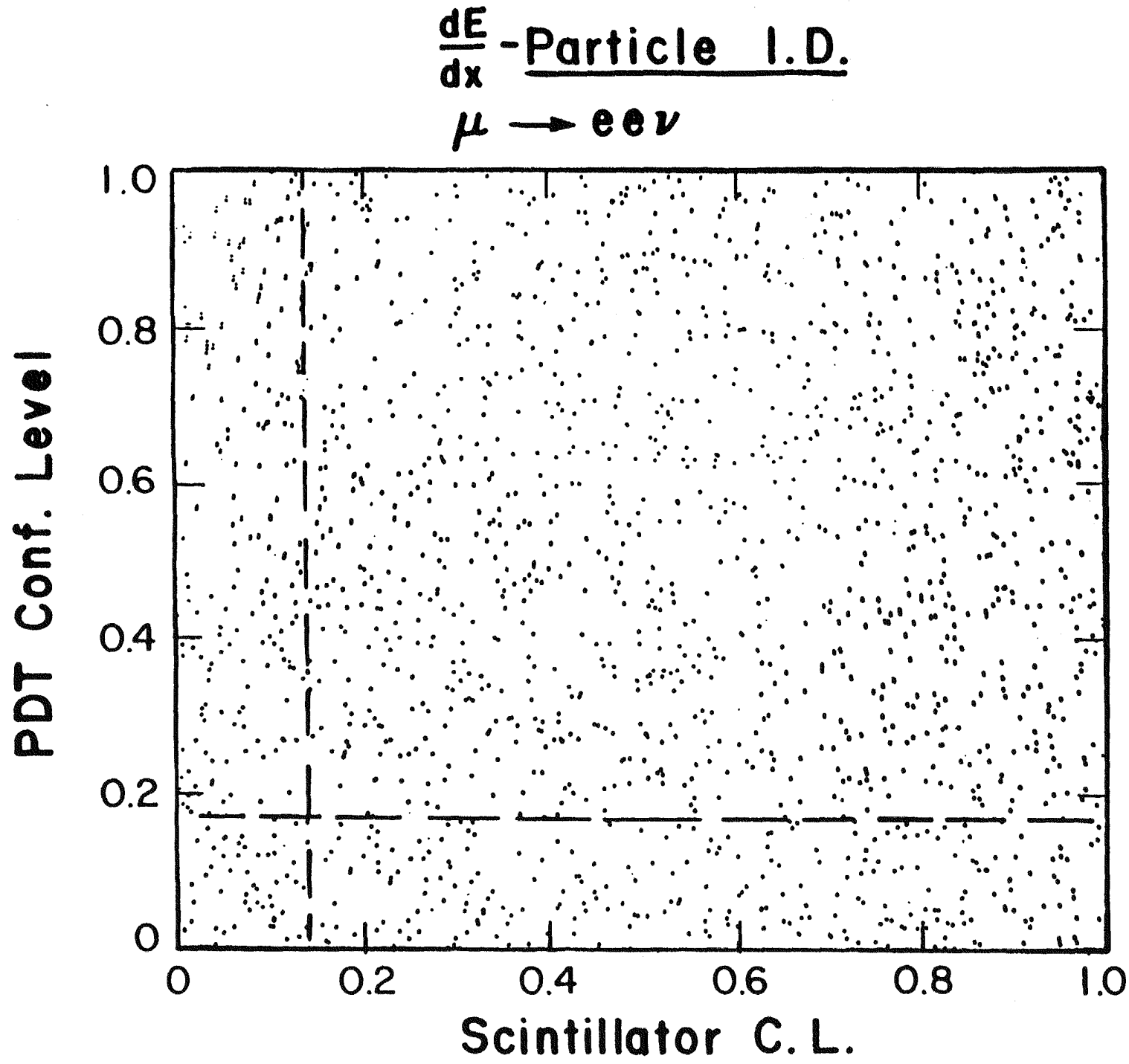
dE/dx - Particle I.D.
μ → eeν
PDT Conf. Level
1.0
0.8
0.6
0.4
0.2
0
0
0.2
0.4
0.6
0.8
1.0
Scintillator C. L.

Figure 10a

Figure 10b

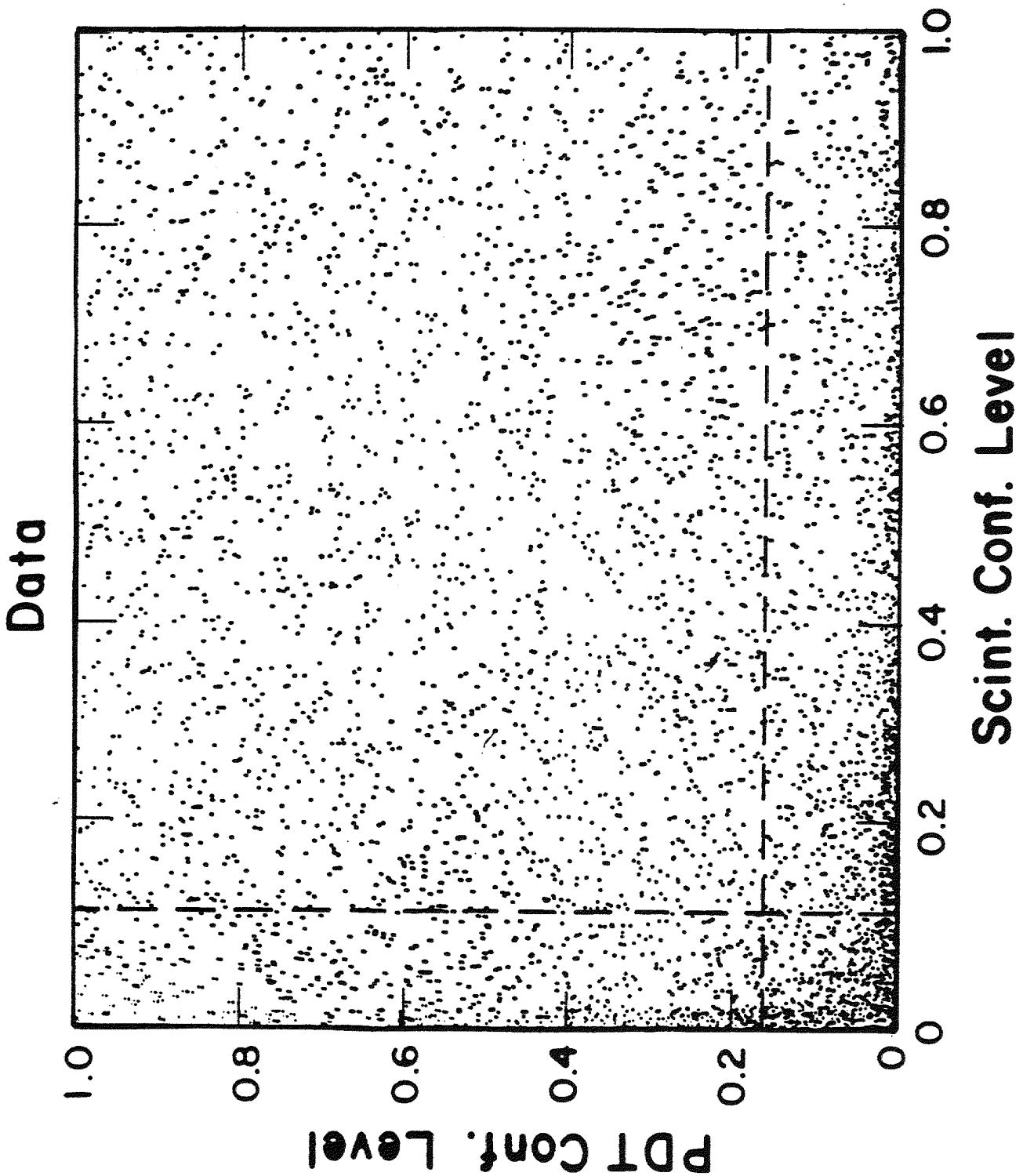

and (2) push limits further into the unexplored region of $\sin^2 2\theta$ and Δm^2. We were also motivated by the fact that the experiment then ran smoothly and data analysis procedures were well developed. Further, we do not expect competitive measurements soon in the new regions of $\sin^2 2\theta$ and Δm^2 that our experiment will explore. Table I indicates the division of responsibility and cost for the 1989 run. The LSU and OSU technicians, Anderson and Marterer and the LSU Research Associate Fazely were present for the entire run and handled most of the data taking. Imlay helped for 2-1/2 months in the summer and Metcalf made several trips to LAMPF. The OSU physicists needed to concentrate their effort on HERA and thus the LSU physicists provided the leadership for this last run.

Table I

Responsibilities For 1989 Run

LSU

- Scientific spokesman (Imlay and Metcalf).
- Postdoctoral Research Associate (Fazely).
- Technical Associate (Marterer).
- 25k$/year computer maintenance, miscellaneous.
- Analysis support.

Los Alamos

- Technical coordinator (Donahue).
- Analysis help (Bill Louis)
- Mechanical support (MP7).
- Electronics support for the shield (Sandberg, MP4).
- 20k$/year for P-10 gas.

OSU

- Technician and electronics support (Anderson).
- 5k$/year miscellaneous.

ANL

- Shield support

CEBAF

- Analysis support

8. Analysis Status

The 1988 data has been analyzed with the same selection criteria as the 1987 data. We are in the process of determining the detector efficiency and selection cut efficiencies for the 1988 data which may be slightly different from the 1987 data. We expect to also analyze the 1989 data with these selection criteria by the end of November. The larger event sample will then permit a better comparison of observed distributions with those expected from processes such as ν_e C and ν_e e elastic scattering as well as a better search for possible systematic effects. Results from experiment 866 at LAMPF indicate our neutrino flux normalization is correct. We are checking over the theoretical estimate of the ν_e C cross sections. Progress is also occurring on the analysis with slow neutron detection. This work, mainly by Brian Fujikawa (a graduate student at California Institute of Technology) is now giving preliminary limits comparable to those obtained without neutron detection.

We are also searching for electrons or muons above 60 MeV in order to set limits on $\pi^\circ \rightarrow \nu\bar{\nu}$ and exotic decays of muons such as $\mu^+ \rightarrow e^+ + \bar{\nu}_e + \nu_\mu$. This study is being done primarily by Ali Fazely, the LSU Research Associate. We also are studying the neutrinos from pion decay in flight ($\pi^+ \rightarrow \mu^+ + \nu_\mu$) in the beam stop region. We will compare our observed ν_μ sample with that expected from Monte Carlo calculation. Once we have confidence in our ν_μ DIF rate we can set neutrino oscillation limits on $\nu_\mu \rightarrow \nu_e$ by searching for electrons above 60 MeV.

9. Status of Neutrino Oscillation Studies

Developments in grand unified theories and the problem of missing mass in the universe have stimulated interest in neutrino oscillation experiments. The apparent signal observed by Reines, et. al.[9] has, however, been followed by null results at reactors[10] and accelerators.[11] . More recently, there have been reports of possible neutrino oscillations in an experiment at the Bugey reactor in France[12] (now withdrawn) and in an experiment at CERN[13] at a level which should be easy to see in E645. Recently, limits comparable to our published results have been reported for an experiment at BNL.[14] Since there is no theoretical guidance as to what mass or mixing angle to expect, it is important to extend the sensitivity over as broad a range of these parameters as possible. Experiment E645 will enable us to substantially improve existing limits on mixing angle as shown in Figure 1.

C. AMY Experiment at TRISTAN

1. Introduction

The AMY experiment at the TRISTAN e^+e^- storage ring at the the National Laboratory for High Energy Physics (KEK) in Japan, is an international collaboration of institutions and universities from Japan, Republic of Korea, People's Republic of China, and the United States. AMY is a high resolution, magnetic detector specialized for lepton detection. Until this year, TRISTAN had the world's highest e^+e^- energy, 61.4 GeV, and is designed to produce e^+e^- annihilations in the previously unexplored region $50 \leq \sqrt{s} \lesssim 70$ GeV.

In the first two years of TRISTAN operation its e^+e^- c.m. energy was the highest in the world. Consequently, it was of great interest to search for the onset of the production of new particles such as the top quark or a 4^{th} generation quark or lepton. Now, limits on new particle masses from $p\bar{p}$ colliders as well as new results from the SLC e^+e^- collider[15] , put most new particles out of the range accessible at TRISTAN. Consequently, the thrust of the AMY analysis effort is shifting towards precision measurements in the still unexplored TRISTAN energy region. In the TRISTAN energy region s/M_Z^2 is of the order of 30 to 60% and the interference between the electromagnetic and weak interaction is expected to be maximum, providing for important tests of the Standard Model. The high center of mass energy of the e^+e^- collision allows for good separation of the jets and their association with the underlying parent partons. These multi-jet events can thus be used to carry out a detailed study of QCD. Hence, there are still plenty of important physics topics to pursue at TRISTAN even though it is no longer the highest energy e^+e^- machine.

The Louisiana State University high energy group assummed primary responsibility in 1984 for the construction and operation of the AMY Muon Detector. The LSU group members have also been deeply involved in the analysis of e^+e^- annihilation to final states with leptons. Their efforts have directly contributed to some of AMY's most important physics results. Prof. Paul Kirk's intermediate energy group at LSU joined AMY in 1985 and was responsible for construction of the Ring Veto counters in the end-cap region of the AMY detector. Kirk is presently working on electronics for the forward tracking chambers to be installed this year as part of an AMY End-Cap Detector upgrade.

The first e^+e^- data at TRISTAN was recorded in November of 1986. To date TRISTAN has delivered over 30 pb^{-1} of e^+e^- luminosity in the CM energy range $50 < \sqrt{s} \leq 61.4$ GeV. AMY has concentrated its analysis effort on those

topics which could be studied with this limited luminosity. These results will be discussed following a brief description of the AMY detector.

Planned upgrades for TRISTAN should result in about a factor 3 increase in luminosity. The AMY detector is also being upgraded to increase the charged and neutral particle acceptance in the forward region and to improve the electron identification by the addition of a Xenon X-ray Detector.

2. The AMY Detector

The AMY detector, shown in Fig. 11, is based on a high field solenoid magnet. The 3.0 Tesla field makes possible precise momentum measurements in a small volume. Final state electrons, while traversing the strong field, emit synchrotron radiation which will be detected and used in conjunction with the barrel calorimeter to distinguish electrons from charged hadrons. The small tracking volume makes AMY particularly well suited for good muon identification. Background due to decay in flight are reduced and the hadron absorbing material can be made unusually thick without prodigious expense. Electron and single photon identification are enhanced by placement of a barrel electromagnetic calorimeter within the magnet coil preceeded by very little uninstrumented radiator.

The entire detector is compact and readily accomodates low-beta configurations of the storage ring. High luminosity is important because the e^+e^- annihilation cross section is expected to have a minimum in the TRISTAN energy region. Since our detector is specialized for lepton identification, we will also have superior sensitivity in studying the quark flavor composition of the annihilation data. AMY's emphasis on high luminosity, high quality lepton identification and good momentum resolution represents, in our view, the best match to the physics opportunities at this new facility.

a. The Tracking Chambers

Charged particile tracking is accomplished by a 4-layer cylindrical array of tube-type drift cells (Inner Tracking Chamber ITCH) followed by a 40-layer (25-axial and 15-stereo) cylindrical drift chamber (Central Drift Chamber CDC). Charged particles traverse all 44 layers down to polar angles $\theta = 33^\circ$ ($|\cos\theta| \leq 0.85$). Tracks as low as $\theta = 25^\circ$ are detected by 12 of the Central Drift Chamber layers as well as the inner 4-tube layers. The tracking chambers are located in a magnetic field volume supplied by a 3-Tesla super-conducting solenoidal magnet coil, so that despite the small tracking volume (the entire 44 layers span only the radii from 12.5 cm to 65 cm), a momentum resolution of $\Delta p_t/p_t = 0.6\% \times p_t$ (GeV/c) is achieved.

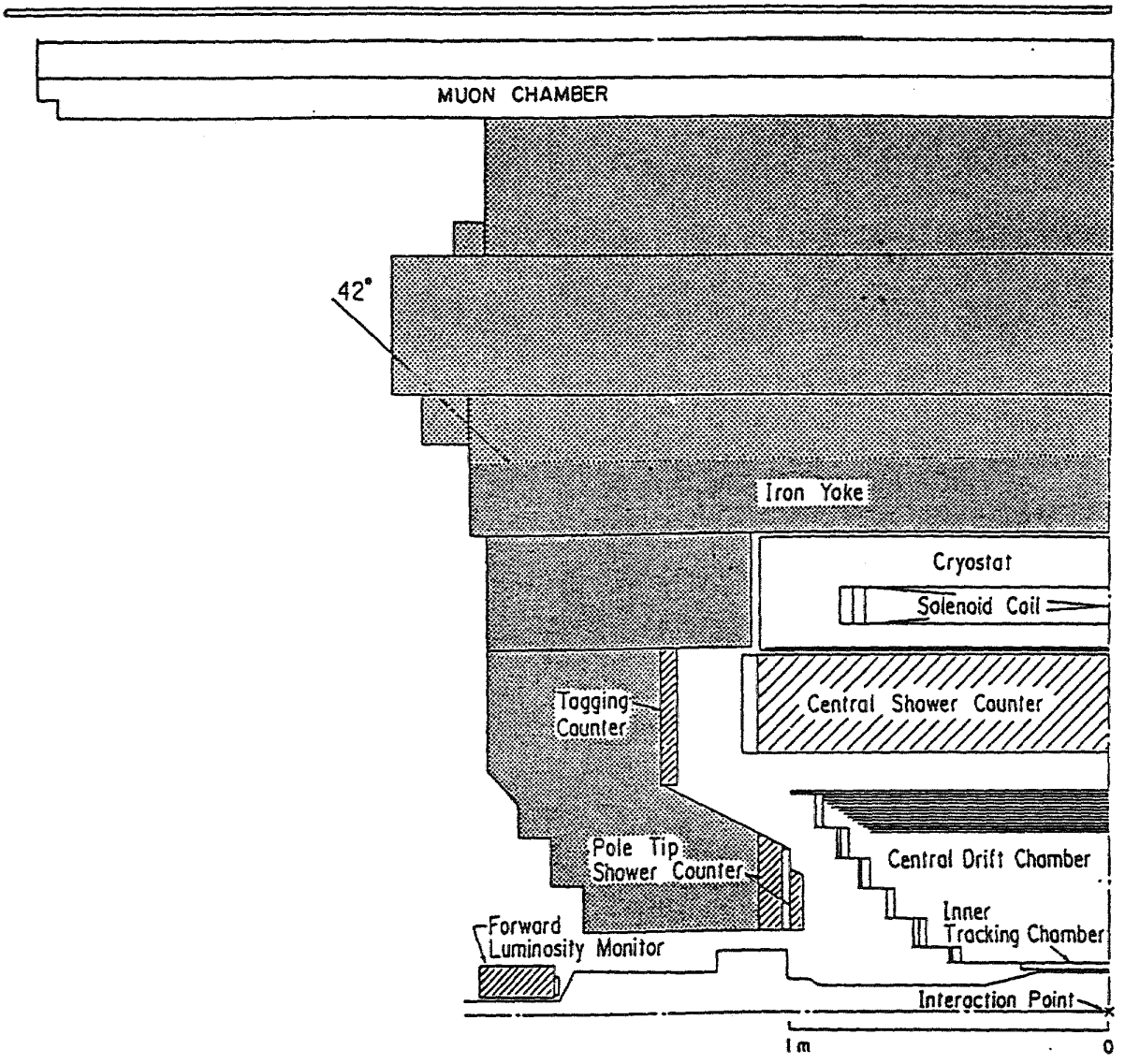

Figure 11. The AMY Detector

b. The Barrel Calorimeter

Situated radially outside the tracking chambers and inside the magnet coil is a cylindrical electromagnetic calorimeter (Central Shower Counter SHC) consisting of 20 alternating layers of lead and gas proportional tubes made of resistive plastic. Anode signal are recorded at each of the 20 layers; signals induced on othogonal cathode strips on either side of the anode wires are tower ganged into 5 depth groups. The SHC fully covers the angular region $|\cos\theta| \leq 0.73$. Using a combination of $e^+e^- \rightarrow e^+e^-$, $e^+e^- \rightarrow \gamma\gamma$, $e^+e^- \rightarrow e^+e^-e^+e^-$, and $e^+e^- \rightarrow e^+e^-\gamma$, the energy resolution is determined to be $\sigma_E/E(GeV) = 21\%/\sqrt{E} + 6\%$. The angular resolution is $\sigma \sim$ 5 mrad in both θ and ϕ. The energy resolution is worse than was observed in a test beam ($\sigma_E/E(GeV) = 25\%\sqrt{E}$) primarilly due to delta ray electrons which spiral in the 3-Tesla field depositing large energy on a single anode wire. These effects are being studied to determine corrections. The fine spatial resolution allows good separation of single photons from π^o decays. From analysis of test beam data, the π/e rejection factor for momenta greater than 3 GeV/c is expected to be better than 100 to 1 which is quite a bit better than the 40 to 1 rejection determined from monte carlo simulation of pions in AMY including the magnetic field. The difference is now under study.

During the summer of 1988, when TRISTAN was shutdown for the installation of RF cavities, repairs to faulty layers of the shower counter were attempted and resulted in severe damage to two of the six sextants of the device. These sextants were partially repaired in place during the subsequent down periods. Afterwards, while the repaired sextants were capable of measuring the gross properties of events; they were not suitable for performing the detailed measurements that constitute the long-range AMY program. Thus two new sextants were constructed and installed in September 1989 into AMY. They are ready to take data in the next run period.

c. The X-ray Detector

Sandwiched between the Central Drift Chamber and Central Shower Counter, is a 10 cm thick Xenon gas detector[16] . This device (called the X-ray Detecter – XRD) will detect the synchrotron x-rays emitted by final state electrons as they spiral through the high magnetic field. The converted x-rays will show up as extra, highly localized patches of ionization several millimeters to one side of the electron trajectory. The state of the art π/e discrimination provided by this device in conjunction with the SHC is necessary to fully achieve AMY's objectives. The three XRD modules were completed and extensively tested using HRS gas with cosmic rays prior to installation in Spring of 1989. The efficiency per wire for minimum ionizing tracks was found to be 90% and spacial resolution of $\sigma_{r\phi} \sim$ 1mm and $\sigma_z \sim$ 20mm was achieved. The XRD appears to be in good

shape and we are looking forward to getting useful data from this detector in the coming run periods. It is hoped that the device will achieve a π/e rejection of at least 100 to 1 at all TRISTAN energies while providing a superior 80% tagging efficiency for electrons.

d. The Muon Detector

AMY's muon detectors are located behind a hadron absorber that consists of 25 cm equivalent of iron in the SHC and magnet coil and 130 cm of iron in the flux return yoke. For the sake of muon identification, the yoke was made much thicker than required by the magnet coil. Particles must penetrate at least 9 absorption lengths of material and therefore AMY has a hadron rejection factor an order of magnitude better than other e^+e^- detectors. The extra iron reduces the background from hadron punch-through to a level less than decay in flight, which was already reduced due to the compact size of the tracking volume. One drawback of the thick hadron absorber is the minimum momentum necessary for a muon to penetrate it, 1.9 GeV/c. The penetration probability only approaches 100% for transverse momenta greater than 2.5 GeV/c. However, we consider the benefits of superior muon identification capabilities as far out-weighing the loss of detection efficiency for low momentum muons.

The Muon Detector consists of 6 large area drift tube chambers. The chambers cover with overlaps, the six rectangular faces of the hexagonal magnet yoke. In the radial direction each chamber has four layers, two layers (staggered by a half-cell) with transverse wires followed by two with axial wires. The double layer structure ensures high efficiency as well as allowing resolution of the right-left ambiguity. The position resolution of these chambers (a few mm) far exceeds that necessary to match muon tracks with tracks extrapolated from the Central Drift Chamber which undergo significant multiple scattering in the hadron absorber. The muon wire chambers cover the angular region $|\cos\theta| \leq 0.74$. Outside of the wire drift chambers is a layer of scintillation counters providing timing necessary ($\sigma_t \sim 3$ ns) to distinguish muons originating from the e^+e^- interaction from cosmic rays. The counters were obtained from stocks of previously used scintillator supplied by LSU, VPI, and University of Rochester with new tubes purchased by LSU. The counters are grouped into 12 half-sextants and this facilitates the making of a muon trigger. Altogether there are 1184 separate wire channals and 163 separate counter channals. The entire Muon Detector, associated electronics, and online and offline detector software, has been and continues to be the primary responisibility of the LSU group. The detector is 100% operational with only a handfull of dead wire channals, which we are fixing. Maintenence of the hardware is now being accomplished by one LSU on-site post-doctoral researcher, Seong Myung, and one LSU graduate student, Jit Ning Lim; with

the assistance of LSU based personnel who travel periodically to KEK. Maintenance to the detector typically involves replacement of electronics endboards and preamp-discriminator cards on the wire chambers and photo-multiplier tubes on the counter system. Only a handfull of such replacements were made during the previous year of running of the detector.

e. End-Cap Detectors

This past summer the AMY End-Cap detectors were upgraded to provide improved energy resolution and hermiticity. Removed were the original Pole-Tip Calorimeter (PTC) and Ring Veto Counter (RVC) (built by Paul Kirk's Intermediate Energy Group at LSU). These detectors were replaced by a Pb-Scintillator Counter with an energy resolution of $\sigma_E/E \sim 15\%/\sqrt{E(GEV)} + 2\%$ (measured in a test beam) covering the region $11^\circ \leq \theta \leq 38^\circ$ and an upgraded small angle luminosity monitor covering the region $2^\circ \leq \theta \leq 11^\circ$. This will allow precise measurements of the electromagnetic energy from particles in the forward region. Paul Kirk during his Sabatical leave worked on the design of the upgraded End-Cap Calorimeter. The device was built by KEK personnel.

Improvements to the end-cap calorimetry are complimented by tracking improvements in this region. In di-lepton, two-photon, and hadronic events it is important to cover as much solid angle as possible. Di-lepton and hadronic events are produced with a cross section that includes and overall factor $(1 + \cos^2\theta)$ and two photon interactions produce final states with even more forward-backward enhancement. With the increased tracking coverage afforded by the new AMY End-Cap Detector, muon-pair production ($e^+e^- \rightarrow \mu^+\mu^-$) can be studied in angular regions where the asymmetry due to weak interference is pronounced. Thus, the overall detection efficiency for final state particles and the ability to reconstuct jets will be improved by installation of forward tracking. The University of Rochester group has designed and proto-typed the forward tracking chamber. The complete design for the new AMY End-Cap is shown in Figure 12, including the micro-beta focusing magnets to be installed in Summer of 1990 for high luminosity TRISTAN operation.

Paul Kirk of LSU is responsible for the electronics associated with the forward tracking system. The electronics includes boards to perform high and low-voltage distribution and pre- and post-amplification of the signals. Like the muon drift chamber electronics developed 3-4 years ago, electronics for the forward tracking chamber are being developed primarilly outside of LSU at the Univ. of Rochester. While LSU is capable of developing the electronics, it lacks the facilities to take on all the work and must rely of Rochester to provide designs and artwork for the electronics and then outside companies to make the PC boards. These extra links in the development of electronics have introduced delays and inconvenience. The

forward tracking chamber system is not yet ready for installation while further iteration of the electronics design takes place. Rochester is overburdened to produce the drift chambers and continue to design electronics. On the other hand the forward calorimeter which was developed in Japan is now installed and due to take data this fall without the forward tracking chamber system. Having a PC board making facility including a minimum CAD system, would allow LSU to fully participate in electronics and nuclear instrumentation development and produce results on a timely basis. Such a facility has been proposed to the LSU board of Regeants this past October.

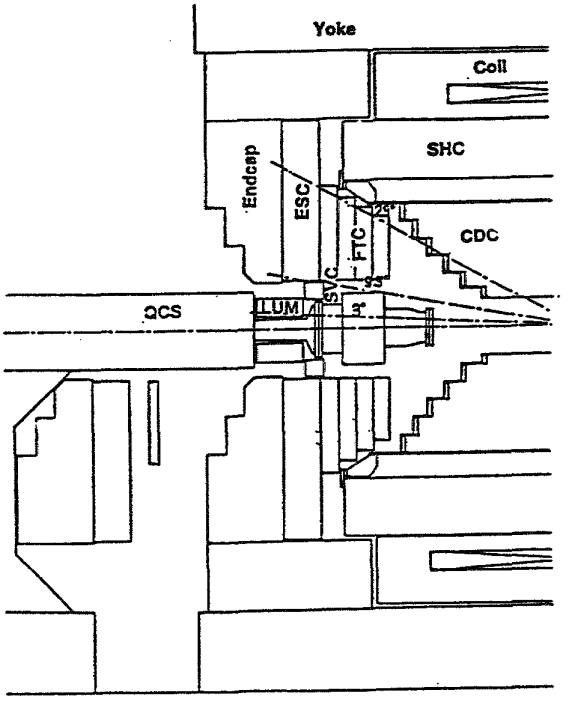

Figure 12. Proposed AMY End-Cap Detector Upgrade

3. Physics Results from AMY

To date, AMY has published eight papers in journals in Physical Review Letters, three more are accepted for publication and will appear in print very soon, and two more were submitted in the last month. A list of these papers is provided in the CVs. Additional papers are in the preparation phase after the preliminary results were presented at international conferences this past summer. Many of the results contained in the papers rely heavily on the analysis of muons identified in the AMY Muon Detector, and three of the papers have been written and/or heavily contributed to by LSU personnel. These analyses will be presented in the following selection of physics results.

a. Lepton Pair Production

Since the leptonic reactions $e^+e^- \rightarrow \mu^+\mu^-$ and $e^+e^- \rightarrow \tau^+\tau^-$ have only point-like particles in both the initial and final state, they provide sensitive and unambiguous tests of the standard SU(2) × U(1) theory of the electro-weak interactions.[17] In this theory, the differential cross sections far above threshold is expressed in the lowest order[18] ($\ell = \mu$ or τ)

$$\frac{d\sigma}{d\Omega} = \frac{\alpha^2}{4s} R_{\ell\ell}[(1+\cos^2\theta) + \frac{8}{3} A_{\ell\ell}\cos\theta], \tag{1}$$

where θ is the angle between the outgoing negative μ or τ direction and the e^- direction, $R_{\ell\ell}$ is the ratio of the total cross section for $e^+e^- \rightarrow \ell^+\ell^-$ to that expected from QED alone, and $A_{\ell\ell}$ is the forward-backward asymmetry. $R_{\ell\ell}$ and $A_{\ell\ell}$ can be expressed in terms of the vector and axial-vector weak neutral coupling constants g_V and g_A, and the Z^0 contribution χ, as

$$R_{\ell\ell} = 1 - 8g_V^e g_V^\ell \chi + 16(g_V^{e\,2} + g_A^{e\,2})(g_V^{\ell\,2} + g_A^{\ell\,2})\chi^2 = \frac{\sigma_{\text{total}}}{\sigma_{\text{QED}}} \tag{2}$$

$$A_{\ell\ell} = -6 g_A^e g_A^\ell \chi \tag{3}$$

$$\chi = \frac{1}{16\sin^2\theta_W \cos^2\theta_W} \frac{s}{(M_Z^2 - s)} \tag{4}$$

where the standard model predictions for the couplings are $g_A^e = g_A^\ell = -0.5$ and $g_V^e = g_V^\ell = -1/2(1 - 4\sin^2\theta_W)$. Despite the relatively large value of the factor χ at TRISTAN energies ($\chi \sim -0.2$ at $\sqrt{s} = 52$ GeV), the effect on the cross section is weak due to the small value of $g_v \sim -0.04$. However, the forward-backward asymmetry $A_{\ell\ell}$ are sensitive to the axial coupling $g_A^e g_A^\ell$ and are expected to

be large at TRISTAN energies. Previous measurements of the differential cross section at PEP[19] and PETRA[20] are in good agreement with the predictions of the model. Here I report on results from AMY[1] published earlier this year, and the subject of Ph.D. Theses by Angelina Bacala of LSU and Rusty Malchow of UC Davis. Bill Metcalf of LSU directed the Di-lepton analysis effort and wrote the paper.

Various track patterns in the tracking chambers and signals in the central shower counter were used to trigger the reactions $e^+e^- \rightarrow \mu^+\mu^-$ and $e^+e^- \rightarrow \tau^+\tau^-$. The triggers were enabled both at the beam crossing time (beam gate) and for an equal time midway between beam crossings (delayed gate) to monitor cosmic ray backgrounds. The trigger efficiency within the geometric acceptance of the detector was determined to be $94 \pm 2.6\%$ for $e^+e^- \rightarrow \mu^+\mu^-$ events and $96.0 \pm 3.0\%$ for $e^+e^- \rightarrow \tau^+\tau^-$ events.

The topology of $e^+e^- \rightarrow \mu^+\mu^-$ events is two back-to-back tracks, where each track: i) is consistent with originating from the interaction point ii) has a momentum that is consistent with the beam energy, iii) has a shower counter energy deposition consistent with minimum ionizing particles, and iv) has hits in the muon detection system ($|\cos\theta| \leq 0.74$) consistent with extrapolations of the observed tracks. In addition, the flight times of the particles from the interaction point to the muon detector, measured by scintillation counters, was required to be in time and consistent with two particles emerging from the beam-beam collision and inconsistent with a single cosmic ray particle traversing the detector (the cosmic ray transit time is typically 25ns). The detection efficiency of muon pair production is 59% including geometrical acceptance and the background from cosmic rays is about 2%.

Tau-pair events were searched for among all events that had two or more charged particle tracks with $|\cos\theta| \leq 0.73$. Events were selected if they had either two nearly back-to-back tracks or one track recoiling against a tightly collimated cluster of two or more tracks. The total invariant mass of the particles in a cluster was required to be below 2 GeV/c^2. In addition, the total visible energy was required to be greater than 20% of the total c.m. energy. Two-track events where both tracks were muons or electrons were rejected in order to reduce backgrounds from Bhabha scattering $e^+e^- \rightarrow e^+e^-$ and two-photon processes $e^+e^- \rightarrow e^+e^-e^+e^-$ and $e^+e^- \rightarrow e^+e^-\mu^+\mu^-$. The overall detection efficiency including geometrical acceptance and accepted branching decay modes is determined to be 25% and the background level about 5%.

The differential cross sections for the combined data from c.m. energies 50-57 GeV are shown in figure 13. Acceptance, trigger efficiency, and radiative corrections[23] have been applied to the data on a bin-by-bin basis in $\cos\theta$. In all

cases, a forward-backward asymmetry is readily apparent. The solid curves are fits to the data and the dotted curves are the standard model predictions with $\sin^2\theta_W = 0.23$ and $M_Z = 92.5 GeV/c^2$.

By fitting the differential cross section to eqn. 1, $R_{\ell\ell}$ and $A_{\ell\ell}$ are extracted. The measurements of $A_{\ell\ell}$ and $R_{\ell\ell}$ are summarized in Table 2. The measured asymmetries are shown together with previous measurements at lower energies,[19,20] and the results of VENUS[21] and TOPAZ[22] at TRISTAN in Figure 14. The experimental results show a large increase in the forward-backward asymmetry between the previously highest available energies and AMY. The theoretical prediction for the asymmetry, using the values for $\sin^2\theta_W$ and M_Z given above, are included in Fig. 14. The measured asymmetries for muons and taus are in good agreement with the electroweak predictions. Consequently, the extracted axial-vector couplings also agree with the model. On the other hand, the extracted vector couplings have large errors and a meaningful comparison with the theory is not yet possible. Analysis of data from recent running is being carried out by Univ. of South Carolina, LSU, and UC Davis.

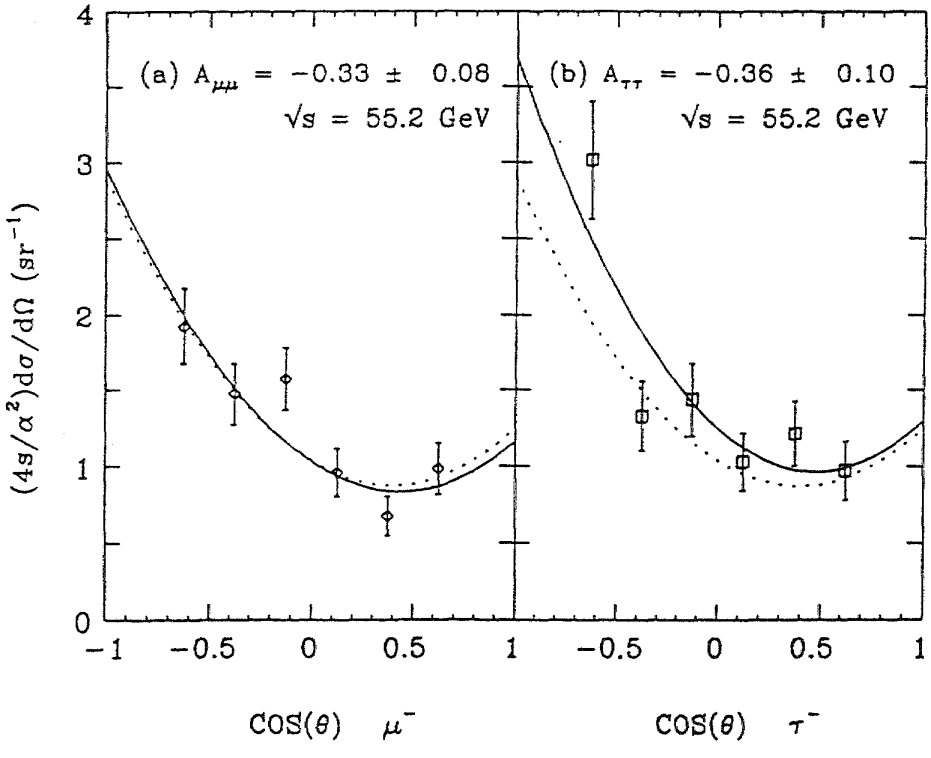

Figure 13 The differential cross sections for (a) $e^+e^- \to \mu^+\mu^-$ and (b) $e^+e^- \to \tau^+\tau^-$

Table 2. The measured Asymmetries and Weak coupling Constants

Energy (GeV)	52	55	56	57[10]	55.2 (AVERAGE)
$A_{\mu\mu}$	-.434 ±.170	-.110 ±.165	-.300 ±.124	-.462 ±.149	-.327 ±.074
$A_{\tau\tau}$	-.184 ±.192	-.177 ±.261	-.459 ±.166	-.495 ±.180	-.363 ±.096
$A_{\ell\ell}$ Std model	-.249	-.294	-.312	-.330	.298
$R_{\mu\mu}$	1.02 ±0.14	0.80 ±0.16	1.09 ±0.12	1.12 ±0.13	1.03 ±0.07
$R_{\tau\tau}$	1.43 ±0.26	1.12 ±0.26	1.16 ±0.20	1.36 ±0.27	1.25 ±0.12
$R_{\ell\ell}$ Std model	1.026	1.037	1.041	1.046	1.037
$g_A^e g_A^\mu$	0.44 ±0.17	0.10 ±0.15	0.25 ±0.10	0.36 ±0.12	0.26 ±0.06
$g_A^e g_A^\tau$	0.19 ±0.19	0.15 ±0.23	0.37 ±0.14	0.38 ±0.14	0.32 ±0.08
$g_A^e g_A^\ell$ Std model	0.25	0.25	0.25	0.25	0.25
$g_V^e g_V^\mu$	0.07 ±0.17	0.14 ±0.11	-.04 ±0.09	-.02 ±0.12	0.03 ±0.06
$g_V^e g_V^\tau$	-.36 ±0.23	-.08 ±0.19	-.06 ±0.19	-.21 ±0.23	-.16 ±0.10
$g_V^e g_V^\ell$ Std model	.002	.002	.002	.002	.002

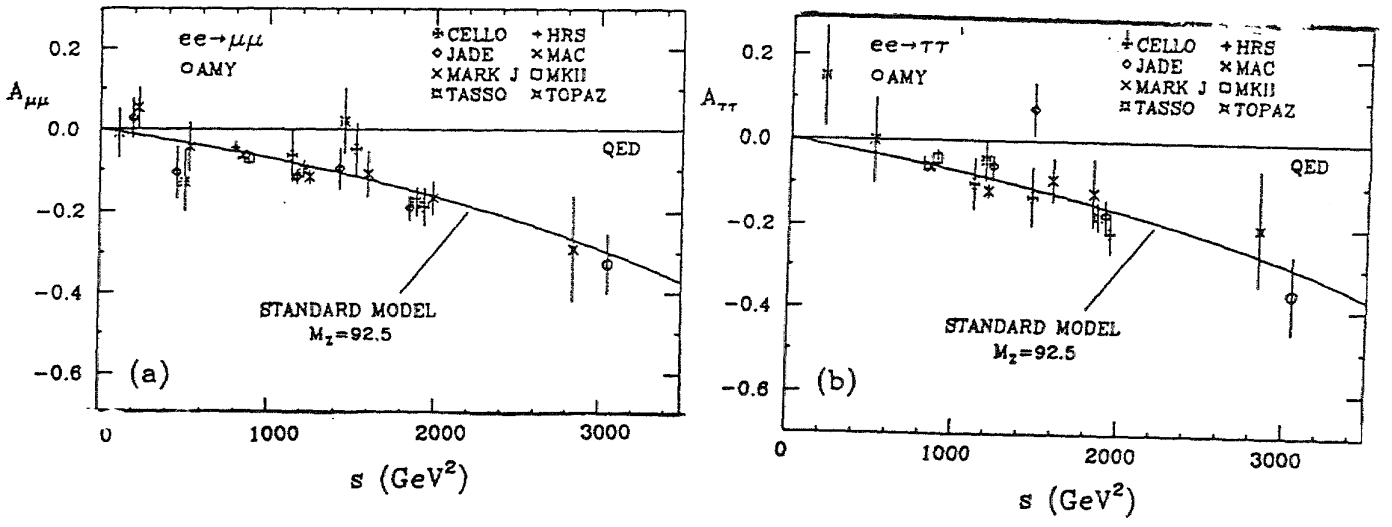

Figure 14 The forward-backward charge asymmetry for (a) $e^+e^- \to \mu^+\mu^-$ and (b) $e^+e^- \to \tau^+\tau^-$

b. Hadronic Events with Leptons

The following analyses were heavily contributed to by R. McNeil, S. Myung, and Jit Ning Lim of LSU. The process considered was $e^+e^- \rightarrow$ Hadrons + ℓ where $\ell = e, \mu$). A brief description of the event selection and lepton identification will preceed a report of the results.

The detector is triggered for multi-hadronic annihilation events by energy deposition in the barrel, and by a variety of track patterns from the ITC and CDC chambers. The latter includes two track and multi-track triggers. Multi-hadronic annihilation events were selected using the criteria described in ref. 24, namely: (a) five or more charged tracks in the CDC with $|\cos\theta| \leq .85$; (b) the total visible energy (E_{vis}) in the CDC and SHC in excess of half the total CM energy; (c) the total longitudinal momentum imbalance is less than $0.4E_{vis}$; and (d) at least 3 GeV (5 GeV for $\sqrt{s} \geq 56$) of energy deposited in the SHC. These cuts reduce the contamination from two-photon initiated processes, tau pairs and beam gas interactions to a level of less than 2%.

Muons are identified by the ability to penetrate the SHC, coil, and hadron absorber (over 9 interaction lengths). Muons in multi-hadronic events are selected by requiring hits in any three of the four muon chamber layers and by matching the hits to an extrapolated CDC track. The muon counter timing information is used to reject cosmic ray tracks that are out of time with the beam crossing. When a track is within a hadronic jet, the CDC reconstruction efficiency is about 95%. The reconstruction efficiency of the muon detection system was determined to be 98% from a study of cosmic ray muons. Backgrounds to the muon signal (hadron fakes) arise principally from hadron showers in the hadron filter, where the debris reaches the muon chamber (punchthroughs), or from the decay of $\pi^{\pm}$ and $K^{\pm}$ mesons, before they are absorbed in the hadron filter, to a muon that reaches the muon chamber (decay). A matching distance cut was chosen to maintain high efficiency for muons orginating from the decay of a heavy quark (prompt) and suppress the above hadron fake background. This matching distance cut was determine from a study of true muons (from the $e^+e^- \rightarrow e^+e^-\mu^+\mu^-$ data sample and those in the prompt muon fraction orginating from the c and b flavor hadrons in a Monte Carlo simulation). It is a smooothly varying function of the extrapolated track momentum at the muon chamber, becoming almost constant (at 14cm) above 5 GeV/c. About 88% of the true muons that are reconstructed by the CDC and the muon chamber system satisfy the matching distance cut. A minimum momentum of 1.9 GeV/c is required for the muons to penetrate the hadron filter. The overall detection efficiency for muons above

3 GeV/c in the angular region of $|\cos\theta| \leq 0.74$ is 82%. The estimated hadron fakes amount to about 35% of the data sample of which 60% are punchthroughs and about 40% are decays. Even though our punchthrough calculation, which is based on the GHEISHA program[25], agrees well with available experimental data from pions, data from kaons is not available in our energy range. We estimate that about half of the punchthrough are induced by K^+ mesons, mainly because of its smaller absorption cross section in the iron. This will be a main source of systematic uncertainty in analyses where a punchthrough background subtraction is performed. The number of muon candidates with a matching CDC track of momentum greater than 1.9 GeV/c selected for each beam energy run is given in Table 2.

Electrons in the multi-hadronic events are selected by their energy deposition in the SHC ($|\cos\theta| \leq 0.73$). A shower in the SHC is defined as an energy cluster greater than 0.2 GeV within the region of $\pm 3°$ in both θ and ϕ direction. Charged tracks with momentum greater than 2.5 GeV/c and within $\pm$3cm of a shower are classified as electron candidates if the ratio of the energy measured in the calorimeter to the momentum of the charged track and the longitudinal shape of the shower is consistent with that of an electromagnetic shower. The efficiency for selection of isolated electrons is determined to be 71% for P > 2.5 GeV/c, by applying the electron selection requirements to a sample of electrons from $e^+e^- \rightarrow e^+e^-e^+e^-$ events. The Monte Carlo simulator gives comparable efficiency. The algorithm misidentifies isolated charged hadrons as electrons with probability 1/55, according to the Monte Carlo simulation. Measurements in a test beam suggest even better hadron rejection.

The data taken at the higher c.m. energy $\sqrt{s} > 57$ GeV are marked by a decreased energy resolution in two out the six units that comprise the SHC. To compensate for this effect, the electron identification criteria were loosened to maintain an efficiency comparable to that obtained at the lower energies. In this case for these two units, the e/π rejection factor was reduced to 1/20. The number of electron events selected for each beam energy run is given in Table 3.

Table 3. The Luminosity, number of hadronic events, and the number of inclusive lepton events for various c.m. energies.

$\sqrt{s}$ (GeV)	50~52	55~57	> 57	total
$\int Ldt(\mathrm{pb}^{-1})$	4.62	14.65	10.28	29.54
hadronic events	570	1710	1269	3549
muon events	30	93	57	180
electron events	44	154	202	400

Search for Isolated Leptons

At e^+e^- energies just above production threshold, the decays of new heavy quarks, which are nearly at rest, result in isotropic event topologies that are quite distinct from the 2-jet structure characteristic of lighter quark production. Quarks carrying a new flavor quantum number would have three-body semileptonic weak decays with branching fraction of 1/9 for each of the e, μ and τ channels. The kinematics of the semileptonic decay process results in final state leptons that are usually well separated from the associated hadrons. Thus, multi-hadronic e^+e^- annihilation events with final state isolated leptons are a good signature for the production of new heavy quarks . The observation[26] at CM energies $46.3 \leq \sqrt{s} < 46.8$ GeV of events with low thrust containing muons at wide angles relative to the thrust axis by the Mark J and JADE experiments at the PETRA e^+e^- storage ring has been interpreted as an indication of the production of a new charge $-1/3$ quark.[27] However, since an excess of such muon events has not been seen by the CELLO experiment at PETRA,[28] and since none of the PETRA experiments have seen similar events with electrons, the experimental situation remains unsettled. The AMY experiment at TRISTAN has previously reported[3] on a search for such events at $\sqrt{s} = 50$ and 52 GeV with a total integrated luminosity of 4.7 pb^{-1}. We continue to search for an excess of hadronic events with isolated leptons in both the muon and electron channel using Mark J criteria for isolation and criteria developed by the AMY group which were found to be more sensitive to new heavy quarks. Recently, the VENUS group at TRISTAN reported[29] an anomalous yield of events with isolated leptons for c.m. energies of 60 GeV and higher. LSU's S. Myung and former LSU graduate student Angelina Bacala (now at Rutgers) performed the AMY analysis which was reported at this year's Lepton-Photon Conference. The following is a summary of the analysis.

The topological event shape is parameterized by means of the variable thrust, which ranges in value from 0.5 (for perfectly isotropic events) to nearly 1.0 (for back-to-back two-jet events). We select events that contain identified leptons (electrons and/or muons) and have a thrust value less than 0.9 when the lepton is excluded from the calculation of thrust. We also require that the energy sum of charged and neutral particles within a cone of half-angle 30° coaxial with the lepton direction to be less than 1 GeV. A primary background source for isolated electron events (not present in the muon case) is the two-photon process $e^+e^- \rightarrow e^+e^- +$ hadrons. To reduce the number of events from this reactions, isolated electron events are required to satisfy two additional requirements: 1) the invariant mass of all detected particles other than the electron is greater than 10 GeV/c^2; and 2) the electron momentum is less than 16 GeV/c. Details

of these selection criteria are described in reference [30].

For comparison, we have also selected isolated leptons using criteria used by the VENUS and Mark-J experimental groups. The VENUS group requires the lepton momentum to be above 4 GeV/c, thrust less than 0.9 and isolation cone energy to be less than 1.0 GeV. The Mark-J group requires thrust less than 0.8 and cosine of the angle between the lepton direction and the thrust axis to satisfy $|\cos\theta| \leq 0.7$.

We have used the LUND 6.3 event generator[31] to generate five flavor $q\bar{q}$ Events, and t quark ($Q\overline{Q}$) events, and the EPOCS[32] generator for $b'\bar{b}'$ events. From an analysis of simulated events we determine that our selection criteria are 15.5% (21%) effiecient for the $b'\bar{b}'$ ($t\bar{t}$) events while the rejection for the background five flavor $q\bar{q}$ events is about 1/900.

In the entire data sample we have observed six isolated electrons and one isolated muon event that pass the AMY criteria. Table 4 shows the number of observed isolated lepton events for different beam energies together with the number expected from the five flavor MC. In addition we have applied the same analysis to simulated events for two-photon processes using the quark parton model (QPM), the vector dominance model (VMD), and the high p_t vector dominance model. In these estimates we used a new radiative correction, including full electroweak effects up to $O(\alpha^3)$, developed by Fujimoto and Shimizu (FS)[33] .

The observation of seven isolated leptons is consistent with the sum of the expected backgrounds of 4.70 ± 0.69 for the five flavor $e^+e^- \rightarrow q\bar{q}$ annihilation process and 0.44 ± 0.10 for the two-photon process. In table 3, we also show our results using the VENUS and Mark-J criteria for isolated leptons. Using the VENUS criteria, we observed 9 isolated lepton events (0 muon and 9 electron) compared to an expected 2.95 ± 0.54 events from ordinary five-flavor quark production plus 1.20 ± 0.16 events from the two-photon process. Five of the observed events are in the 55 to 57 GeV c.m. energy data and four occur at 60 GeV and above. Using the Mark-J criteria, there are eleven observed events (9 electron and 2 muon) compared to an expected total of 13.7 ± 1.07 events.

In the absence of an excess of isolated lepton events, we can set limits on the pair production of heavy quarks. Table 5 compares the observed number of isolated leptons with a Monte Carlo determined expectation for heavy quark production. As can be seen from the table, we find no evidence for heavy quark production for any of the isolation criteria.

In order to obtain lower limits on the masses of new heavy quarks, we have compared our observations with theorectical predictions. We make no background subtraction to the observed number of events, making the mass limit

conservative.

The expected number of events for the case of heavy quark production is given by

$$N_{Q\bar{Q}} = \epsilon_{Q\bar{Q}}(1+\delta)\int Ldt \times \sigma_{Q\bar{Q}}$$

where $\epsilon_{Q\bar{Q}}$, the efficiency for finding isolated leptons from heavy quark events, is $15.5 \pm 1.5\%$ for b' and $21.0 \pm 2.0\%$ for t quark. The quoted error for the efficiency includes both statistical errors and uncertainties in the fragmentation function and the inefficiency of lepton identification. The radiative correction factor for heavy quark production, $(1+\delta)$, is obtained from the FS calculation and parameterized as $\delta = -\exp(-4.13\beta - 0.69)$, where β is the velocity of the heavy quark. Errors from the luminosity measurement are included as a statistical error and 2.4% overall systematic error. We include weak and first order QCD effects for the calculation of $\sigma_{Q\bar{Q}}$.

Using the AMY isolated lepton selection criteria, we set 95% confidence-level mass limits for b' and t quarks of 28.9 GeV/c^2 and 30.4 GeV/c^2 repectively. In conclusion, our observation of seven isolated leptons events is consistent with Monte Carlo expectation for five flavors quark production and two-photon hadron production. We do not confirm the VENUS report of a new source of isolated leptons for c.m. energies of 60 GeV and above.

Isolated Muon

$\sqrt{s}$ (GeV)		50~52	55~57	> 57	total
Data	AMY cut	0	1	0	1
	Venus cut	0	0	0	0
	Mark-J cut	0	1	1	2
5-flavor MC	AMY cut	0.47±0.21	0.98±0.35	0.33±0.13	1.78±0.43
	Venus cut	0.28±0.16	0.84±0.33	0.11±0.08	1.23±0.38
	Mark-J cut	1.13±0.33	2.05±0.53	0.77±0.21	3.96±0.65

Isolated Electron

$\sqrt{s}$ (GeV)		50~52	55~57	> 57	total
Data	AMY cut	0	3	3	6
	Venus cut	0	5	4	9
	Mark-J cut	0	3	6	9
5-flavor MC	AMY cut	0.47±0.21	1.23±0.42	1.21±0.27	2.92±0.54
	Venus cut	0.19±0.13	0.61±0.29	0.92±0.23	1.72±0.39
	Mark-J cut	0.47±0.21	2.62±0.56	6.28±0.60	9.37±0.85
2γ MC	AMY cut	0.08±0.02	0.24±0.08	0.12±0.05	0.44±0.10
	Venus cut	0.19±0.04	0.59±0.13	0.42±0.09	1.20±0.16
	Mark-J cut	0.06±0.02	0.19±0.07	0.12±0.05	0.37±0.09

Table 4. The number of observed isolated lepton events for different isolation cuts, compared with expectations for five quark flavors. For the isolated electrons, background estimates from two-photon processes are also given. Only statistical errors are listed.

		AMY cut	Venus cut	Mark-J cut
Electron	Data	6	9	9
	b′ quark MC	21.9±1.44	20.3±1.39	17.2±1.28
	t quark MC	80.5±4.74	63.3±3.79	67.7±3.80
Muon	Data	1	0	2
	b′ quark MC	25.3±1.55	21.6±1.43	20.1±1.38
	t quark MC	98.0±4.57	76.9±4.05	69.6±3.86

Table 5. The number of observed isolated lepton events compared with expectations for the pair production of heavy quarks (t or b′) with full excitation. The heavy quark mass is taken to be 27.5 GeV/c^2. Only statistal errors are listed.

Measurement of the b quark forward-backward Asymmetry

In the standard model of electroweak interactions, the quarks and leptons form left-handed doublets and right-handed singlets in the weak isospin representation. While there is as yet no direct evidence for the sixth quark (t quark), the scheme with three families of doublets of leptons and quarks, including the t quark as a counterpart of the b quark, has been successful in explaining a wide range of experimental phenomena. It is therefore generally accepted that the t quark will eventually be found as higher energy accelerators become operational. Meanwhile, in the absence of direct experimental evidence for the t quark, it is an important test of the standard model to continue to check whether the properties of the b quark are consistent with the interpretation of the b quark as a $T_3 = -1/2$ member of a $(t\ b)_L$ weak isopin doublet, where T_3 is the third component of weak isospin. Production of $b\bar{b}$ in e^+e^- annihilation at c.m. energies with significant contributions from the Z^0 provides an excellent testing ground for this interpretation. The coupling of the $b\bar{b}$ pair to the Z^0, expressed in terms of the vector- and axial-vector coupling constants, g_A^b and g_V^b, depends of T_{3L} and T_{3R}, where L and R stand for left-handed and right-handed, respectively. Thus the coupling varies depending on whether the b quarks are assigned to a doublet or a singlet. While this difference has some effect on R_b, the b quark contribution to the total hadronic cross section in units of lowest order QED cross section for $e^+e^- \rightarrow \mu^+\mu^-$, its effect on the forward-backward charge asymmetry in the $e^+e^- \rightarrow b\bar{b}$ process, A_b, is rather dramatic. The angular distribution for the $e^+e^- \rightarrow b\bar{b}$ is described by

$$\frac{d\sigma}{dcos\theta} = \frac{\pi\alpha^2}{2s} R_b[(1+\cos^2\theta) + \frac{8}{3}A_b\cos\theta], \qquad (5)$$

where α is the fine structure constant, s is the square of the c.m. energy, and θ is the angle between the outgoing $b(\bar{b})$ direction and the $e^-(e^+)$ direction. Ignoring QCD corrections, which amount to about 5% in our energy region, R_b and A_b are

expressed in terms of the vector and axial-vector weak neutral coupling constants g_V and g_A, and the Z^0 contribution χ, as

$$R_b = 3\left[Q_b^2 - Q_b 8 g_V^e g_V^b \mathrm{Re}(\chi) + 16(g_V^{e\,2} + g_A^{e\,2})(g_V^{b\,2} + g_A^{b\,2})|\chi|^2\right] \quad (6)$$

$$A_b = 3[-6Q_b g_A^e g_A^b \mathrm{Re}(\chi) + 48 g_V^e g_V^b g_A^e g_V^b |\chi|^2]/R_b \quad (7)$$

where Q_b is the charge of the b quark and χ is the contribution from the Z^0 given by

$$\chi = \frac{1}{16 \sin^2\theta_W \cos^2\theta_W} \frac{s}{(s - M_Z^2 + i\Gamma_Z M_Z)} \quad (8)$$

As can be seen in the above formula, the asymmetry A_b strongly depends on g_A^b, which in the standard model is simply T_{3L}. The aymmetry is expect to reach maximum at TRISTAN energies. As an example, using $\sqrt{s} = 57$GeV, $M_Z = 92$ GeV, $\Gamma_Z = 2.5$ GeV, $\sin^2\theta_W = 0.230$, and including QCD corrections up to third order, the standard model prediction for A_b is -0.56. Here, $g_A^b = -1/2$, corresponding to the left-handed and right-handed b quarks belonging to a doublet and singlet respectively. For the simplest alternative model without the t quark, in which both left-handed and right-handed b quarks are assigned to singlets[34], we have $g_A^b = 0$ and, consequently, A_b becomes zero. On the other hand, changing g_A^b from $-1/2$ to 0 changes R_b from 0.55 to 0.38; a difference that is not as striking as that for A_b.

We have extracted the forward-backward charge asymmetry of the $e^+e^- \to b\bar{b}$ process using multihadronic inclusive muon events. The analysis was performed by physicists from KEK and LSU and is the subject of the Ph.D. dissertation of J.N. Lim of LSU. The paper has been accepted from publication in Physical Review Letters.

The presence of prompt muons with hadronic jets indicates that the events originated either from c or b quarks. The charge of each muon reflects the sign of the parent quark charge. The selection of hadronic events and the identification of muons have been previously described. In a data sample corresponding to an integrated luminosity of 18.6 pb^{-1} accumulated between $\sqrt{s} = 52$ and 57 GeV, we find 123 events passing the multihadronic inclusive muon selection criteria. This data sample contains events of interest, namely $e^+e^- \to b\bar{b}$ with subsequent semileptonic decay either directly, $b \to \mu^-(\bar{b} \to \mu^+)$, or by the cascade decay, $b \to c \to \mu^+(\bar{b} \to \bar{c} \to \mu^-)$ (ref). It also containes additional prompt muons coming from $e^+e^- \to c\bar{c}$, followed by $c \to \mu^+(\bar{c} \to \mu^-)$, and hadron fakes. For the determination of the forward-backward charge asymmetry for $e^+e^- \to b\bar{b}$, we assume that the yield and asymmetry of $e^+e^- \to c\bar{c}$ is correctly described

by the standard model. We estimate the contributions from the $c\bar{c}$ production as well as those from hadron fakes by using a Monte Carlo simulater where five flavors are generated according to the standard model using the LUND 6.3 event generator[31] . We subtrack these contributions from the data in order to obtain the $e^+e^- \rightarrow b\bar{b}$ sample. Estimation of the fraction of hadron fakes coming from b flavored hadrons requires knowledge of $e^+e^- \rightarrow b\bar{b}$, which are trying to determine. While such an assumption is not strictly valid, we apply it to the present case because the fraction of hadron fakes coming from the b flavor hadrons is only $\sim 1/10$ of those originating from u,d,s, and c flavor hadrons. The Monte Carlo is also used for estimating the ratio of muons from $b\bar{b}$ cascade decays to those from direct decays. This is justified because this ratio depends only on the decay kinematics of the b quark and not on the dynamics of the $b\bar{b}$ pair production. The cascade decay produces muons with charge opposite to those produced by direct decay, and thus contributes oppositely to the asymmetry. We use our estimated ratio of the cascade decay to direct decay to correct for this effect.

The Monte Carlo study indicates that we can enhance the fraction of b quark by applying a cut of P_T greater than 0.7 GeV/c, where P_T is the transverse momentum of muons with respect to the event thrust axis. Thus, we divide the data into two P_T regions, below and above $P_T = 0.7$ GeV/c. The distributions for muon P_T and $\cos\theta$ of the data are shown in Figure 16 together with the estimated contributions of $c\bar{c}$, hadron fakes, and the $b\bar{b}$ contribution obtained in this analysis. The muons from $b\bar{b}$ extend toward higher P_T values compared to with those from $c\bar{c}$ and hadron fakes. This is expected because the muons from semileptonic decays of b flavored hadrons tend to have larger P_T values, reflecting the fact that these hadrons are heavier than those of other flavors. The angle θ used in Figure 16 is defined as the direction of the thrust axis associated with $\mu - (\mu^+)$ with respect to the incoming $e^-(e^+)$ direction. As expected, the angular distribution for hadron fakes does not show any asymmetry, while the $c\bar{c}$ contribution has a positive asymmetry.

We have extracted A_b and R_b using the distributions for $P_T \geq 0.7$ GeV/c. After subtracting $c\bar{c}$ and hadron fakes from the data sample, the resulting distribution was converted to the $e^+e^- \rightarrow b\bar{b}$ differential cross section by first correcting for: 1) the effect of different θ difinitions; 2) the efficiency for detecting the b quark by requiring a muon; 3) the effect of the cascade decay $b \rightarrow c \rightarrow \mu$; and 4) the muon detection efficiency of 82%, and then normalizing to the luminosity. We obtain a θ dependent correction factor by dividing a Monte Carlo generated $e^+e^- \rightarrow b\bar{b}$ angular distribution, where θ was defined as the direction of the b quark, by an angular distribution of simulated $b\bar{b}$ events in which θ was defined as the direction of the thrust axis. We first used a $(1+\cos^2\theta)$ angular distribution. The observed asymmetry using this correction factor was calculated. Unlike the

first, which is symmetric in $\cos\theta$, the second correction factor has a slight $\cos\theta$ asymmetry caused by a combination of the non-zero asymmetry for $e^+e^- \rightarrow b\bar{b}$ and the non-zero ratio for $b \rightarrow c \rightarrow \mu/b \rightarrow \mu$. This second factor incorporates the effects described in items 1) through 4) listed above. The $e^+e^- \rightarrow b\bar{b}$ differential cross section was fitted to equation (5) in the region of $|\cos\theta| \leq 0.6$ and the asymmetry parameter A_b was obtained. The R ratio of the $b\bar{b}$ prodution, R_b, was also obtained from the fit. The results are shown in Figure 17. In order to estimate systematic uncertainties, we repeated the analysis by varying the hadron fake contribution by $\pm 30\%$, which corresponds to the fraction contributed by the K^+ induced punchthroughs. We use the largest shift in this analysis as our estimate of the systematic error.

Our final results, measured at average c.m. energy of $\sqrt{s} = 55.2$GeV, are $A_b = -0.72 \pm 0.28 \pm 0.13$ and $R_b = 0.57 \pm 0.16 \pm 0.10$, where the first and the second errors are statistical and systematic, respectively. The effect of $B^0 - \overline{B}^0$ mixing[35] is to reduce the observed asymmetry by an amount ranging from 6% to 36%[36]. The amount of this reduction depends on poorly known processes such as $B_s^0 - \overline{B}_s^0$ mixing and the semileptonic branching ratios for all b mesons. We did not make any correction. These observed results are consistent with the standard model predictions of $A_b = -0.56$ and $R_b = 0.51$. Figure 18 compares our result for A_b with those from previous measurements at lower energies[37], which are also not corrected for $B^0 - \overline{B}^0$ mixing. The measurements are consistent with the standard model prediction throughout the energy region explored so far. Thus the axial-vector coupling of the $b\bar{b}$ to the Z^0 is consistent with being $g_A^b = -1/2$. This in turn is consistent with the weak isospin asignment $T_{3L} = -1/2$ and $T_{3R} = 0$ for the b quark, therefore requiring the existence of the t quark.

Measurements of Heavy Quark Fragmentation Using Inclusive Muons

The following is a report of an Analysis performed by S. Myung of LSU. The paper is in preparation which would be submitted to Physical Review (or equiv.) within the next six months.

Fragmentation is a process in which quarks are transformed into observable particles. The fragmentation of heavy quarks into heavy hadrons is of both theoretical and experimental interest. The $e^+e^- \rightarrow q\bar{q}(g)$ cross section can be calculated exactly to the 2nd order perturbative QCD. However, the subsequent transformation of quarks into hadrons at large distance(at low energy) where perturbative QCD no longer applies is described by a phenomenological model such as string fragmentation. In this model a string is stretched between final quarks, the gluons being kinks on the string. As the q and $\bar{q}$ move apart, the potential energy stored in the string increases and a new pair of $q\bar{q}$ is produced

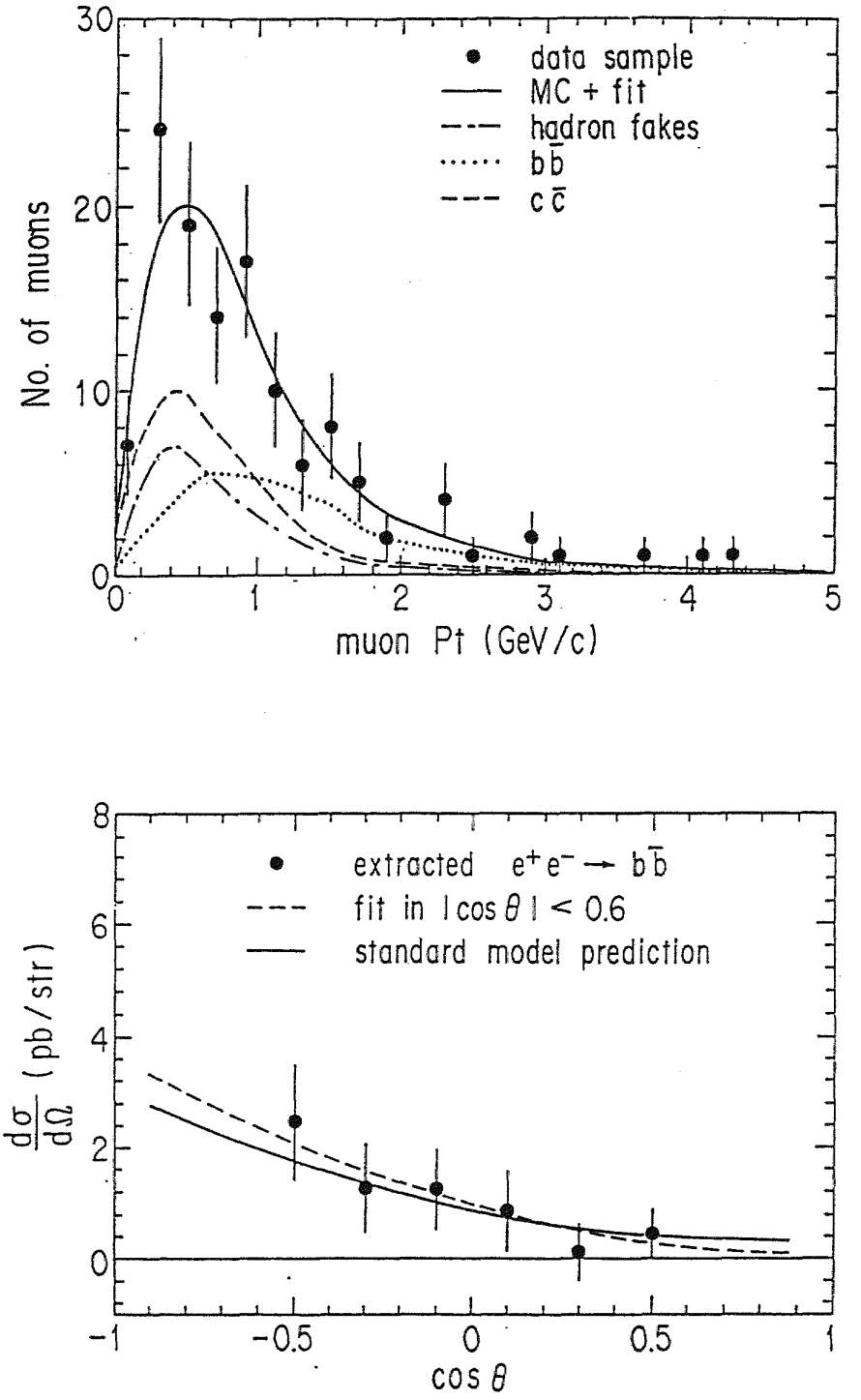

Figure 16 Transverse momentum and angular distribution for the data and the estimated contribution for $c\bar{c}$ and hadron fakes.

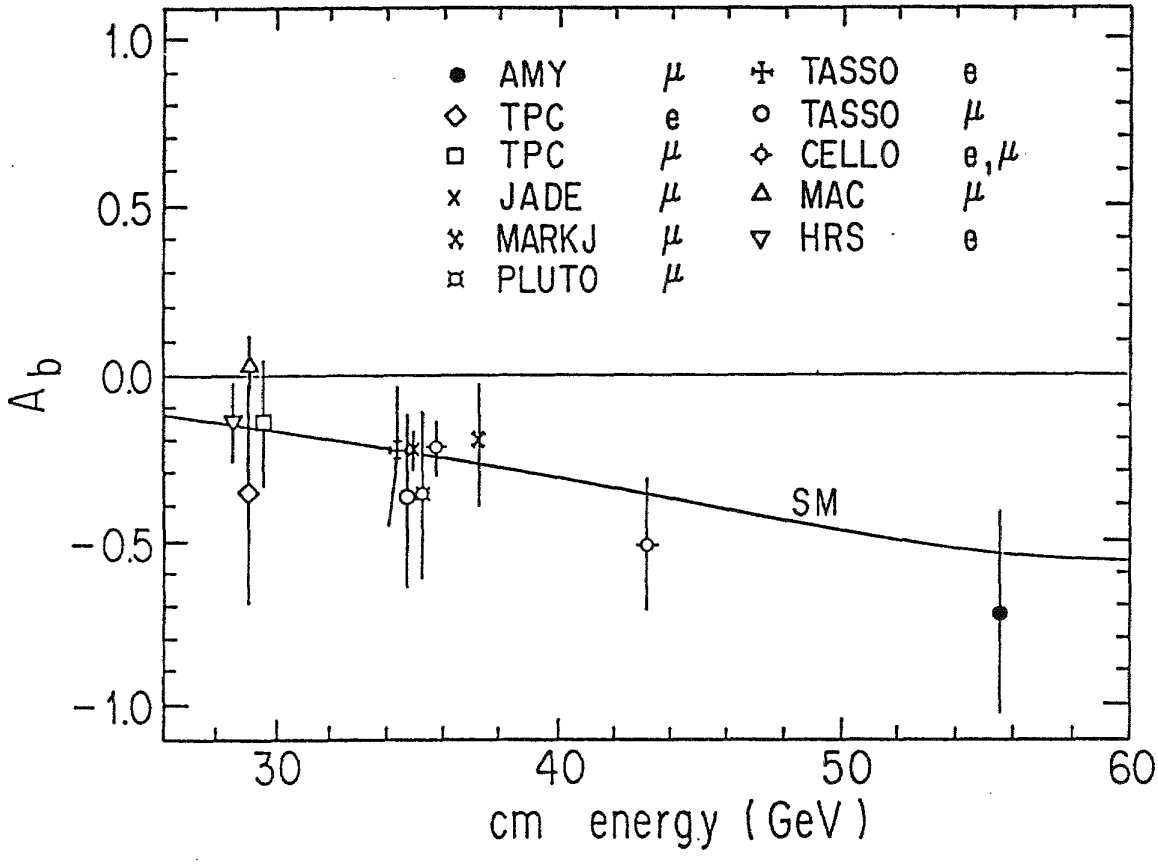

Figure 17 b quark forward-backward asymmetry measured by AMY compared with theoretical predictions and the results from lower energy experiments.

when the string is broken. This procedure continues if the invariant mass of the string pieces is large enough. A parton will then form hadrons by combining with a neighboring q(or $\bar{q}$). The transverse momentum distribution of hadrons with respect to the fragmentation direction can be parametrized by a gaussian distribution with a width of ~260 MeV. The longitudinal momentum of hadron can be parametrized by a scaling function f(z), where z is the fraction of available energy-momentum,(E+p), carried by the primary hadron.

The actual form of this function still is the subject of theoretical and experimental endeavor. Originally it was assumed that f(z) for heavy quarks,Q, was similar to that for light quarks,q, which fragment principally into pions and kaons, with a distribution of z which steeply falls as z increase.[38] However, kinematic consideration[39] for a heavy quark fragmenting into a hadron($Q\bar{q}$ or Qqq) suggest that the momentum of the heavy quark is retained by the hadron containing Q, leading to a 'harder' distribution in z(i.e. peaked towards higher values of z) than for the light quarks,q. Calculating the transition probability for the process $Q \rightarrow Q\bar{q} + q$, Peterson et al. developed the following fragmentation function[40] :

$$f(z) \propto \frac{1}{z[1 - \frac{1}{z} - \frac{\epsilon_Q}{(1-z)}]^2} \tag{9}$$

where z is defined as

$$z = \frac{(E + p_{\parallel})_{\text{hadron}}}{(E + p)_{\text{quark}}} \tag{10}$$

where $(E + p_{\parallel})_{\text{hadron}}$ is the sum of the energy and momentum component parallel to the fragmentation direction carried by the primary hadron and $(E + p)_{\text{quark}}$ is the energy-momentum of the quark after accounting for initial state radiation, gluon bremsstrahlung and photon radiation in the final state. The only free parameter, ϵ_Q is to be determined experimentally for each heavy quark Q. It is expected to be approximately equal to

$$\epsilon_Q \sim \frac{M_q^2}{M_Q^2} \tag{11}$$

i.e. the ratio of the squares of the masses of the light and heavy quarks forming the primary(or leading) meson. Even if z is theoritically preferred z_e is widely used, which is defined as

$$z_e = \frac{E_{\text{hadron}}}{E_{\text{quark}}}. \tag{12}$$

We observed that there was very little difference between them so for our analysis

we have used z_e instead of z.

Another form of fragmentation function which is proposed by the Lund group is

$$f(z) \propto \frac{1}{z}(1-z)^a \exp(-\frac{bm_t^2}{z}) \tag{13}$$

where m_t is the transverse mass of the produced hadron and the parameters a and b are to be determined experimentally. Even though the Lund functional form was tuned to provide a good description of a number of particle distributions in multihadronic events, in analyses specific to the determination of the 'hardness' of the heavy quark fragmentation functions, Peterson function has been widely adopted because it has only one parameter for each quark flavor.

The production of heavy charm and bottom quarks in the fragmentation process is expected to be suppressed due to their heavy masses[41] . Thus, heavy mesons and baryons contain either the primary quark or its weak decay product. Experimentally there are two kinds of analyses on determining the'hardness' of heavy quark fragmentation functions; one is the reconstruction of heavy mesons from their hadronic decay products and obtaining momentum spectra of them. However the fragmentation of b quarks into b flavored mesons and baryons in the e^+e^- annihilation continuum is not well explored due to the small b quark cross section and the very inefficient reconstruction of the b flavored hadrons. Alternatively, one can study the semi-leptonic decay of heavy hadrons. Since lepton momentum is dependent upon the momentum of the parent hadron, it contains information on the fragmentation of the heavy quark. The transverse component of the lepton momentum relative to the jet axis has information on the quark flavor. Figure 19 shows transverse momentum of muon relative to the thrust axis for different kinds of quark flavors.

The data were collected at center of mass energies in the range 50-61.4 GeV and corresponding integrated luminosity of 33.8 pb^{-1}. From 3861 hadronic events we selected 197 inclusive muon events(202 inclusive muon candidate tracks). These inclusive muons were divided into 10 (p,p_t) bins, here p_t is transverse component of the muon momentum relative to the thrust axis. We divided into four categories for the sources of inclusive muons: 1) $b \rightarrow c\mu^-\bar{\nu}_\mu$; 2) $c \rightarrow s\mu^+\nu_\mu$ 3) cascade decay; $b \rightarrow cX$; $c \rightarrow s\mu^+\nu_\mu$; and 4) Hadron Fakes composed of 4a) decay of hadron; $\pi, K \rightarrow \mu\nu_\mu X$ 4b) hadron punch through. Figure 20 shows the momentum and p_t for the various catagories.

We performed minimum χ^2 fit to the inclusive muon data according to following formula. The number of expected inclusive muon in each p and p_t bin

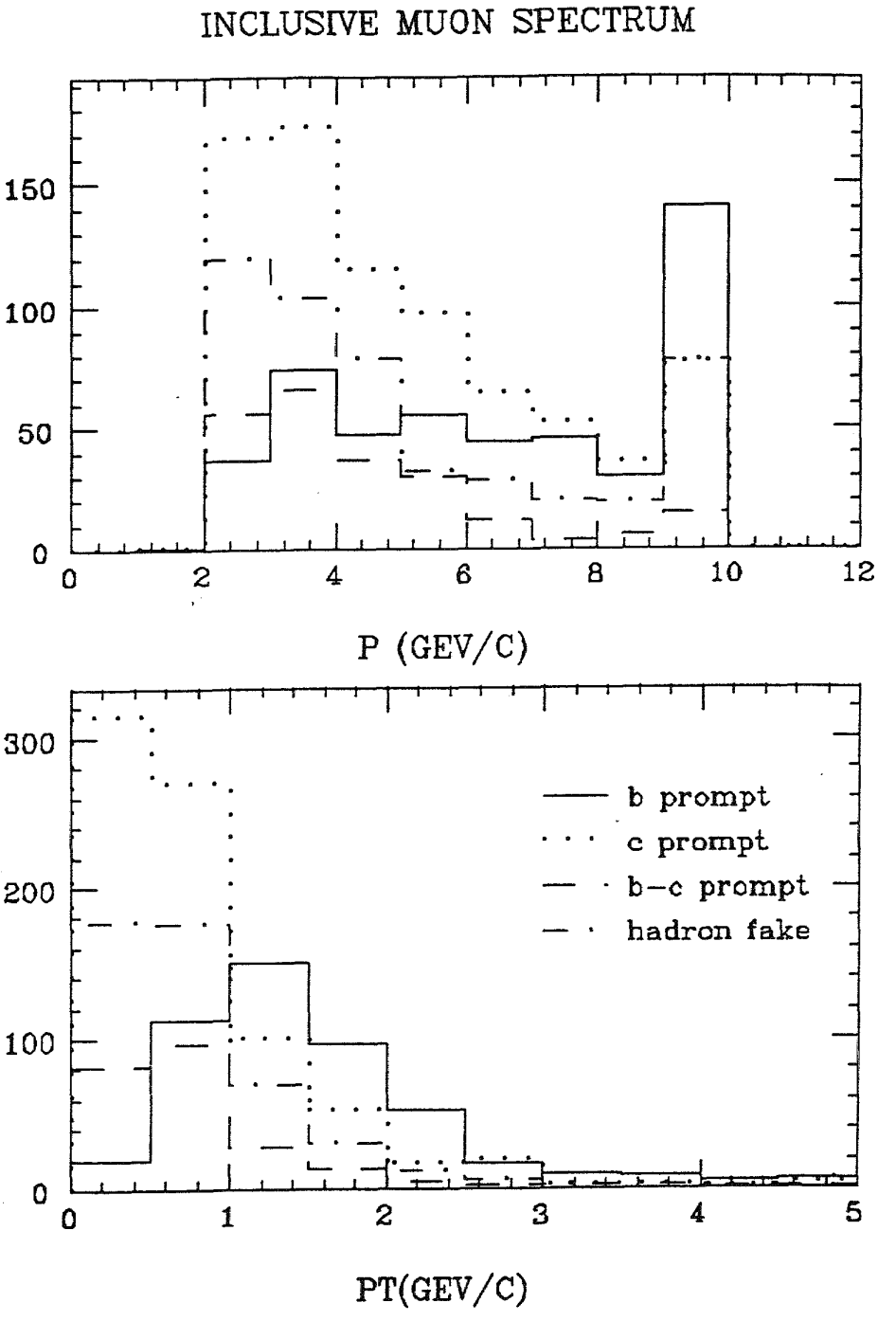

Figure 19 Momentum and transverse momentum distribution of muons from a Monte Carlo simulation.

is given by

$$\begin{aligned} N_{exp}(p, p_t) = & N_{background}(p, p_t) + \\ & \epsilon(p, p_t)[2N_{cc} \cdot BRc \sum_j W(j) P_c(j, p, p_t) + \\ & 2N_{bb}\{BRb \sum_j W(j) P_b(j, p, p_t) + BRc \sum_j W(j) P_{bc}(j, p, p_t)\}]. \end{aligned} \tag{12}$$

Here, $\epsilon(p, p_t)$ is the efficiency of finding prompt muons in a bin of p and p_t including the fiducial volume cut and identification efficiency, BRb and BRc are the average semi-muonic branching ratio of the b and c meson respectively.

$$W(j) = \int_{zmin(j)}^{zmax(j)} dz\, \beta\, f_Q(z).\ j = 1, 5$$

$$f_Q(z) = N/[z(z - 1/z - \epsilon_Q)/(1 - z)]^2.$$

$P(j, p, p_t)$ is the probability that the semi-muonic decay of a heavy hadron with z in jth bin will produce a muon. To obtain this we have generated muon p and p_t spectra with a flat fragmentation function.

As can be seen from the formula there are 4 parameters to be determined; ϵ_b, ϵ_c, BRb and BRc. Because of the limited statistics we fixed two of the four parameters to the world average values and performed fit with two parameters at a time, which gives 6 fits. From these 6 we excluded two cases where the correlation between to parameters are excessive (the one where ϵ_b and BRb are parameters and the other where ϵ_c and BRc are parameters).

Table 6 displays the fitted values. Once we obtain ϵ_Q we can determine $< z_Q >$ by integrating f(z) from $z_{min} = M_Q/E_{beam}$ to 1.

There are the following systematic error sources:

- uncertainty of hadron punchthrough background; $\pm 30\%$
- uncertainty of efficiency of finding prompt muon;
- uncertainty of number of $b\bar{b}$ and $c\bar{c}$ events(related with the branching ratio in Monte Carlo); $\pm 10\%$
- uncertainty of world average values of fixed parameters;
- $\star$ uncertainty in P_b, P_c and P_{bc}.
- $\star$ uncertainty in the calculation of jet axis.(or. direction of fragmentation)

- $\star$ uncertainty in fragmentation model.
- $\star$ uncertainty due to binning.

Items with $\star$ are not considered yet. Table 6 shows fitted values with statistical error, correlation between parameters and systematic errors.

Our results on heavy quark fragmentation value and muon branching ratio are compared with results from other experiments[42] in figure 20.

Table 6 Results of the fit to heavy quark fragmentation and average semileptonic branching ratio obtained from inclusive muon data.

	case 1	case 2	case 3	case 4
	ϵ_b, ϵ_c	BRb,BRc	ϵ_b,BRc	ϵ_c,BRb
ϵ_b	$0.0030^{-0.0026}_{+0.0057}$	fixed	$0.0042^{-0.0036}_{+0.0075}$	fixed
ϵ_c	$0.028^{-0.014}_{+0.030}$	fixed	fixed	$0.023^{-0.010}_{+0.017}$
BRb(%)	fixed	13.22±4.55	fixed	14.29±4.28
BRc(%)	fixed	11.42±2.37	$10.63^{+3.11}_{-2.74}$	fixed
$< Z_b >$	$0.86^{+0.07}_{-0.05}$	—	$0.85^{+0.07}_{-0.06}$	—
$< Z_c >$	$0.73^{+0.05}_{-0.06}$	—	—	$0.75^{+0.04}_{-0.04}$
χ^2/dof	1.88	1.86	1.84	1.92

Fixed value: ϵ_b=0.0075, ϵ_c=0.04, BRb = (11.8±0.5)%, BRc=(8.6±0.9)%. Corresponding $< Z >$ values of ϵ_b and ϵ_c are $< Z_b >$=0.818 ± 0.03, $< Z_c >$=0.70 ± 0.03.

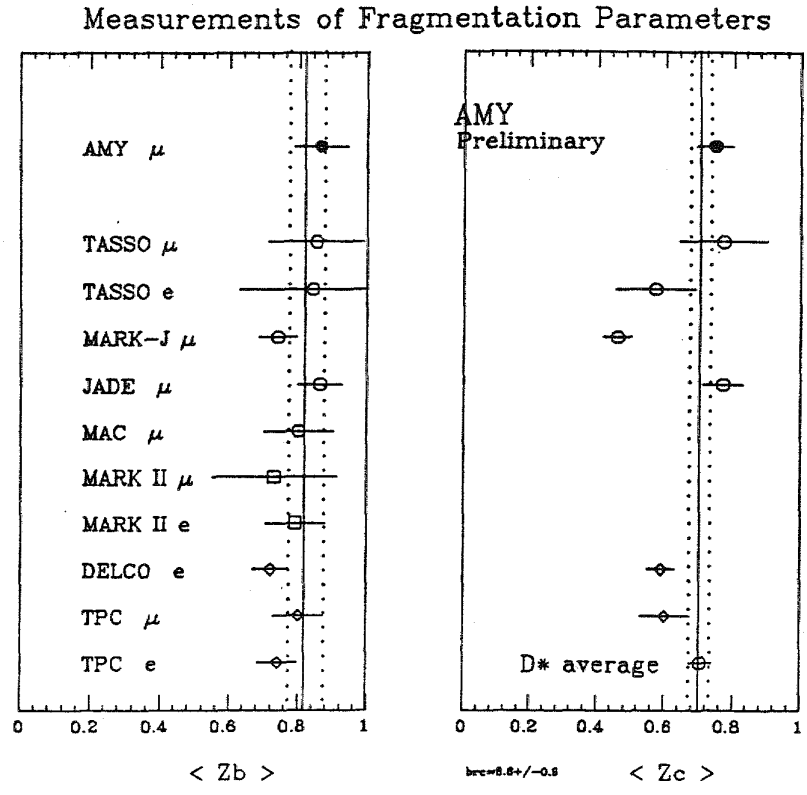

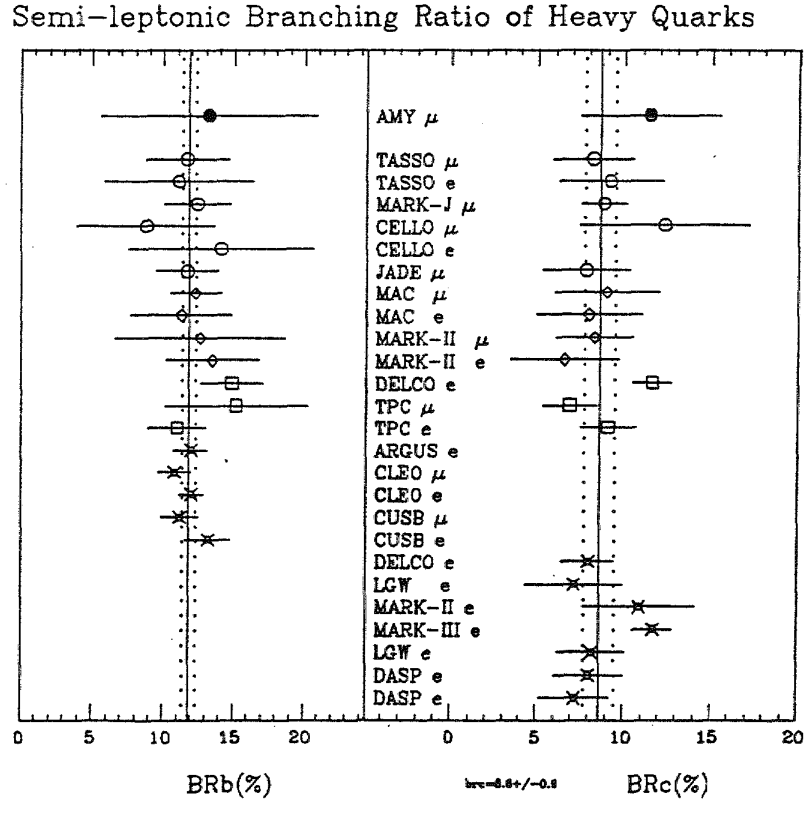

Figure 20 Comparison of AMY result on fragmentation and and semi-leptonic branching ratio with results from lower energy experiments.

3. Future of AMY

a. U.S. Computing

Despite having success in arriving at early physic results, AMY has been hampered by the limited computing resources available to it at KEK. For example, a typical multi-hadronic Monte Carlo event takes about five minutes of CPU on the KEK based Fujitsu FACOM M-383 computer which AMY does its analysis on at KEK. We presently record about one such data events every 10 minutes when we are running at TRISTAN (luminosity ~ 10 nb^{-1}/hr). By summer '90, TRISTAN will be operating in high luminosity mode and the luminosity is expected to increase by a factor near 3 and even if all we did was simulate Monte Carlo events of this one process, we could not keep up the accumulation of such events in the data and our systematic uncertainties will be excessive. The answer lies in streamlining our software and in expanding our computing resources. Only then can we hope to maintain the current level of output AMY has been internationally recognized for.

At home in AMY US-member institutions, we presently have a combined computing power equal to that allocated to us at KEK. With the detector and offline analysis and Monte Carlo simulation software stabalizing, an effort has begun to utilize these resoureces. The hope is not only to unload some of the computing burden off of the KEK computing facilities, but to allow US-based physicists a chance to contribute significantly to AMY results while at home. This certainly applies to LSU professors Imlay and Metcalf, who have used up their sabaticals, and McNeil who has just started as a faculty member and will only have summers for long stays at KEK during the next few years.

The first phase of the distribution of AMY software to US-based computers began this past spring by first transfereing all of the relavent AMY software to a KEK-based VAX 8500 and using the CMS software Management System to maintain the integrity of that sofware as revisions are made. Then, each participating member institution updates a like set of software on a VAX computer at home via DECNET link to KEK in Japan. There are 2000 individual software files to be maintained in this fashion and a computer job which merely checks the revision dates of these files with those in the "original" set at KEK (and copies any new files) takes about 7 hours of real time (only a few minutes of CPU) due to the limited speed and bandwidth of the DECNET link to JAPAN. Therefore, the reliability of the AMY software at the US institutions crucially depends on the "live time" of the DECNET link and the frequency of link failures during this 7 hour job. This job is presently submitted automatically at night a few times a week, and link failures are frequent. We are currently working with DECNET representatives at the Space Physics Analysis Network SPAN (this is the network

which LSU utilizes, although we also belong to HEPNET) to improve the link reliability and performance.

This past summer, the LSU HEP group purchased a VS3200 workstation with Maxtor Disk and 8mm Tape Drive to combine with an existing VS2000 workstation with color graphics monitor. This allow us to begin AMY analysis work as well as run our ZEUS Test station (see next section). In order to increase the computing resources available to the LSU HEP group for AMY analysis we have joined a computing consortium with the LSU Space Physics Group, Intermediate Energy Group, and Gravity Wave Group. The VAX cpus in the consortium form a local area cluster consisting of a VAX 11-750, 3500 server, two VS3200s (one is ours), a VS3100, and a VS2000 (ours) which totals about 13 VAX 780 equivalents. Besides the additional CPU power, we have thus obtained use of peripherals such as a laser printer, and 6250bpi tape drive. We share maintenance costs of the hardware and software for the whole system with the other members of the consortium. We also purchased an additional RA81 disk to install on a VAX in the cluster to facilitate analysis of data by the entire consortium. Our intent is to use this cpu to simulate Monte Carlo generated events of various processes in the AMY detector. We hope to make a significant contribution to AMY's Monte Carlo simulated data sample and AMY data analysis.

b. TRISTAN and AMY Schedule

The TRISTAN program of energy increase runs parallel to one of luminosity upgrade that in the summer of 1990 will include the installation of superconducting quadrupole focusing magnets. The micro-beta configuration will provide a minimum factor of 3 increase in luminosity. The increased luminosity will allow TRISTAN experiments including AMY to perform the precise measurements necessary to further test the standard model of the electro-weak interaction and QCD.

The AMY detector operated very well during its first two years of operation. However, due to a mishap, there was recent damage to two sextants of the Shower Counter (SHC). These sextants have been replaced and are ready for data. The AMY Muon Detector presently is stable and maintained by one LSU graduate student and one LSU post-doctoral researcher on-site at KEK. As necessary, the electronics endboards will be replaced on the detector. Major changes to AMY are in progress, increasing the solid angle acceptance of AMY for charged and neutral particles, and improving the electron identification (see sections 2.c and 2.e). The LSU group will continue maintaining the AMY Muon Detector and performing analysis of new data from AMY.

c. LSU at AMY

The LSU high energy group has taken a leading role in the analysis of e^+e^- annihilation to final states with muons including muon pairs and hadronic events with muons. With the addition of S. Myung we gained expertise in the area of the analysis of electrons in the central detector. She has taken an active role in several important areas of analysis. Recently, we hired post-doctoral researcher Hong Joo Kim from Korea Univ. He has worked on the AMY experiment as a Graduate Student. Although Kim's primary responsibility will be on the ZEUS effort, he will also easily be able to pursue part-time, analysis of AMY data from LSU. As the AMY experiment enters the high luminosity phase with stable running it will become increasingly important that the US institutions be able to contribute to results from home. Hong Joo Kim will ensure that the AMY analysis software at LSU is up to date and running properly, and keep the analysis production continuous. With a full-time researcher at LSU, the three professors in the high energy group will be able to use their research time doing analysis of data as opposed to simply getting up to date.

D. The ZEUS Experiment at HERA

1. Introduction

Last year the LSU HEP group started looking at possible new experimental projects because our neutrino experiment was nearing completion and because a new Assistant Professor, Roger McNeil, had joined our group. We decided in late 1988 to join the ZEUS experiment. This experiment will study collisions of 30 GeV electrons with 820 GeV protons at HERA, a new storage ring at DESY. HERA is attractive because of its physics potential and because it is an unique facility. Participation in ZEUS will also allow the LSU group to maintain a strong collider program in the period preceding SSC operations.

The ZEUS barrel calorimeter is being built by U.S. Institutions. When we joined ZEUS a prototype module was being tested at ANL and preparations were underway to start construction of the 32 barrel modules. With HERA scheduled for completion in 1990 it is important to build the modules as rapidly as possible. We decided we could best help out by taking over the preparation of the wave length shifter bars for the electromagnetic part of the calorimeter from Ohio State University. Then OSU could concentrate on the rest of the optical components.

2. Physics at HERA

HERA will permit the study of e-p collisions at four-momentum transfer squared, Q^2, up to 10^5 GeV^2 at a center of mass energy $\sqrt{s}$ of 310 GeV. At HERA the neutral current ($ep \rightarrow eX$) and charged current ($ep \rightarrow \nu X$) reactions will have comparable rates since $Q^2_{max} > M^2_w$. (see Fig. 21). Expected rates for 200 pb^{-1} of data are shown in Fig. 22. Measurement of the proton structure function in this newly opened kinematic region will be a priority for ZEUS. The large Q^2 range will permit a much more stringent test of QCD as well as searches for quark or lepton substructure.

HERA will also be able to search for new particles such as excited leptons, leptoquarks, the t quark, SUSY particles and new bosons (Z', Z_R, $W_R^{\pm}$). The most complete discussion is in the report "Physics at HERA" from the 1987 DESY workshop.[43] The 1988 Snowmass Summer Study[44] reviews the physics potential of HERA and other machines for new particle searches. Overall HERA compares well. We note that studies of lepton nucleon scattering have had a major role in forming our present picture of particle physics (scaling, neutral currents, partons, QCD). We expect

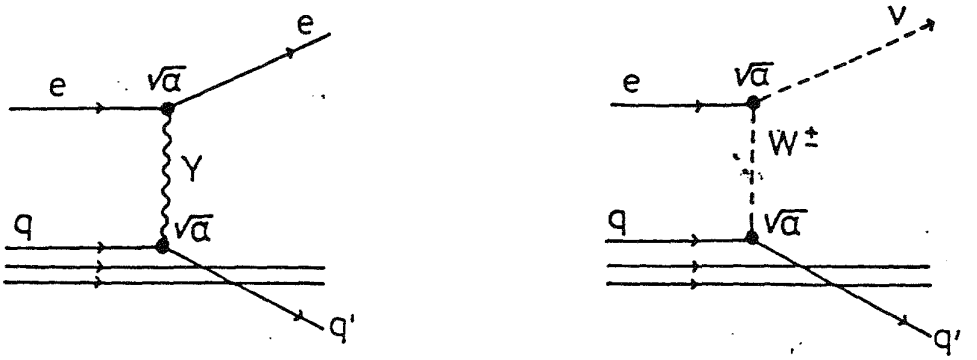

Fig. 8a,b NC and CC scattering by γ and W exchange, respectively.

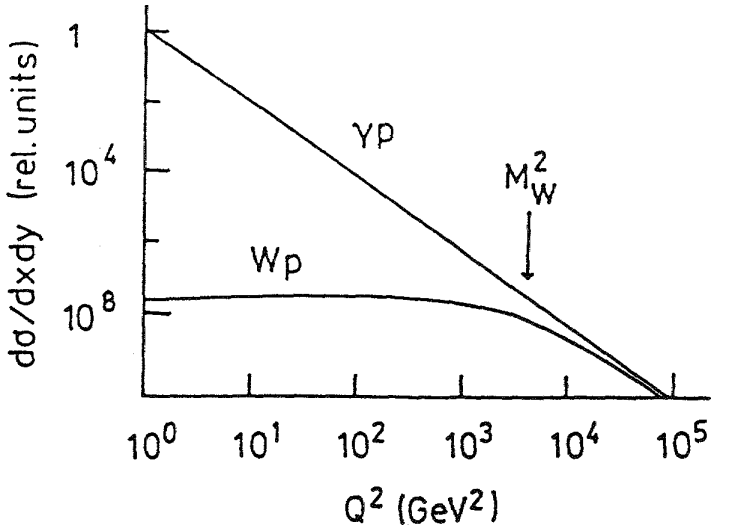

c) Qualitative behaviour of NC scattering by γ exchange and CC scattering by W exchange.

Fig. 21

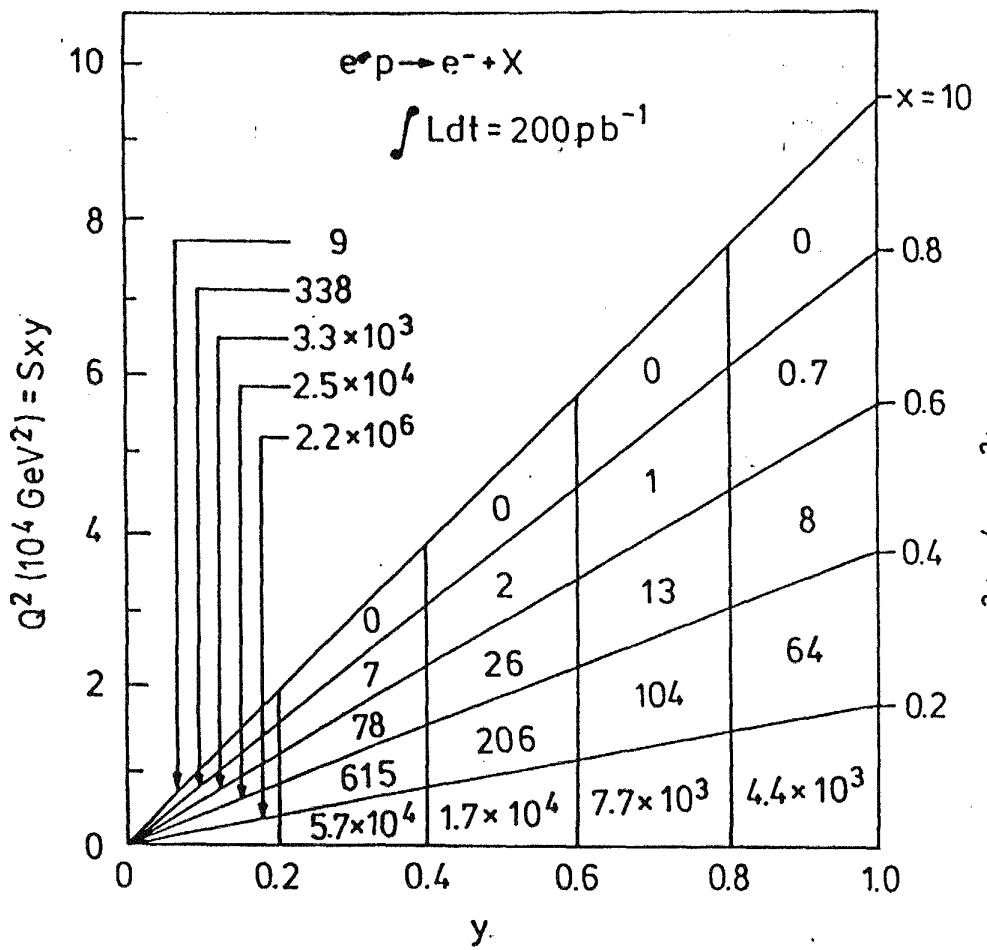

Fig. 9 Event rates for $e^-p \to e^-X$ with $x > 0.01$ and $y > 0.01$.

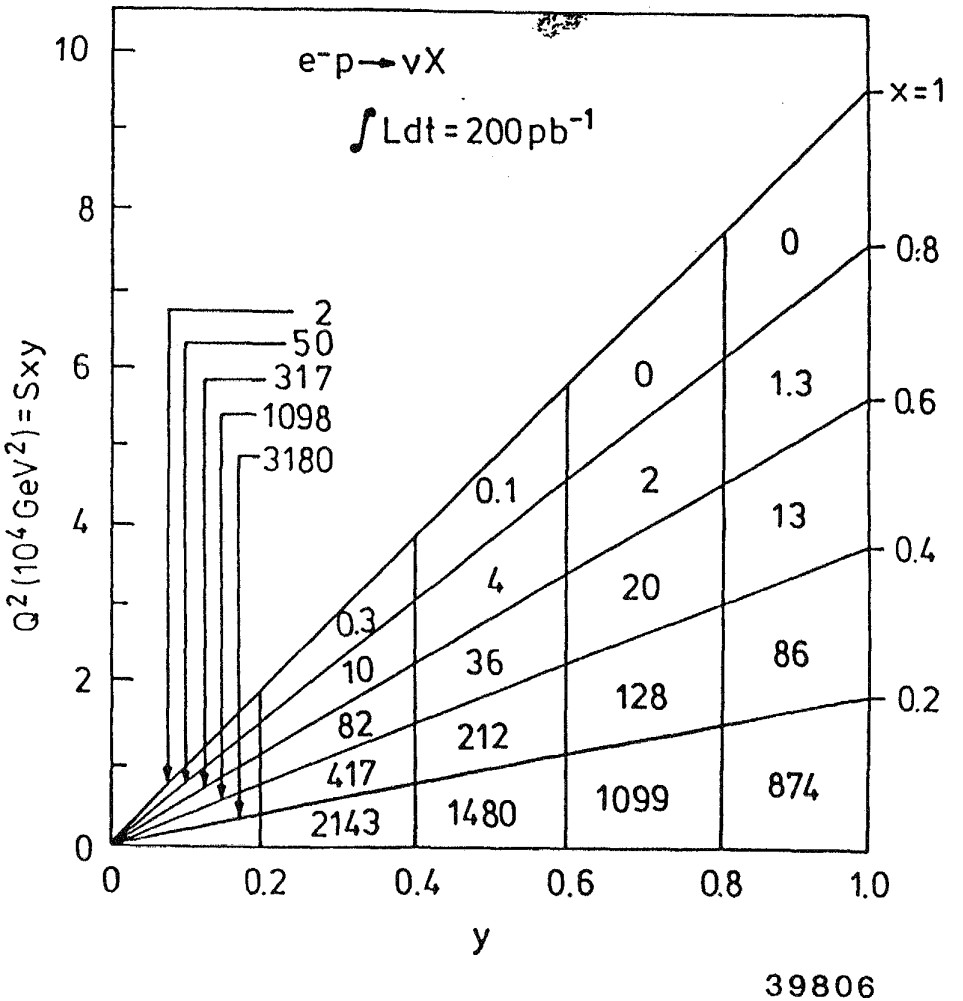

Fig. 10 Event rates for $e^-p \to \nu X$ with $x > 0.01$ and $y > 0.01$.

that HERA will have a similar impact.

3. The ZEUS Detector

The ZEUS detector is shown in Fig. 23. Inside the coil of the 1.8 T solenoidal magnetic field are a vertex detector (VXD) and a central tracking detector (CTD). In the forward (proton) direction are the forward tracking chamber (FTD) and a transition radiation detector (TRD). In the rear (electron) direction is the rear tracking detector (RTD). Surrounding the coil and tracking detector are three high resolution calorimeters (FCAL, BCAL, and RCAL). All three calorimeters are similar in construction. U.S. Institutions are responsible for the Barrel Calorimeter (BCAL) which is discussed in more detail in the next section. Surrounding these calorimeters are the backing calorimeter (BAC), the forward muon spectrometer (FMU) and the barrel and rear muon detector (MU).

The decays of short lived particles can be detected in a vertex detector which has a time-expansion type drift cell.

The central track detector consists of a cylindrical jet type drift chamber with an outer radius of 85 cm and an overall length of 240 cm. Track position and dE/dx loss are measured in 9 superlayers each with 8 layers of sense wires. Four of the superlayers have stereo wires. A resolution of 100 μm is expected, leading to a momentum resolution of$\sigma(p)/p = 0.002 \cdot p \oplus 0.003$ (p in GeV/c) for a magnetic field of 1.8 T. Particle tracking at small forward and backward angles to the beam is aided by four planar drift chambers providing a momentum measurement with $\sigma(p)/p = 0.01 \cdot p$ at a forward angle of 140 mrad.

Electron identification is performed with dE/dx information from the tracking detectors and with the calorimeter. In the forward direction a transition radiation detector, consisting of four modules, yields an additional hadron rejection factor of about 100 for momenta below 30 GeV/c. In order to identify electrons within dense jets a silicon pad detector will be inserted in the calorimeter at a depth of 3-6 radiation lengths. A hadron-electron rejection of 30-200 can be obtained with one layer. The combined hadron rejection including the information from the silicon pad detector is well above 10^4.

The purpose of the backing calorimeter is to measure the energy of late showering particles. The backing calorimeter uses as absorber the iron plates which form the magnet yoke. Aluminum tubes operated in proportional mode are used for read out. The expected energy resolution for hadrons is $\sigma(E)/E = 1.0/\sqrt{E}$. (E in GeV).

Muons are detected in the forward direction in a spectrometer using drift- and

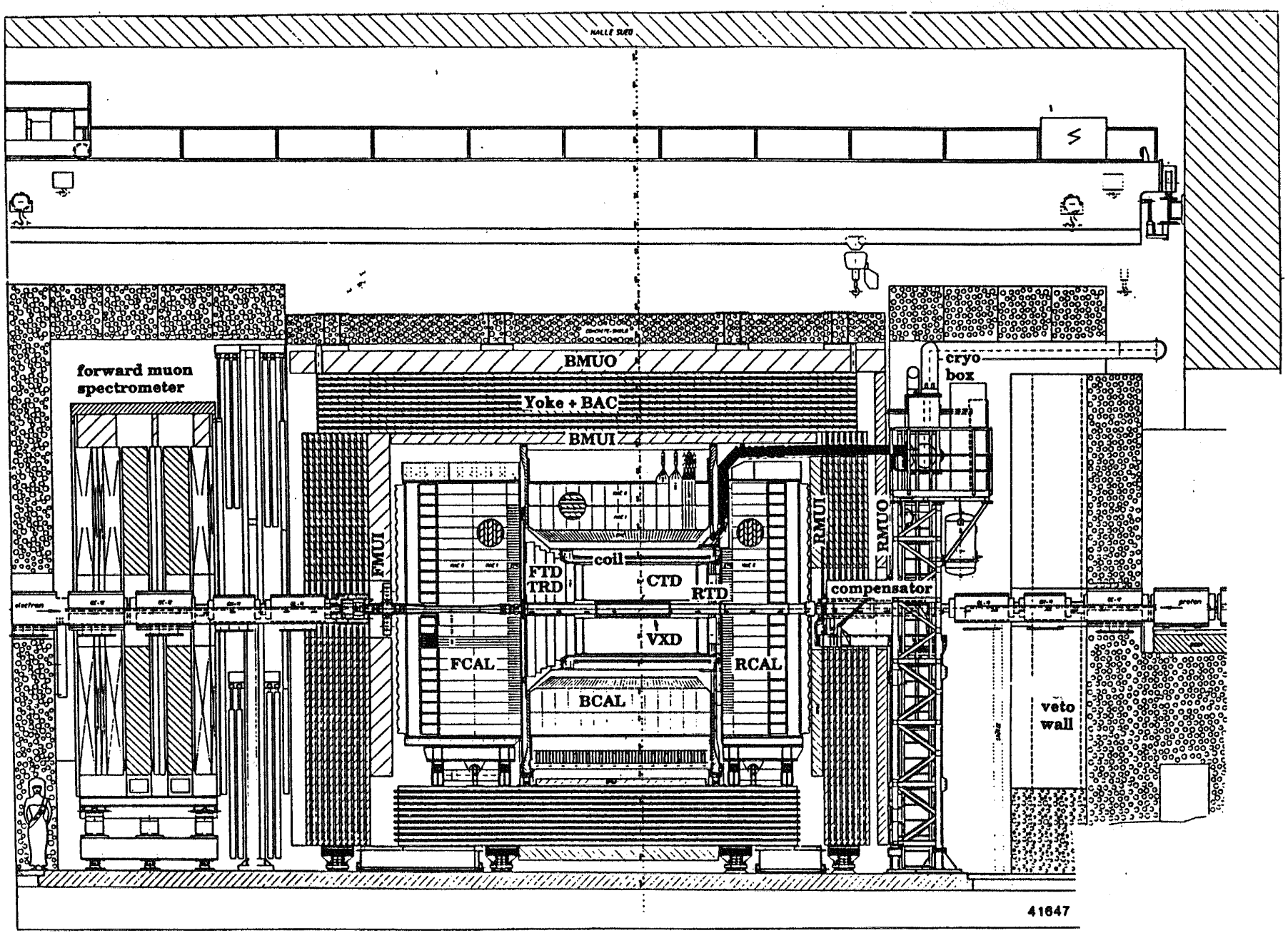

Fig. 23a Section of the ZEUS detector along the beam.

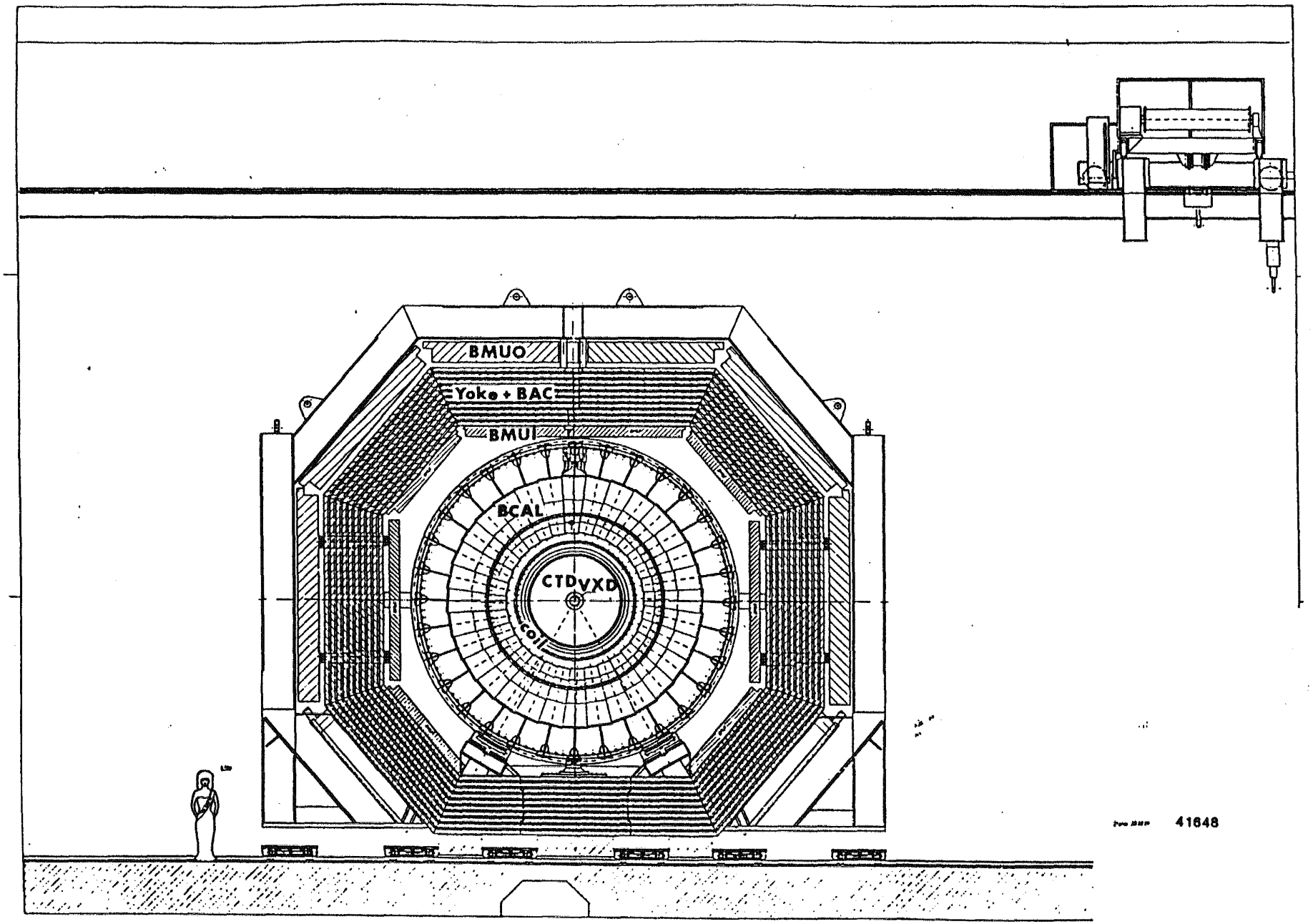

Fig 23b Section of the ZEUS detector perpendicular to the beam.

limited streamer tube chambers plus scintillator counters interspersed between the magnetized iron yoke and magnetized iron toroids. The momentum resolution for 100 GeV/c muons is $\sigma(p)/p = 23\%$. In the barrel and rear detectors muons are detected by limited streamer tube chambers before, in between and behind the backing calorimeter. The momentum resolution is 30% at 20 GeV/c. The pion (kaon) rejection factors are 1000 (100) at 40 GeV/c in the forward direction, and 700 (350) at 10 GeV/c in the barrel region.

A leading proton spectrometer detects very forward produced protons with $\chi_L > 0.3$. The spectrometer uses proton beam line magnets and six miniature high resolution chambers installed in Roman pots very close to the beam at distances between 20 and 90 m from the interaction point. A momentum resolution of $\sigma(p)/p < 1\%$ is expected.

Electron and photon detectors are installed some 30 to 100 m downstream in electron beam direction to measure the luminosity and tag small Q^2 processes.

The magnetic solenoid is superconducting and provides a field of 1.8 T. It has an inner radius of 86 cm, a length of 280 cm and is 0.9 radiation lengths thick. A compensating solenoid is installed in the rear of the detector.

The detector is structurally subdivided into the inner components supported by the bottom yoke, and the clam shells carrying most of the backing calorimeter and the muon detectors. The clam shells can be retracted sideways by as much as 6.5 m on one side and 4.6 m on the other. In this way fast and simple access is provided to all components of the detector. Furthermore, the modular construction of the calorimeter allows installation of calorimeter modules also when the detector is in the beam position (see Fig. 24).

4. The ZEUS Calorimeter

a. General Description

The calorimeter consists of depleted uranium plates interleaved with plastic scintillator in order to achieve compensation and the best possible energy resolution for hadrons.[45] The scintillator plates form towers which are read out via wave length shifter bars, light guides and photomultipliers. The calorimeter is segmented longitudinally into an electromagnetic and one or two hadronic sections. Typical tower sizes are 5 cm x 20 cm in the electromagnetic section and 20 cm x 20 cm in the hadronic section. The calorimeter is divided into a forward, a barrel and a rear part with 7,5, and 4 absorption lengths, respectively. The active area in the forward direction (proton beam direction)

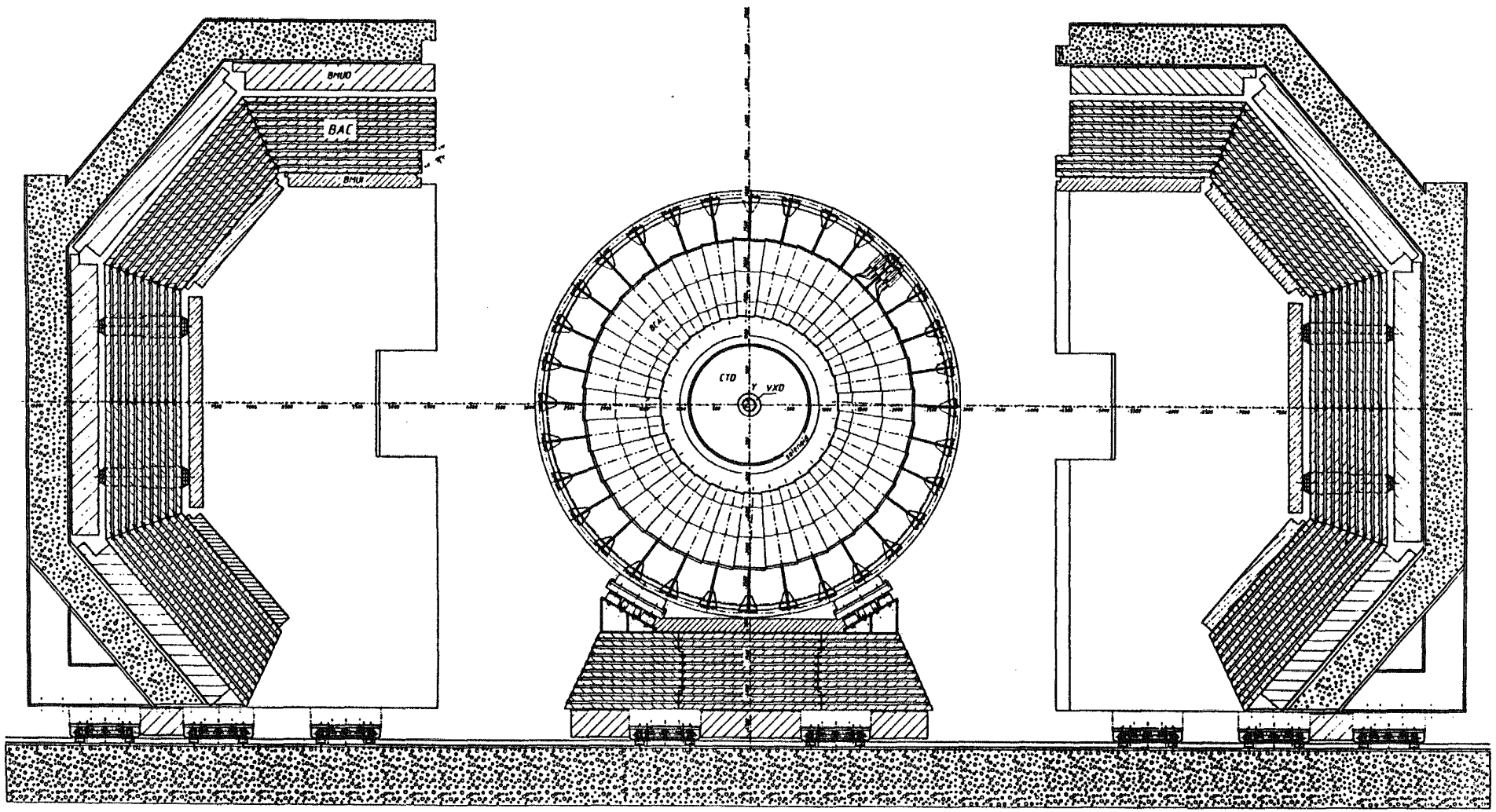

Fig. 24 Section of the ZEUS detector perpendicular to the beam. The clam shells are far retracted to give access to the inner detector components.

starts at about 60 mrad. The solid angle coverage corresponds to 99.8% in the forward hemisphere and 99.5% in the backward hemisphere. The expected energy resolutions are for electrons $\sigma(E)/E = 0.18/\sqrt{E} \oplus 1\%$ ($\oplus$ stands for addition in quadrature) and for hadrons $\sigma(E)/E = 0.35/\sqrt{E} \oplus 2\%$ (E in GeV).

The barrel calorimeter (BCAL consists of 32 identical modules (see Fig. 25), each covering an 11.25^{o} wedge in azimuthal angle. The inside radius for each module is 122 cm. The polar angle coverage is from $\theta = 36.7^{o}$ to $\theta = 129.1^{o}$. A module is divided into three segments in depth, called the electromagnetic section (BEMC), consisting of 21 layers of depleted uranium 23 χ_o or 1λ deep, and the two hadronic sections (BHAC1 and BHAC2), each 49 layers of depleted uranium, 53 χ_o or 2λ deep.

Within each module, the electromagnetic section is divided into projective towers with nominal dimensions of 5 cm x 24 cm at the front face. In the two hadronic sections, the towers are nonprojective in θ. Except at the ends four BEMC subtowers are followed by a single hadronic tower. Readout of the scintillation light from the individual towers in all three sections is accomplished using the two wave length shifter bars (WLS), placed one on each of the included faces of the modules and connected through light guides to photomultiplier tubes. Each module is closed by aluminum side panels that are used to retain the WLS plates and provide a gas-tight box. Each aluminum side panel will have a 1 mm lead sheet attached to it to reduce the effects of photons showering in the WLS. The BEMC is projective both in θ and ϕ, while the BHAC is only projective in ϕ, resulting in rectangular WLS-tiles.

b. Optical components

As discussed in the introduction to the ZEUS section LSU agreed to take over the production of the wavelength shifter bars for the electromagnetic part of the barrel calorimeter (BEMC) from OSU in order to speed up production of modules. OSU is still preparing the BHAC wave length shifters and the scintillators.

We hired three technicians in May 1989 to work on setting up the production facility at LSU for BEMC waveshifter bars. A duplicate scanning table was prepared at OSU and sent to LSU. A commercial oven for annealing pipes at LSU was bought. Our technicians made a number of trips to OSU in the summer to both learn the procedures and to help in the preparation of waveshifters for the first module at OSU. Our technicians also went to ANL to install the EMC waveshifters on the first module.

The procedure for preparation of the WLS is now briefly described.:

The Y-7 WLS sheets are laser cut by Laser Services Inc., of Westford, Mass into

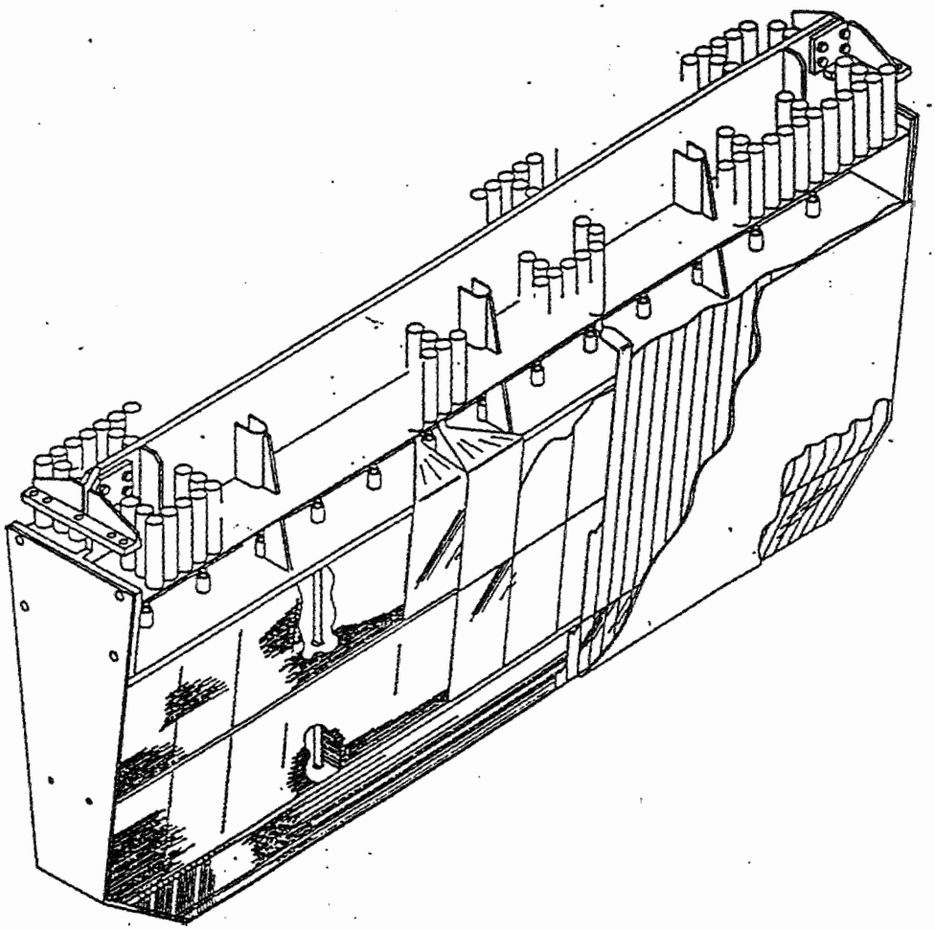

Fig. 25. Isometric view of a BCAL module

final EMC optical components. They are bent at LSU to conform to the final geometry of the barrel calorimeter. Ninety degree bends in the pipes are formed using infrared lamps and special jigs which make no contact with the hot plastic. Fingers leading to the transition piece are hand formed after heating. After bending, the finger ends are milled to join a transition piece leading to the photomultiplier tube. The transition piece is also made of Y-7 doped acrylic to allow for shifting of UV light from the laser calibration system. The milled light pipes are glued to the transition piece using acrylic optical glue. To avoid crazing in the milled pipes, the WLS are annealed for 8-10 hours before gluing. This is done using a large annealing oven purchased by Argonne National Laboratory for LSU. Finally each WLS is washed in an ultrasound bath of mild soap and distilled water. The bottom of each WLS piece is painted with Bicron reflecting paint to decrease longitudinal non-uniformities, and the long straight section of the pipe which transports the light to the photomultipliers is wrapped with 100 μm aluminized mylar.

The scintillator tiles and waveshifters will have light-yield non-uniformities caused by thickness variations (±5%) in the manufacturing of such thin plates. The light-yield also depends on the distance the scintillator tiles are from the phototubes. If not corrected, these non-uniformities would contribute to the energy resolution and decrease the performance of the calorimeter. We correct for light-yield non-uniformity by application of a reflective mask onto the waveshifter. LSU is preparing these reflection masks. The light collection uniformity of each piece of scintillator and coupled waveshifter is measured using computer controlled x-y scanning tables. These scanning tables are computer controlled via a CAMAC based data acquisition system modeled after the Ohio State University system, but utilizing the Vaxstation 3200 computer and Kinetic Systems Model 3922/2922 CAMAC controller and interface we purchased this past year. The scan results prove to be reproducible point by point to slightly better than 1%. Figure 26 shows the response of a WLS measured at LSU.

The results of the scans for the WLS and scintillator tiles are used to prepare the reflection masks. First, a pattern (negative image) of black rectangles whose density reflects the light-yield results from the scan is printed on a transparency. Presently, the results of the scan are used to prepare a graphics file which is then sent to a printing company to make the transparency at a cost of about $7/transparency. We are looking into the possibility of purchasing a laser printer and producing the transparencies ourselves. The transparency is then used to expose photo-sensitive aluminum plates which are then attached to the face of the WLS opposite the scintillator tiles. The reflection masks have been shown to remove the non-uniformities in a prototype module leaving a residual non-uniformity of less than 1%. As part of the ZEUS production effort, LSU now has a photographic exposure facility to make reflection masks.

By September, LSU was able to begin production of module 2 of the EMC WLS.

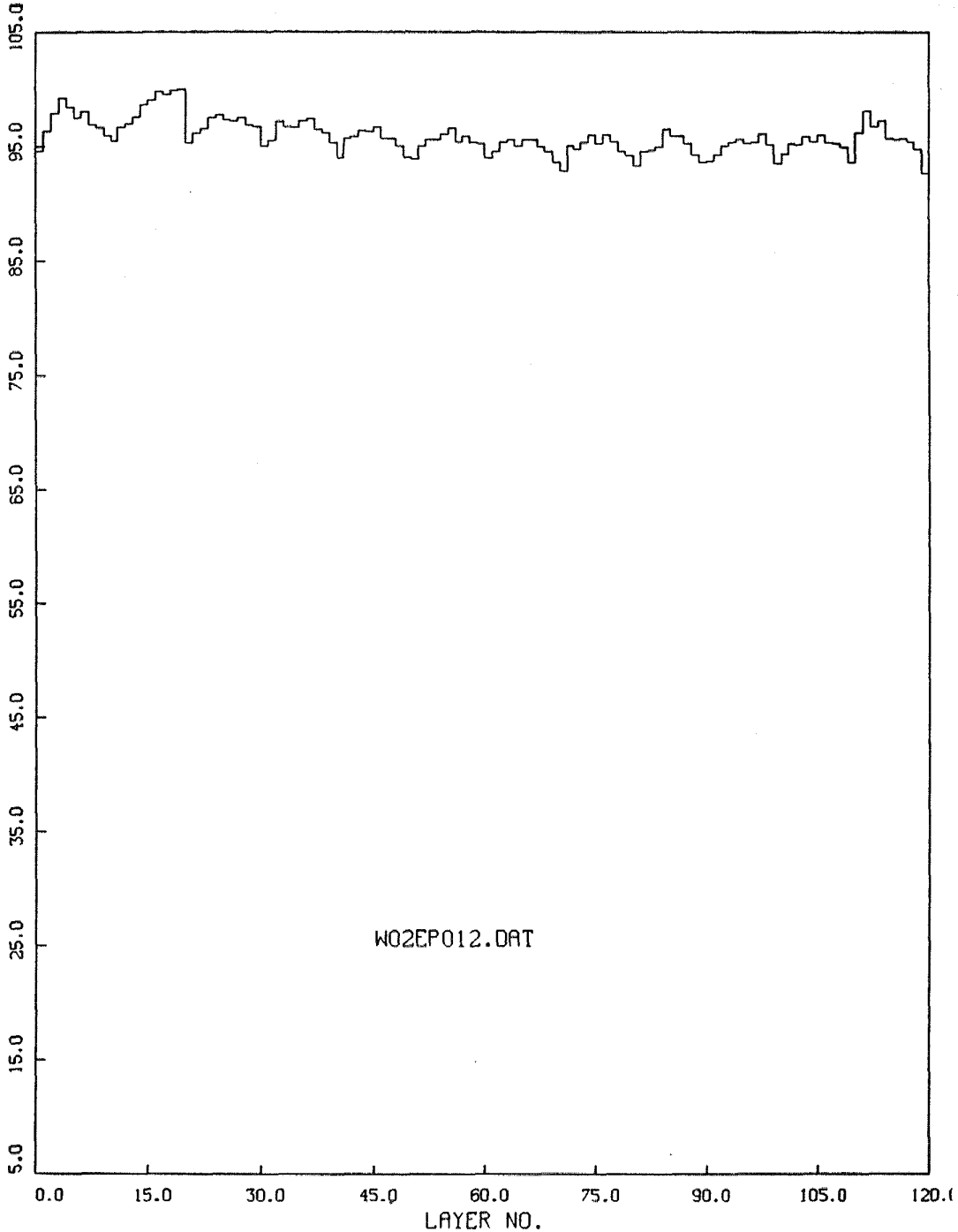

Fig 26 Response of a BEMC-WLS before correction, measured at LSU

leaving a residual non-uniformity of less than 1%. As part of the ZEUS production effort, LSU now has a photographic exposure facility to make reflection masks.

By September, LSU was able to begin production of module 2 of the EMC WLS. We are currently building up to a production speed of two modules a month which is necessary to have all 32 calorimeter modules completed by the end of 1990. Extra production jigs have been machined at LSU. With the 10 machining/bending jigs and the size of the oven we presently have, we can produce at least 10 completed waveshifter bars per day. The WLS scanning runs in parallel to the production effort. It takes about 40 minutes per waveshifter bar to complete a scan. At this rate we can keep a pace of completing 2 modules worth of WLS per month and finish the project near the end of 1990. Once the WLS production effort is streamlined, we plan to undertake the scanning of the scintillator tiles for the EMC as well. This will make the production of the reflection masks easier as we will be in total control of the EMC optical components testing.

5. LSU Plans for ZEUS

The LSU group joined ZEUS early in 1989. So far we have considered it a priority to get our EMC wavelength shifter production facility into operation. We consider ZEUS our major project for the next several years and want to substantially increase our ZEUS effort as our other projects wind down. As discussed elsewhere in the proposal, we expect to complete the analysis of our neutrino experiment next spring. Next year we plan to continue on AMY but to devote the majority of our effort to the ZEUS experiment.

On ZEUS we want to participate as the calorimeter beam tests at Fermilab and start working on ZEUS software. Roger McNeil plans to work on Monte Carlo calculation for the test beam. A post-doctoral associate, Hong Joo Kim, has just joined our group to work primarily on the ZEUS experiment. In the future, it will be essential to have a post-doctoral associate at DESY as well as one at LSU. Thus, when the post-doctoral associate on the neutrino experiment leaves we plan to replace him with someone who will work on ZEUS. We also want to find two graduate students to work on ZEUS to replace the two we have had on AMY. With this size group we could pursue a reasonable analysis effort at LSU and have a reasonable size contingent on site at /desy. This is particularly important given the fact that the 3 faculty members will have to spend the majority of their time at LSU.

E. SSC ACTIVITY

It will take nearly a decade to construct the Super Conducting Super Collider (SSC) in Texas, and may take as long to build experimental detectors capable of extracting physics at the SSC. Consequently, particle detection technologies must be vigorously studied now, and detectors designed very soon so that construction of them may commence. Over the next few years there will be significant research and development efforts culminating in SSC Detector proposals.

The primary motivation for the SSC is the expectation that it will lead to new discoveries, such as Higgs bosons, supersymmetric particles, heavy W's or Z's, new heavy fermions, or composite particles. Many of the predicted particles produce W's and Z's in their decay chains and it will thus be necessary for an SSC detector to be able to measure W and Z production through their decay products - e, μ, Jets, and νs. Detecting new physics such as the Higgs at SSC will be a challenge. The cleanest signals will be observed in the leptonic decays of the W's and Z's produced. These events will have very low rates and must be observed on top of large backgrounds requiring innovations in particle detectors and nuclear instrumentation. Furthermore, all SSC detector components must operated in the SSC environment of very high collision rate and for those components in the immediate vicinity of the accelerating beams, high radiation.

The pace of SSC Research and Development has increased dramatically over recent months. On October 2, 1989 proposals for major SSC detector Subsystems Research and Development were submitted to the SSC laboratory. LSU is involved with two of these SSC Subsystem R & D proposals:

A Proposal for Development of Super conducting Air Core Toroids as a Precision Muon Spectrometer for SSC Experiments.

and

A Proposal to develop an Uranium Scintillator-plate Calorimetry System for the SSC.

a. Muon Identification

In the proposal to develop super conducting air core toroids, McNeil is involved in making Monte Carlo simulation studies of hadron backgrounds to rare physics processes.

A very important consideration in the optimization of the design of any muon spectrometer for SSC detectors is the level of backgrounds from hadron punchthrough and decay. These backgrounds not only affect the ability to observe signals from rare physics processes at SSC, but also the ability to form low-rate triggers for muons. The punchthrough background is of particular importance to the development of a precision muon spectrometer system based on air core toroids where the insertion of extra filter material for punchthrough suppression sets the scale for the toroid system both in size and cost. An outstanding issue that must be understood before one could embark on the construction of a muon spectrometer is the minimum hadron absorber thickness demanded by SSC physics needs. Another issue is the impact of the hadron punchthrough and muon radiation on the performance requirements for the design of the muon spectrometer including the toroid system, muon measuring system, and trigger system. We propose to study these issues through simulation of the hadron punchthrough and to study the effects of this background on the detailed design choices for the toroid system.

The work proposed is as follows: First, determine the overall rate and spectrum of punchthrough background as a function of hadron absorber thickness and lab angle,θ. This will be for a general purpose detector and not be specific to air core toroids. First, a FAST Monte Carlo detector simulation will be developed including exit punchthrough shower parameterizations. This simulation will then be combined with an event generator such as ISAJET to study absolute rates; then, for detailed design choices of the toroid system, transport the punchthrough particle through the field and determine requirements for the forming of a muon trigger including minimum P_T and linkage to tracks before and after the calorimeter. Finally, for detailed design choices of the muon spectrometer, determine by simulation the impact of punchthrough background and muon radiation on momentum resolution and the ability to observe physics signals involving muons.

b. Scintillation Calorimetry for SSC

In the proposal on Scintillation Calorimetry we are involved in the testing and optimization of optical components in the calorimeter.

A major technical challenge facing the builders of detectors for the SSC is to achieve an optimum design for the calorimeter. This is because the dominant characteristics of the 40-TeV pp collisions will be final states containing jets of hadrons as well as leptons. In addition to the jets from the primary partons, there will be copious production of the W and Z bosons, which much be identified via their decays to either jets or leptons. A calorimeter must, therefore, measure jets as well as electrons from heavy boson decays. Accurate measurements of electrons in the calorimeter are necessary to

be sensitive to new physics.

There are very severe operating requirements for an SSC calorimeter. In addition to the general questions of sampling granularity, transverse tower segmentation, longitudinal shower sampling, and total calorimeter thickness, the SSC imposes additional constraints related to the interaction rate of 62 MHz and the anticipated radiation damage of more than one Mrad per operating year. These requirements put severe constraints on the technologies that can be used for a calorimeter. Parallel efforts to optimize various calorimeter technologies such as warm liquids, liquid argon, scintillator plates, scintillating fibers, and silicon are presently underway. Because of its fast response and good energy resolution, we propose to study scintillator-plate technology for the SSC.

LSU is responsible for the production and testing of optical components for the electromagnetic portion of the ZEUS barrel calorimeter (see section D for further discussion of this work) which uses scintillator-plate sampling. This calorimeter is designed expressly for accurate measurements of the energy of both electrons and jets. Besides giving outstanding energy resolution for electrons and jets, this type of calorimetry has several other strengths: its response is very fast, well-matched to the high data rates expected at the SSC; it can measure both the longitudinal and the lateral development of the showers; the construction is simple and allows insertion of position measuring devices in the calorimeter stack to provide accurate spatial position of the electromagnetic showers; and finally, it requires relatively few readout channels. LSU's experience and present setup make it ideally suited to perform studies to optimize this technology for the SSC environment.

The concept which is proposed is a scale-up of the ZEUS calorimeter. The barrel section would consist of 192 modules, 64 in azimuth and 3 modules along the beam direction. As in the ZEUS calorimeter (which has 32 modules) each module would be mechanically stable stand-alone units. Each of the modules would be 2.4 m deep, 6.75 m high and 0.25 m thick and contain towers of between 256 layers (2.6 mm thick scintillator) and 333 layers (2.0 mm thick scintillator) of scintillator and depleted Uranium (or lead).

The work proposed by LSU is in regard to the optical system of the calorimeter. We must ensure an adequate efficiency in the coupling of the scintillator light via a waveshifter plate and light guide to the photon detector so that the photon statistics will not dominate the resolution. The main tasks assigned are:

Measure the light detection efficiency. Measure the system efficiency of the optical design proposed for the calorimeter (scintillator, waveshifter, lightguide, and photon detector).

Optimize the optical structure. Determine the structure of filters and reflectors required to obtain the necessary detector uniformity consistent with the chosen optical geometry. Optimize the structure to maximize the light yields.

Evaluate the optical performance of radiation exposed scintillator and wavelength shifter material to determine the light transmission, light output, and radiation damage recovery.

Participation in production and testing of the optical components for three full scale prototype modules to be constructed as part of the subsystem proposal.

Participate in testing of the prototype modules using radioactive sources, cosmic rays, and e/π test beams.

F. REFERENCES

1) T.Y. Ling, T.A. Romanowski, The Ohio State University; L.G. Hyman, B. Musgrave, Argone National Laboratory; R. Imlay, W.J. Metcalf, Louisana State University; R.D. McKeown, California Institute of Techology. A search for Neutrono Oscillations at LAMPF, Proposal submitted to LAMPF.

2) "New limits on $\bar{\nu}_\mu \rightarrow \nu_e$ Oscillation",L.S. Durkin *et al.*, Phys. Rev. Lett., **61**, 1811 (1988).

3) S. Igarashi *et al.*(AMY), Phys. Rev. Lett. **60**, 2359 (1988).

4) "Measurement of Cross Sections and Charge Asymmetry for $e^+e^- \rightarrow \tau^+\tau^-$ and $e^+e^- \rightarrow \mu^+\mu^-$ for $\sqrt{s} = 52\text{to}57\text{GeV}$", A. Bacala *et al.*(AMY), Phys. Lett. **B 218**, 112 (1989).

5) "A Measurement of $e^+e^- \rightarrow b\bar{b}$ Forward-Backward Charge Asymmetry Between $\sqrt{s}$ = 52 and 57 GeV", H. Sagawa, J. Lim *et al.*(AMY), Accepted for publication in Phys. Rev. Lett. (1989).

6) L.S. Durkin *et al.*, NIM **A277**, 386 (1989).

7) M. Timko, Ph.D. Thesis, The Ohio State University; C. Choi, Ph.D. Thesis, Louisiana State University.

8) J. Mitchell, Ph.D. Thesis, The Ohio State University.

9) F. Reines *et al.*, Phys. Rev. Lett. **45**, 1307 (1980).

10) K. Kwon *et al.*, Phys. Rev. **D24**,1097 (1981); F. Boehm *et al.*, Phys Lett. **97B**, 310 (1980); J.L. Vuileumier *et al.*,Phys. Lett. **114B**, 298 (1982); K. Gabathuler *et al.*, Phys. Lett. **138B**, 449 (1984); G. Zacek *et al.*, Phys. Rev. **D34**, 2621 (1986).

11) F. Dydak *et al.*, CDHS Collab., Phys.Lett. **134B**, 281(1984); F. Bergsma *et al.*, CHARM Collab, Phys.Lett. **142B**, 103 (1984); L.A. Ahrens *et al.*, Phys. Rev. **D31**, 2732 (1985); C. Angelini *et al.*, Phys. Lett. **179B**, 307 (1986); E.B. Brucker *et al.*, Phys. Rev. bf D34, 2183 (1986); J. Bofill *et al.*, Phys. Rev. **D36**, 3309 (1987).

12) Indication for Neutrino Oscillation from a High Statistics Experiment at the Bugey Reactor, J.F. Cavaginac *et al.*, Phys. Lett. **148B**, 387 (1984).

13) "Anomalous Electron Production Observed in the CERN PS Neutrino Beam", G. Bernardi *et al.*, Phys. Rev. Lett. **53**, 641 (1984); Phys. Lett. **139B**, 115 (1984).

14) B. Blumenfeld *et al.*, Phys. Rev. Lett., **62**, 2237 (1989).

15) See for example Proc. of the Lepton-Photon Conference, SLAC, Aug. 1989.

16) H. Harada *et al.*, Nucl Inst. and Meth. **A265**, 141 (1988).

17) S.L. Glashow, Nucl. Phys. **22**, 579 (1961); S. Weinberg, Phys. Rev. Lett. **19**, 1264 (1967); A. Salam, Proc. of the 8th Nobel Symposium, Aspenasgarden, 1968, p.367 (Almqvist and Wiksell, Stockholm).

18) R. Budny, Phys. Lett. **B55**, 227 (1975); J.Ellis and M.K. Gaillard, CERN 76-18.

19) M. Derrick et al. (HRS), Phys. Rev. **D 31**, 2352 (1985); W. Ash et al. (MAC), Phys. Rev. Lett. **55**, 1831 (1985); M.E. Levi et al. (MARK-II), Phys. Rev. Lett. **51**, 1941 (1983).

20) B. Adeva et al. (MARK-J), Phys. Rev. Lett. **55**, 665 (1985); W. Bartel et al. (JADE), Z. Phys. **C 26**, 507 (1985); Ch. Berger et al. (PLUTO), Z. Phys. **C 27**, 341 (1985); H.J. Behrend et al. (CELLO), DESY Report 87-005; M. Althoff et al. (TASSO), Z. Phys. **C 22**, 13 (1984).

21) K. Abe *et al.*(VENUS), paper contributed to the 24th International Conference on High Energy Physics, Munich, August 1988.

22) I. Adachi *et al.*(TOPAS), paper contributed to the 24th International Conference on High Energy Physics, Munich, August 1988.

23) M. Igarashi et al., Nucl. Phys. **B263**, 347 (1986); S. Kawabata, Comput. Phys. Commun. **41**, 127 (1986). The difference in the radiative corrections between $\mu^+\mu^-$ and $\tau^+\tau^-$ is due to the different selection criteria in the two cases.

24) H. Sagawa *et al.*(AMY), Phys. Rev. Lett., **60**, 93 (1988).

25) H. Fesefeldt, Nucl. Instr. and Meth., **A263**, 114 (1987).

26) B. Adeva *et al.*(MARK J) ,Phys. Rev. **D 34**, 681 (1986); W. Bartel *et al.*(JADE), Z. Phys. **C36**, 15 (1987) .

27) F. Cornet *et al.*,Phys. Lett.,**B174**,224 (1986); V. Barger,R.J.N. Philips and A. Soni, Phys. Rev. Lett. **57**, 1518 (1986).

28) H.J. Behrend (CELLO)*et al.*,Phys. Lett., **B 193**, 157 (1987).

29) K. Ogawa *et al.*(VENUS), Topical Conference at KEK, (1989).

30) S. Eno *et al.*(AMY), KEK Preprint 88-47.

31) LUND 6.3, T. Sjostrand and M. Bengsston, Comput. Phys. Commum., **43**, 367 (1987).

32) EPOCS, see K. Kato and T. Munehisa, KEK87-5(1987) (Unpublished).

33) F. Fujimoto and Y. Shimimzu, *Mod. Phys. Lett.***A 3**, 581 (1988).

34) Various theorectical models of this type and their consequences were studies by several authors. See for example, G.L. Kane and M.E. Peskin, Nucl. Phys. **B195**, 29 (1982). The mostr striking feature of the simplest of these models is the appearence of a flavor changing neutral current, which was subsequently ruled out experimentally. See P. Avery *et al.*, Phys. Rev. Lett. **53**, 1309 (1984). Various schemes to suppress the FCNC were proposed. References may be found in G.L. Kane and M.E. Peskin. For a more recently proposed model, based on supersymmetry, see Ernest Ma, Phys. Rev. **D35**, 851 (1987).

35) H. ALbrecht *et al.*(ARGUS), Phys. Lett. **B192**, 245 (1987); M. Artuso *et al.*(CLEO), Phys. Rev. Lett. **62**, 2233 (1989).

36) K. Hagiwara *et al.*, Phys. Lett. **B219**, 369 (1989).

37) W. Bartel *et al.*(JADE), Phys. Lett **B146**, 437 (1984); M. Althoff *et al.*(TASSO), Phys. Let. **B146**, 443 (1984); C. Kiesling, Talk in the 29th Moriond Conference (March, 1989); F. Ould-Saada, DESY report 88-177 (1988); H.R. Band *et al.*(MAC), Phys. Lett. **B218**, 369 (1989); C.R. Ng *et al.*(HRS), ANL-HEP-PR-88-11; S.L. Wu, Nucl. Phys. **B** (proc.Suppl.) 3.

38) L.M. Sehgal, P. Zerwas, *Nucl. Phys.*, **B108**, 484(1976); V. Barger et al., *Phys. Lett.*, **70B**, 51(1977).

39) Ya.I. Azimov *et al.*, Leningrad preprint, **LNPI-222** (1976); M. Suzuki, Phys. Lett., **71B**, 51 (1977); J.D. Bjorken, Phys. Rev., **D17**, 171 (1978); D.M. Scott, Phys. Rev., **D18**, 210 (1978).

40) C. Peterson et al., *Phys. Rev.*, **D27**, 105(1983).

41) B. Andersson et al.,*Phys. Rep.*, **97**, 33(1983); T. Sjöstrand, *Comp. Phys. Commun.*, **27**, 243(1982).

42) JADE Collaboration: W. Bartel et al., *Z. Phys. C*, **33**, 339(1987); MARK II Collaboration: M.E. Nelson et al., *Phys. Rev. Lett.*, **50**, 1542(1983); TASSO Collaboration: M. Althoff et al., *Phys. Lett.*, **146B**, 443(1984); *Z. Phys. C*, **22**, 219(1984); MARK J Collaboration: B. Adeva et al., *Phys. Rev. Lett.*, **51**, 443(1983); MAC Collaboration: B. Fernandez et al., *Phys. Rev. Lett.*, **50**, 2054(1983).

43) "Proceedings of the Summer Study on High Energy Physics in the 1990s", June 27-July 15, 1988 Snowmass, Colorado, Published by World Scientific Pub.

44) "Proceedings of the HERA Workshop", October 12-14, 1987, Hamburg, F.R. Germany, Published by DESY.

45) H. Tiecke *et al.*, Nucl. Inst. and Meth., **A277**, 42 (1989).

IV. REPORTS

ORO-5490-1 Comments on Electromagnetic Mass Differences in the Charmed Quark Model, Lai-Him Chan, LSU Preprint, 1977).

ORO-5490-2 The Spin Structure of the Effective Quark Hamiltonian and the Hyperfine Splittings of Charmonium, Lai-Him Chan, Phys. Lett., **71B**, 422 (1977).

ORO-5490-3 Quark-Loop Dominance in the SU(3) Sigma Model, ,Lai-Him Chan, Phys. Rev. Lett., **39**, 1124 (1977).

ORO-5490-4 Charmonium - The $^1P_1$ State, Lai-Him Chan and R. F. O'Connell, Phys. Lett., **76B**, 121 (1978).

ORO-5490-5 Progress Report, March 1978.

ORO-5490-6 The Gross-Neveu Model as a $Z_3 = 0$ Limit of the Two-Dimensional SU(N) Sigma Model, R. Haymaker and F. Cooper, Phys. Rev. **D19**, 562 (1979).

ORO-5490-7 Renormalization of the Broken Symmetry 2D SU(N) Sigma Model and the $\bar{\psi}\psi$ Model, R. Haymaker with F. Cooper,G. Guralnik, and K. Tamvakis, Phys. Rev. **D20**, 3336 (1974).

ORO-5490-8 Progress Report, March 1979.

ORO-5490-9 The Effect of Heavy Particle in Low Energy Light-Particle Processes, Lai-Him Chan, T. Hagiwara and B. Ovrut, Phys. Rev., **D20**, 982 (1979).

ORO-5490-10 How to Measure the Number of Quark and Lepton Generations without Building Ultrahigh Energy Accelerators, Lai-Him Chan and T. Hagiwara, Phys. Rev. **D20**, 1968 (1979).

ORO-5490-11 Progress Report, January 1980.

ORO-5490-12 A Goldstone Pion with Bag Confinement, T. Goldman and R. Haymaker, LSU Preprint, (1980).

ORO-5490-13 A Goldstone Pion with Bag Confinement, T. Goldman and R. Haymaker, Invited Talk Presented at the XX International Conference on High Energy Physics, Madison, Wisconsin, July 1980. (Published in the Proceedings, American Institute of Physics, 1981).

ORO-5490-14 Dynamically Broken Chiral Symmetry with Bag Confinement,T. Goldman and R. Haymaker, Phys. Rev. **D24**, 724 (1981).

ORO-5490-15 Bag Confinement Chiral Breaking Effect on a Goldstone Pion,T. Goldman and R. Haymaker, Phys. Lett. **1OOB**, 276 (1981).

ORO-5490-16 Bag Boundary Condition for Confinement in the qq - Relative Coordinate, R. Haymaker and T. Goldman, Phys. Rev., **D24**, 743 (1981).

ORO-5490-17 Observation of the Upsilon" at the Cornell Electron Storage Ring, G. Finocchiaro et al. (including G. Levman, LSU) Phys. Rev. Lett., **45**, 222 (1980).

ORO-5490-18 Observation of the Transition $\Upsilon' \rightarrow \Upsilon\pi^+\pi^- \rightarrow e^+e^-\pi^+\pi^-$, G. Mageras et al (Including R. Imlay and G. Levman, LSU) Phys. Rev. Lett. **46**, 1115 (1981).

ORO-5490-19 Hadron Electromagnetic Mass Differences and a Prediction of $B^+ - B^\circ$ Lai-Him Chan, LSU Preprint, (1980).

ORO-5490-20 Progress Report, February 1981.

ORO-5490-21 Measurement of B-meson Semileptonic Decay, (including Imlay, Metcalf, Levman, Sreedhar, LSU), Phys. Rev. Lett. **47**, 771 (1981).

ORO-5490-22 Closed-Form Bound-State Effective Potential and Exact Solutions for Dynamical Symmetry Breaking in a 4D Gauge Theory, R. Haymaker and J. Perez-Mercader, Phys. Lett. **1O6B**, 201 (1981).

ORO-5490-23 Dynamical Symmetry Breaking. R. Haymaker, Lecture Notes for the XXI Cracow School of Theoretical Physics; Acta Physica Polonica **B13**, 575 (1982).

ORO-5490-24 Progress Report, December 1981.

DOE/ER/05490-25 Dynamics and Stability of Dynamical Symmetry Breaking without Fundamental Scalars, R. Haymaker and Juan Perez-Mercader, Phys. Rev. **D27**, 1353 (1983).

DOE/ER/05490-26 Dynamics of the Light Mesons Lai-Him Chan, LSU preprint, (1982).

DOE/ER/05490-27 Search for Structure in $\sigma(e^+e^- \rightarrow \text{hadrons})$ between $\sqrt{s}$ =10.34 and 11.6 GeV, E. Rice, et al.(including Imlay, Metcalf, Levman, and Sreedhar, LSU), Phys. Rev., Letters **48**, 906 (1982).

DOE/ER/05490-28 Thrust Distributions and Decays of the Y Bound States, D. Peterson, T. Bohringer, et al. (including Imlay, Metcalf, Levman and Sreedhar, LSU), Phys. Letters, **1114B**, 277 (1982).

DOE/ER/05490-29 Upper Limit for Axion Production in Radiative Gamma Decay M. Sivertz, et al.(including Imlay, Metcalf, Levman and Sreedhar, LSU), Phys. Rev. **D26**, 717 (1982).

DOE/ER/05490-30 Search for $B^* \rightarrow B + \gamma$ and limits on the B-meson mass, R. D. Schamberger, Jr., et al., (including Imlay, Metcalf, Levman, and Sreedhar, LSU), Phys. Rev., **D26**, 720 (1982).

DOE/ER/05490-31 InclusiveK° Production in e+e- Annilhilation at the Upsilon Resonances, G. Giannini, et al, (including Imlay, Metcalf, Levman and Sreedhar, LSU), Nuclear Physics **B206**, 1 (1982).

DOE/ER/05490-32 Convexity of the Effective Potential, R. Haymaker and J. Perez-Mercader, Phys. Rev. **D27**, 1948 (1983).

DOE/ER/05490-33 Observation of $\pi\pi$ Cascade Decays of the Upslion" G. Mageras,et al. (including Imlay, Levman, Metcalf, and Sreedhar,LSU), Phys. Lett. **118B**, 453 (1982).

DOE/ER/05490-34 Hadron Electromagnetic Mass Differences and a Prediction of B^+-B°, Lai-Him Chan, LSU preprint. (Revision) Phys. Rev. Lett, **51**, 253 (1983).

DOE/ER/05490-35 Observation of P-wave $b\bar{b}$- Bound States, K. Han, et al.,(including Imlay, Levman, Metcalf, and Sreedhar, LSU), Phys. Rev. Letters, **49**, 1612 (1982).

DOE/ER/05490-36 Evidence for χ_b' Production in the Exclusive Reaction $Y'' \rightarrow \gamma\chi_b' \rightarrow (\gamma\gamma Y'$ or $\gamma\gamma Y)$, G. Eigen, et al., (including Imlay, Levman, Metcalf, and Sreedhar, LSU, Phys. Rev. Lett.,**49**, 1616 (1982).

DOE/ER/05490-37 Progress Report, December 1982.

DOE/ER/05490-38 Stability of a Chiral Breaking Vacuum, R. Haymaker and J. Perez-Mercader, preprint, to be published in the Proceedings of the Workshop on Non-Perturbative QCD, Oklahoma State University, 1983; Birkhauser.

DOE/ER/05490-39 Natural, Large, Dynamically Generated Gauge Hierarchies, R. Haymaker and J. Perez Mercader, LANL Preprint LA-UR-83-2332, (1983).

DOE/ER/05490-40 Observation of the Lowest P-Wave $b\bar{b}$- Bound States, C. Klopfenstein et al., (including Imlay, Metcalf, Levman, and Sreedhar) Phys. Rev. Lett., **51**, 160 (1983).

DOE/ER/05490-41 Progress Report, October 1983

DOE/ER/05490-42 Tunneling and the Low Momentum Expansion of the Effective Action, C. Bender, F. Cooper, B. Freedman, R. Haymaker, Nucl Phys., **B256**, 653 (1985).

DOE/ER/05490-43 Anomalous Z° Events and Scalar Bound States, R. Haymaker and T. Matsuki, Phys. Lett. **148B**, 243 (1984).

DOE/ER/05490-44 Association of Supersymmetry with g = 2 for the Electron, R. Haymaker and A. R. P. Rau, LSU Preprint, (1985).

DOE/ER/05490-45 Isospin Mass Splittings of Hadrons with Heavy Quarks, Lai-Him Chan, Phys. Rev. **D31**, 204 (1985).

DOE/ER/05490-46 Observation of χ_b Production in the Exclusive Reaction $Y' \rightarrow \gamma\chi_b \rightarrow \gamma\gamma Y \rightarrow \gamma\gamma(e^+e^-$ or $\mu^+\mu^-)$ F. Pauss et al., (including Imlay, Levman, Metcalf, Sreedhar) Phys. Lett., **130B**, 444 (1983).

DOE/ER/05490-47 Semileptonic Decay of the B Meson, C. Klopenstein, et al,.(including Imlay, Levman, Metcalf, Sreedhar), Phys. Lett., **130B**, 44 (1983).

DOE/ER/05490-48 The CLEO Detector, D. Anders, et al.,(including Imlay) Nuclear Instru. and Meth., **211**, 47 (1983).

DOE/ER/05490-49 Observation of Direct photons in Y and Y' Decays and Determination of the QCD Scale Parameter, R. D. Schamberger, et al., (including Han, Imlay, Levman, Metcalf, Sreedhar) Phys. Lett., **138B**, 225 (1984).

DOE/ER/05490-50 Search for Higgs Scalars in Upsilon Decays, S. Youssef, et al., (including Han, Imlay, Levman, Metcalf, Sreedhar), Phys. Lett., **139B**, 332 (1984).

DOE/ER/05490-51 A Measurement of the Semileptonic Decay of B Mesons into Muons, G. Levman, et al., (including Sreedhar, Han, Imlay, Metcalf), Phys. Lett., **141B**, 271 (1984).

DOE/ER/05490-52 A Study of Hadronic Decays of the Y', V. Fonseca, et al., (including Imlay, Levman, Metcalf) Nucl. Phys., **B242**, 31 (1984).

DOE/ER/05490-53I Improved Method for Studying Tunneling and False Vacuum Decays, R. Haymaker, T. Matsuki, S. Wang, and F. Cooper, Abstract, submitted to AIP Santa Fe meeting DPF, Fall, 1984.

DOE/ER/05490-54 A New Approach to the Low Energy Effective Action Expansion, Lai-Him Chan, Abstract submitted to APS, DPF, Santa Fe meeting, Fall, 1984

DOE/ER/05490-55 Can Baryons be Chiral Solitons in the Effective Lagrangian of the Non-Linear SU(N) Quark Model? Lai-Him Chan, Abstract submitted to the APS DPF Santa Fe meeting Fall, 1984.

DOE/ER/05490-56 General Calculation of the N=4 Supersymmetric Yang-Mills Self Energy in an Effective Light-Cone Gauge Formalism, T. Matsuki, and G. Leibbrant, Phys. Rev., **D31**, 934 (1985).

DOE/ER/05490-57 Chiral and Graviational Anomalies in Any Dimension, R. Delbourgo and T. Matsuki, J. Math. Phys. **26**, 1334 (1985).

DOE/ER/05490-58 Another Resonance observed in a Multi TeV e+e- Collider, T. Matsuki, LSU preprint, (1984).

DOE/ER/05490-59 New Limits on the Mass of Majorana Neutrino and Right-handed Heavy Bosons, A. Fazely, F. Imlay, T. Matsuki and W. Metcalf.

DOE/ER/05490-60 Progress Report October 1984.

DOE/ER/05490-61 Effective-Action Expansion in Perturbation Theory, Lai-Him Chan, Phys. Rev. Lett., **54**, 1222 (1985).

DOE/ER/05490-62 Baryons as Solitons in the Effective Lagrangian of Spontaneously Broken Chiral Symmetry, Lai-Him Chan, Phys. Rev. Lett., 55, 21 (1985).

DOE/ER/05490-63 Lorentz Anomaly in Arbitrary Dimensions, T. Matsuki, to be published in Zeit. f. Phys. C (1985).

DOE/ER/05490-64 Gravitational Counterterms and BRS Symmetry, R. Delbourgo and T. Matsuki, Phys. Rev. **D32**, 2579 (1985).

DOE/ER/05490-65 Quantum Corrections to False Vacuum Decay in the Coleman-Weinberg Potential, F. Cooper, R.W. Haymaker, T. Matsuki, and S. Wang, Phys. Rev. **D32**, 2049 (1985)

DOE/ER/05490-66 Gravitational Counterterms in an Axial Gauge, T. Matsuki, Phys. Rev. **D32**, 3164 (1985).

DOE/ER/05490-67 Effective Lagrangian for the Linear σ Model at $M_\sigma \rightarrow \infty$, Lai-Him Chan, LSU Preprint (1985).

DOE/ER/05490-68 PC Database for High Energy Preprint Collections, R. W. Haymaker, LSU Preprint (1985).

DOE/ER/05490-69 Saddle Point Instability in Models of Chiral Symmetry Breaking, R. W. Haymaker and T. Matsuki,Phys Rev., **D33**, 1137 (1986).

DOE/ER/05490-70 Supersymmetry in Quantum Mechanics, R. W. Haymaker and A. R. P. Rau, Am. J. Phys., **54**, 928 (1985).

DOE/ER/05490-71 Path Integral Derviation of Gravitational Anomalies in Arbitrary Even Dimensions, T. Matsuki, Progrs. Theor. Phys., **75**, 461 (1986).

DOE/ER/05490-72 Masses, Widths and Leptonic Widths of the Higher Upsilon Resonances, D. M. J. Lovelock et al, Phys. Rev. Lett., **54**, 377 (1985).

DOE/ER/05490-73 Observation of B* Production in e+e- Interactions above the b-Flavor Threshold, K. Han et al.,Phys. Lett, **55**, 36 (1985).

DOE/ER/05490-74 Progress Report, September 1985.

DOE/ER/05490-75 Comparison of Alternative Effective Potentials for Dynamical Symmetry Breaking, R. W. Haymaker, T. Matsuki, and F. Cooper, Phys. Rev. **D35**, 2567 (1987).

DOE/ER/05490-76 Derivative Expansion for the one-loop effective actions with Internal Symmetry, L-H Chan, Phys. Rev. Lett, **57**, 1199 (1986)

DOE/ER/05490-77 Is the Nonlinear $M_\sigma \to \infty$ Limit of the Linear σ Model? L-H Chan, Phys. Rev. **D36**, 3755 (1987).

DOE/ER/05490-78 Effective Lagrangian for the Chiral Quark Dynamics, L-H Chan, **Chiral Soliton**, Chapter 2, 64-69, edited by K. F. Lin (World Scientific, Singapore, 1986)

DOE/ER/05490-79 Neutrinoless Double β decay and its Relation to Pion Double Charge Exchange, A. Fazely and L. C. Liu, LS-UR-86-447 (1986), Phys. Rev. Lett. **57**, 968 (1986)

DOE/ER/05490-80 Progress Report, September 1986

DOE/ER/05490-81 Space Structure of Confining Strings, J. Wosiek and R. W. Haymaker, Phys. Rev. **D36**, 3297 (1987)

DOE/ER/05490-82 Complex Langevin Simulations of Nonabelian Integrals, R. W. Haymaker and J. Wosiek, Phys. Rev. **D37**, 969 (1988).

DOE/ER/05490-83 Improvement of the Derivative Expansion, Lai-Him Chan, Phys. Rev. **D38**, 3739 (1988).

DOE/ER/05490-84 Progress Report, October 1987

DOE/ER/05490-85 Complex Langevin Simulation of Non-Abelian Flux Integrals, R. W. Haymaker and J. Wosiek, Nuclear Physics **B4**, 571-575, (1988).

DOE/ER/05490-86 Hierarchies under the Rainbow, R. W. Haymaker and J. Perez-Mercader, LSU preprint, (1988).

DOE/ER/05490-87 Measurements of R and a Search for Heavy-Quark Production in e+e- Annihilation at $\sqrt{s}$ = 50 and 52 GeV, H. Sagawa, et al., Phys. Rev. Lett. **60**, 93-96 (1988).

DOE/ER/05490-88 Search for Isolated Leptons in Low-Thrust e+e- Annihilation events at $\sqrt{s}$ = 50 and 52 GeV, S. Igarashi, et al., Phys. Rev. Lett. **60**, 2359-2362 (1988).

DOE/ER/05490-89 Experimental Mass Limit for a Fourth-Generation Sequential Lepton from e+e- Annihilations at $\sqrt{s}$ = 56 GeV, G. N. Kim, et al., Phys. Rev. Lett. **61**, 911-914 (1988).

DOE/ER/05490-90 Recent Results from AMY at TRISTAN, R. R. McNeil, KEK preprint 87-90 (1987).

DOE/ER/05490-91 Nonanalog 0+(g.s.) → 0+(g.s.) Transitions in Pion Double Charge Exchange Reactions on ^{128}Te and ^{130}Te, A. Fazely, et al., Phys. Letters **B208**, 361-364 (1988).

DOE/ER/05490-92 Effective Action Expansion for the Non-Linear Sigma Model: The Normal Coordinate Method, L.-H. Chan, W. F. Kao, and T. Matsuki, LSU preprint (1988).

DOE/ER/05490-93 Progress Report, October 1988

DOE/ER/05490-94 Convergence of Langevin Simulation for Complex Gaussian Integrals, R. W. Haymaker and Y Peng, LSU HE Preprint #94-1989.

DOE/ER/05490-95 Color Flux Distribution on the Lattice, R. W. Haymaker, presented at the XXIX Cracow School of Theoretical Physics, Zakopane, Poland, June 1989.

DOE/ER/05490-96 Limits on $\overline{\nu_\mu} \rightarrow \overline{\nu_e}$ Oscillations, L. S. Durkin, et al., Phys. Rev. Lett. **61**, 1811 (1988).

DOE/ER/05490-97 Physics from TRISTAN, invited address at the Conference on "Beyond the Standard Model," R. R. McNeil, Iowa State University, Ames Iowa, November 1988, Proceedings to be pubished by Academic Press.

DOE/ER/05490-98 Measurements of Cross Sections and Charge Asymmetries for $e^+e^- \rightarrow \tau^+\tau^-$ and $e^+e^- \rightarrow \mu^+\mu^-$ for $\sqrt{s}$ from 52 to 57 GeV., A. Bacala, et al., Phys. Lett. **B218**, 112 (1989).

DOE/ER/05490-99 Measurements of the e+e- Total Hadronic Cross Section and a Determination of Mz and$\Lambda_{\overline{MS}}$, T. Mori, et al., Phys. Lett. **B218**, 499 (1989).

DOE/ER/05490-100 Experimental Evidence for the non-Abelian Nature of QCD from a Study of Multijet Events Produced in e+e- Annihilations, I. H. Park, et al., Phys. Rev. Lett., **62**, 1713 (1989).

DOE/ER/05490-101 A Fine-Grain Modular Detector for Low-Energy Particles, L. S. Durkin, et al., Nucl. Instrum. Method **A277**, 386 (1989).

DOE/ER/05490-102 Search for the Substructure of Leptons in High Energy QED Processes at TRISTAN, S. K. Kim, et al., Phys. Lett. **B223**, 476 (1989).

DOE/ER/05490-103 "Recent Results from TRISTAN, W. J. Metcalf, invited talk at the 2nd International Conference on the 4th Family of Quarks and Leptons, UCLA, Febrruary 23-25, 1989.

DOE/ER/05490-104 Search for Unstable Heavy Neutral Leptons in e^+e^- Annhilations at $\sqrt{s}$ from 50 to 60.8 GeV, N. M. Shaw, et al., Phys. Rev. Lett., 63, 1342 (1989).

DOE/ER/05490-105 Consequence on Scale Invariance, H. Cheng and W. F. Kao, LSU HE preprint, (1989).

DOE/ER/05490-106 $^{12}C(\pi^{\pm},\pi^{\pm'},p)^{11}B$ Reaction near the Giant Dipole Region, S. H. Yoo, et al., Phys. Rev. Lett., **63**, 738 (1989)

DOE/ER/05490-107 Progress Report, October 1989.